Predicting the Rooftop Wind Climate for Urban Wind Energy in the Rotterdam - Delft - Zoetermeer Region

New approaches for implementing urban height data in the wind atlas method

B.M. van Wijk

TU/e Technische Universiteit **Eindhoven** University of Technology

TUDelft
Delft University of Technology

donQi
urban windmill
independent energy

Predicting the rooftop wind climate for urban wind energy in the Rotterdam - Delft - Zoetermeer region

New approaches for implementing urban height data in the wind atlas method

Submitted in Partial Fulfillment of the Requirements for the Degree of

Master of Science

in Sustainable Energy Technology

B.M. van Wijk

November 1, 2011

Supervisors:

Prof. dr. G.J.W. van Bussel

dr. ir. W.A.A.M Bierbooms

ir. K.T. van der Heijden

Abstract

One of the most crucial aspects for the successful application of urban wind turbines is selecting a site with an advantageous rooftop wind climate, such as a high annual mean wind speed and minimized turbulence. There are demands from industry to be able to predict the rooftop wind climate in a reliable yet cost-effective way. This is challenging because wind in the built environment is inherently complex, and a correct rooftop wind climate prediction should be made in consideration of both the meso-, as well as the micro and building-scale wind climatic effects.

For rooftops extending clearly above the neighboring buildings, this study shows that a realistic prediction may be obtained by roughness parameterization of the surrounding urban surface. This procedure involves analysis of a Digital Elevation Model (DEM) to find the microscale urban roughness lengths and displacement height. The Wind Atlas and Application Program (WAsP) then combines these aerodynamic parameters with a meso-scale wind climate.

A first trial for a 32 m high building in Rotterdam indicated that the sectoral mean wind speed prediction could be improved substantially as compared to an existing wind climate prediction which was based on land-use criteria (LGN3+). A 4-week ultrasonic measurement campaign held at that roof could partially validate the roughness lengths derived from the DEM.

As a second case-study, roughness lengths were calculated from the DEM for a building in the city of Zoetermeer, again enabling a long-term wind climate prediction. After a 5-week measurement campaign held at this site, it was found that the actual sectoral wind climate was again predicted with satisfiable accuracy. Some directions had an inaccurate prediction, but it was shown that a building-induced acceleration played an important role in these sectors. Turbulence measurements done to estimate surface roughness were initially not successful, due to a low anemometer position. A height increase of 1.3 m led to a better surrounding surface roughness measurement, although some distortive effects from the building remained.

The two case-studies illustrate that a digital elevation model indeed holds valuable information about the microscale wind climate, and that this information can be made operational in WAsP by the proposed method. A clear user-guide is supplied indicating the exact steps required to enable this integration. Practical recommendations for future roughness measurements in an urban environment are given based on current experiences. Since experimental evidence in this study is only covers two locations, analyzing a more profound basis of experimental evidence from various urban rooftops should be used to further substantiate the chosen approach.

Acknowledgements

Contents

List of Tables

List of Figures

x

Symbols

General

u	Wind speed [m/s]
u_*	Friction velocity [m/s]
k	Von Kármán constant [-]
z	Height above ground [m]
z_0	Surface roughness length [m]
z_d	Zero-plane displacement height [m]

DEM analysis

H	Obstacle height [m]
$\overline{H}$	Average obstacle height [m]
$\overline{h}$	Average cell height in DEM [m]
A_p	Plan area [m^2]
A_f	Frontal area [m^2]
C_d	Drag coefficient [-]
λ_f	Frontal area density [-]
λ_p	Plan area density [-]
D	Weighing function distance constant [m]

Building scale

D	Virtual building dimension [m]
H	Building roof height [m]
y	Vertical coordinate above roof [m]
x	Longitudinal coordinate from roof edge [m]

WAsP

X	RD horizontal coordinate [m]
Y	RD vertical coordinate [m]
h	Height above ground level [m]
U	Mean wind speed [m/s]
U^J	Sector J mean wind speed [m/s]
P	Power density [W/m^2]

Sonic Measurements

U 10-minute mean longitudinal wind speed [m/s]

σ_u Standard deviation of U [m/s]

N Number of samples

u_i Individual 10 Hz sample wind speed [m/s]

y Logarithm of measured z_0 [log m]

z_0 Measured roughness length [m]

U_{vert} 10-minute mean vertical wind speed [m/s]

Abbreviations

ABL	Atmospheric Boundary Layer
AEP	Annual Energy Production
AGL	Above Ground Level
AHN	Actuele Hoogte van Nederland (Actual Height of the Netherlands)
CFD	Computational Fluid Dynamics
CI	Confidence Interval
DEM	Digital Elevation Model
ESDU	Engineering Sciences Data Unit
KNMI	Koninklijk Nederlands Meteorologisch Instituut (Royal Dutch Meteorological Institute)
LGN3+	Landgebruik Nederland 3+ (Dutch Land Use 3+)
MAE	Mean Absolute Error
MCP	Measure Correlate Predict
NAP	Normaal Amsterdams Peil (Amsterdam Ordnance Datum)
RD	Rijksdriehoekscoördinaat (Dutch National Coordinate)
RIX	Ruggedness Index
TI	Turbulence Intensity
UCL	Urban Canopy Layer
UWT	Urban Wind Turbines
WAsP	Wind Atlas and Application Program

Chapter 1

Introduction

1.1 A challenge for Urban Wind Energy

The recent interest in renewable energy sources has driven the attention to less conventional electricity generators such as Urban Wind Turbines (UWT). Urban wind turbines are machines designed to extract the power that is available in the wind in urban areas. Their limited size allows them to be directly connected to the existing building structure, and a limited rated power enables a direct connection to the low-voltage grid, allowing owners to produce energy on the costumer-side of the electricity grid. In addition to solar cells and micro-Combined Heat and Power, urban wind turbines are part of the radically new technologies for distributed energy production.

Small turbines like the one depicted in figure 1.1 have been subject to ongoing design improvements to anticipate on the different wind characteristics one finds in the urban environment, such as a larger speed and direction variability. Yet, there is a general consensus that the practical success or failure of a small wind turbine is still highly dependent on the specific *local* wind conditions at the roof of installation [60]. Besides an advantageous mean wind speed, these conditions include turbulence levels due to ambient sources, effects caused by direct shelter from nearby obstacles or effects from wind reacting on the geometry of the building. It has been shown that insufficient attention to any of these points can cause turbine under-performance or, in some extreme cases, turbine damage due to cyclic and extreme loads exceeding the design assumptions.
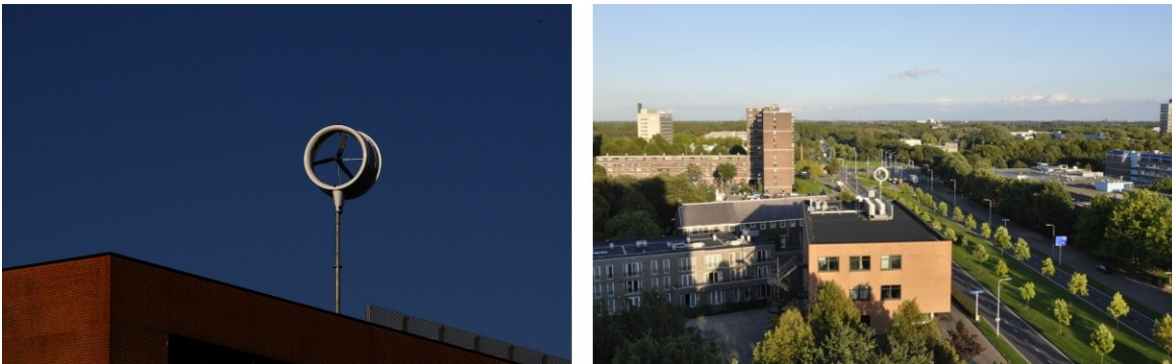
Figure 1.1: The Diffuser-augmented Urban Wind Turbine recently developed by DonQi installed on a roof in Eindhoven, The Netherlands.

1.2 Problem definition

The main objective of this project is to work towards better urban turbine siting, by improving the rooftop wind climate prediction in urban locations. To introduce the problem, it makes sense to shortly discuss three types of analytical approaches which are available for the determination of the rooftop wind climate,

together with their major benefits and disadvantages. These are: on-site measurements, numerical flow simulations and the wind atlas method.

First, on-site measurements involve equipping the roof with anemometers (wind measuring devices) that simply register wind speeds at a fixed spot. One may then derive the long-term wind climate through a time-series correlation –if it exists– with a nearby meteorological station. The main advantage is that it is straightforward and relatively reliable, disadvantages are that it is costly, both financially and in time and effort, and that a solution is only found for a single spot, which may have been affected by unknown building-induced flows. A previous report describes the methods, results and experiences of a measurement campaign and correlation analysis of a building in Rotterdam

Second, Computational Fluid Dynamics (CFD) simulations may be used to model the flow as it is affected by the building and (part of) its surroundings. The main advantage is that it is possible to generate wind profiles with a very satisfying degree of detail, for instance details of zones with advantageous wind speeds and low turbulence. Yet on a project-basis, the complete process seems to be too exhaustive for the UWT industry, with steps including: modeling geometries and flow domain, establishing boundary and initial conditions, generating the grid, simulation, post-processing, validating measurements and sensitivity analyses. The variable climate often implies that multiple wind directions need to be studied.

Third, the wind atlas method employs an extensive set of models for the horizontal and vertical extrapolation of wind climatic data. It has shown its practical and industrial value for the utility-scale wind energy sector, but for the built environment, a direct application of this method generally does not lead to reliable results because the complexity and ruggedness of the surface exceeds the operational limits of the models. Fikirte Yemer tried to applied the wind atlas approach to predict the wind climate for a 32 m high building in Rotterdam using the Wind Atlas and Application Program (WAsP) [62]. She found that indeed errors were large, but it was possible to reduce the sector-averaged mean wind speed error by analyzing a urban height data about the surroundings to model the flow displacement of urban obstacles. More details about this particular approach are presented in section 2.3.3.

While the general approached proved promising, very little theoretical foundation appeared to be available on how one should go about including the urban height data in the wind atlas approach and how it compares to some known aspects of wind through urban areas. This project was started from the motivation of laying better foundation for the integration of this data in the wind atlas framework, by a thorough literature review, followed by new modeling approaches and on-site measurements at two locations.

We adopt a broad central research question that defines the problem:

> In what way(s) could a Digital Elevation Model of the surroundings be used to better predict the rooftop wind climate for urban locations using the wind atlas approach?

Given the objectives, the aim is to finalize the project with practical recommendations or a tool for industry, enabling application readily available height and wind climate data for improved urban wind climate predictions on a project basis.

1.3   Report outline

The outline of this report reflects largely the process followed in the project. Chapter 2 –the literature review– reflects a broad focus which was adopted in the beginning of the project. It attempts to lay a foundation for the remaining parts of the thesis, and treats wind climates on different spatial scales and the role of the Wind Atlas and Application Program WAsP. In Chapter 3, a description is given about the explorative work with the Digital Elevation Data. It also describes the proposed use of WAsP and substantiates the choices made in this program.

At the end of Chapter 3, we come to conclude that three strategies may be adopted. These strategies are applied to a first case-study location in Chapter 4, and each individual strategy is evaluated, eventually leading to the preference of urban roughness parameterization. It is then attempted to partially validate

the roughness parameterization by further experiments on the trail location. These results are presented in Chapter 5. In Chapter 6, the results are presented for a second urban location in an attempt to validate the conclusions developed so far. The report is finalized by a conclusion section in Chapter 7 and recommendations in Chapter 8.

Chapter 2

Literature review

This literature overview is aimed at presenting a relevant selection of topics related to urban wind climatology. The chapter starts out by treating some more fundamental concepts; an introduction is given about the wind layers within the atmosphere and the division of spatial scales often used in meteorology. Then, some parts follow in which the wind characteristics are described on a meso, micro and building scale, a division which is retained throughout this report. There is strong focus on the concept of surface roughness length and its use in urban wind climate studies.

For the micro scale, additional focus is laid on the effect of urban obstacles and the methods to incorporate those effects within the existing frameworks. Specific attention is given to the meaning of urban morphometry and how it could be related to the wind regime or climate.

A further focus in on the fundamentals, internal workings and the use of the Wind Atlas and Application Program (denoted as WAsP) for wind climate modeling. The main limitations of WAsP for the use in complex terrain are discussed, followed by approaches found in literature to partly overcome these limitations.

The chapter is finalized by a short summary and a conclusion about the literature in relation to the current project. The current project is more precisely positioned and further research choices within this project are substantiated.

2.1 Wind in the atmospheric boundary layer

High up in the atmosphere, wind primarily interacts with pressure differences and the force of Coriolis, caused by the rotation of the earth. Lower in the atmosphere, interaction from the earths surface becomes increasingly important. The atmospheric boundary layer (ABL) is the layer in which the wind is related to the drag caused by surface irregularities and by surface heat fluxes.

The adiabatic boundary layer wind can be defined as wind close to the surface under neutrally stable weather conditions. Neutrally stable weather conditions imply that the flow close to the earths surface is neutrally stratified; there is no effective heat flux within the layer. Except noted otherwise, statements in this chapter and throughout this report apply to wind under adiabatic conditions.

The adiabatic ABL can extend vertically over a few hundred meters and is generally divided into two sub layers: the surface layer and the mixing layer. The surface layer is the layer with the largest velocity gradients and, as a result (and cause), the highest production of turbulence. It covers on average the lowest 10% of the ABL. The mixing layer is the layer where turbulent kinetic energy generated in the surface layer is dissipated. Due to the mixing, the speeds in this layer are independent of the direct parameters of the ground directly below it, instead they are a function of the surface characteristics over a larger scale.

For wind engineering purposes, especially for UWTs, the surface layer is the most important layer. Within this surface layer, different phenomena occur at different heights, so it is again convenient to divide this layer into a number of smaller layers. The absolute lowest part of the surface layer is the layer of air between the roughness elements (obstacles) and is often referred to as the Canopy Layer or Urban Canopy Layer (UCL). It stretches to around the height of the tallest roughness element. The layer that overlaps this lowest layer but extends further, to about 1.5 to 2 times the obstacle size, is referred to as the Roughness Sublayer (RS). This layer covers the part of the surface layer where the flow is considered
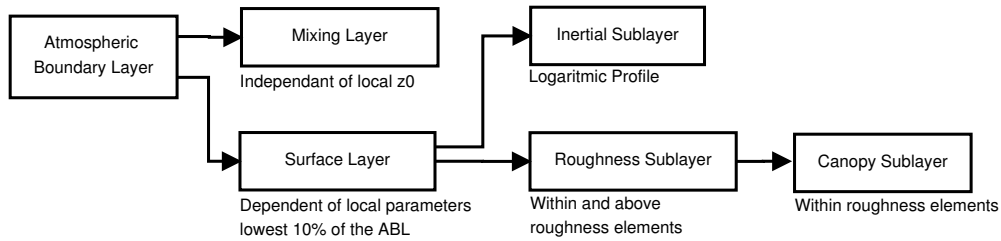
Figure 2.1: Composition of the Atmospheric Boundary Layer.
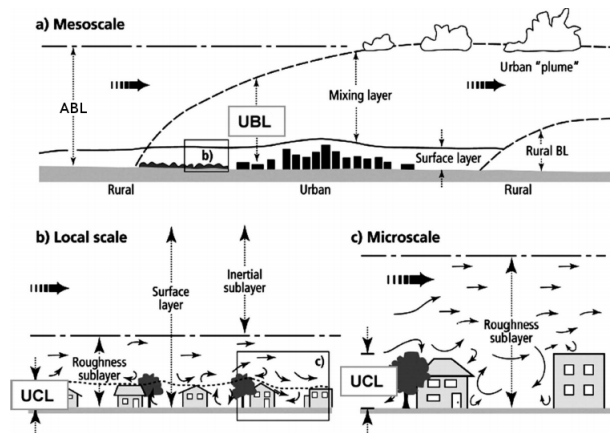
Figure 2.2: Overview of scales and layers within the ABL [44]. Note that in this document the local scale is merged with the microscale for convenience.

to be complex, 3-dimensional and dynamically influenced by the individual roughness elements. The shear stresses in this layer are variable with height. In the remaining upper part of the surface layer, individual obstacle influences diminish. This part is called the Inertial Sublayer (IS) and, in the idealized case, shear stresses in this layer are constant with height implying that a logarithmically shaped wind profile develops.

2.2   Wind climatic scales

A common meteorological division is made on the basis of the spatial scales on which climatic phenomena manifest themselves. The spatial scales are also fundamental in the theories developed so far within meteorology and wind climate studies. Three scales are distinguished:

- The Synoptic Scale (L > 2000 km)

- The Mesoscale (2 km < L < 2000 km)

- The Microscale (L < 2 km)

The synoptic scale is the largest scale on which climate manifests itself, the typical scale of large weather systems such as cyclones and large pressure zones. Air circulation on this scale is primarily driven by the Coriolis force and pressure imbalances originating from differences in temperature and solar radiation on the planet.

6

Within this global synoptic scale there are a number of smaller mesoscales, typically stretching for anywhere between 2 and 2000 km. Wind phenomena on these mesoscales are governed by a different climatic system, with stronger influences from the regional landscape, such as ground level elevation, meso surface roughness, the distance to mountains, the proximity of an ocean or sea, and the location of the region with respect to the global climate. Some mesoscale wind considerations are discussed in section 2.2.1.

The microscale is the smallest climatic scale and stretches for a few kilometers. On this scale, local surface roughness becomes an important parameter and man-made objects as well as vegetation become to strongly affect the wind resource. Micrometeorological processes are limited to the shallow layers of frictional influence close to the earth's surface [21]. With regard to the microscale meteorology, the characteristics of the direct nearby surroundings of the area of interest are important determinants. The micro scale wind climate is discussed in section 2.2.2.

As was noted by B. Blocken [11], the climatic scale division could well be extended by a fourth scale, namely the building scale. It is on this scale that building-related phenomena manifest themselves such as building wakes, speed-up effects and roof separation, see section 2.2.3.

2.2.1   Mesoscale wind climate

The mesoscale is an important scale for wind resource estimations, because on this scale the top part of the ABL can often be assumed to have a comparable wind climate. Only for the lowest part of the ABL, the surface layer, mesoscale distances are too large and effects from microscale drag and turbulence are too important to assume an equal wind climate. There is a practical scaling relationship that can be used to transform the top (equal) ABL wind climate to the lower surface layer, incorporating effective drag from the local microscale landscape; the log-law.

2.2.1.1   Log-law in the inertial sublayer

By a dimensional analysis known as the Monin-Obukhov similarity theory, a relationship can be derived between the mean velocity profile, a surface length scale and wind speed for the inertial sublayer [38]:

$$u(z) = \frac{u^*}{k} \ln\left(\frac{z}{z_0}\right) \tag{2.1}$$

In this formula, u is the wind speed, k is the von Kármán constant, z_0 is the surface length scale (meso surface roughness) and u^* is the friction velocity. This formula follows from the Navier-Stokes equation applied to an air layer with the following characteristics:

- Constant surface stress

- Uniform roughness

- Turbulent viscosity is the only relevant viscosity term

- Negligible thermal effects (neutral stability)

This law has been extensively validated in controlled laboratory environments but also in field studies for wind energy purposes. It is generally accepted, but has known limitations, mainly in cases of non-neutral stratification, low wind speeds or inhomogeneous or large roughness.

The surface roughness parameter is a measure for the surface microstructure and is defined as the height where the logarithmic relationship would result in a zero wind speed. It can also be seen as the height where the effective momentum sink is located.

In this log-law formulation, the surface roughness should be seen as a mesoscale parameter; it is not about the immediate roughness at the location, but rather an average over a certain length called the
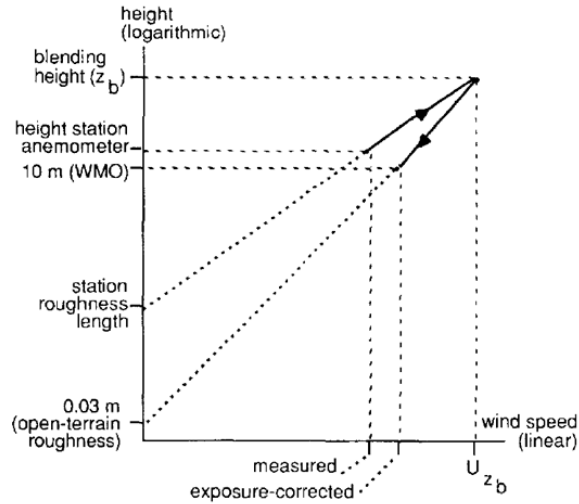
Figure 2.3: Figure showing the concept of blending height. First a local wind observation is extrapolated to an estimate at a height z_b. Consequently, a wind speed estimate for a site with the same mesoscale wind climate but a different local roughness or height can be determined from the value at z_b, by extrapolating downward using a different roughness [58].

fetch distance (which should be relatively invariant under the second assumption). It is possible to relate surface roughness lengths to typical land-use types, currently known as the (revised) Davenport roughness classifications. Typical roughness lengths vary from $z_0 = 0.0002$ m for calm sea, snow or sand-like surfaces to $z_0 > 2$ m for inner cities [57] (see also Appendix F).

2.2.1.2 Two layer 'blending height' model

The practical value of the terrain roughness classifications is that it enables us to use wind observations from inside the logarithmic sublayer and transform it into an wind speed that is independent from local effects. J. Wieringa of the Royal Dutch Meteorological Office hence proposed to define a wind speed at a certain height which is said to be unaffected by the local micro environment [58]. He proposed to use a height of 60 m, see figure 2.3.

Assuming a similar wind velocity at blending height allows directly equating two logarithmic profiles and finding a relation between two friction velocities of two sites which are governed by the same meso climate:

$$u_2^* = \frac{\ln\left(\frac{60}{z_{0,1}}\right)}{\ln\left(\frac{60}{z_{0,2}}\right)} u_1^* \tag{2.2}$$

A note should be made here that the choice of the blending height is empirical and essentially for flat terrain. Also, the two sites should have a good point-to-point representativity, as is put forward by Wieringa. In a recent report of the KNMI, the blending height method in combination with a model for the geostrophic wind was used to (re)produce a wind atlas for the Netherlands [48].

The Wind Atlas and Application Program (WAsP), which we will discuss later, does not use the concept of blending height. Rather, it introduces a way of dealing with variable roughness within the surroundings of a site, by incorporating an internal boundary layer (or roughness change) model [50].

8
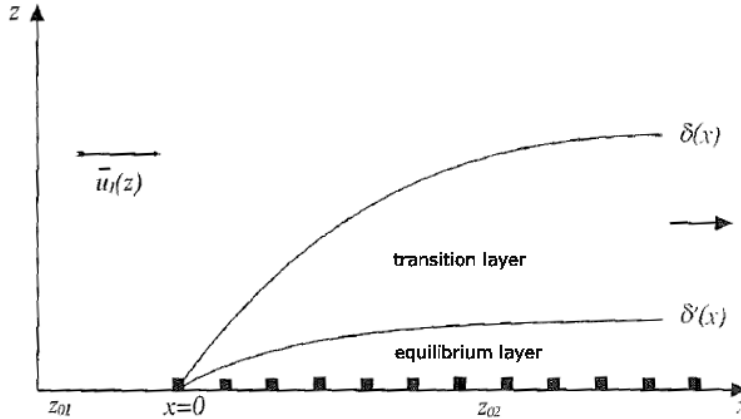
Figure 2.4: IBL development after a roughness transition (adapted from [4])

2.2.1.3 Roughness transition

In case of a roughness transition, the log-law profile given by equation 2.1 cannot directly be applied, because the homogeneous roughness assumption is violated. The most clear example of such an situation is when wind flows over a rural-urban transition. Every roughness transition results in the formation of an internal boundary layer within the original atmospheric boundary layer.

In figure 2.4, $\delta(x)$ shows the height to which the downstream atmosphere is disturbed due to the change in roughness and $\delta'(x)$ shows the height at which the velocity is totally adjusted to the new parameters. Assuming that some transients effects settle (S. Mertens [37] notes that this is achieved after a fetch distance of around 500 m), three layers come to coexist in which different velocity profiles are valid.

In the European Wind Atlas report a description is given of how roughness lengths are used to determine a wind speed in these three different layers [1]. First, the height of the internal boundary layer as a function of the upstream fetch length $h = \delta(x)$ is determined with an empirical relation. Then, three velocity regions are valid:

- Close to the ground, when $z < 0.09h$, the velocity profile is given by the new roughness parameter:

$$\bar{u}(z) = \frac{u_2^*}{k} \ln\left(\frac{z}{z_{0,2}}\right) \tag{2.3}$$

- For $0.09h \leq z \leq 0.3h$, the velocity profile is given by a combination of new and original roughness parameters:

$$\bar{u}(z) = \frac{u_2^*}{k} \ln\left(\frac{0.09h}{z_{0,2}}\right) + \left(\frac{u_1^*}{k} \ln\left(\frac{0.3h}{z_{0,1}}\right) - \frac{u_2^*}{k} \ln\left(\frac{0.09h}{z_{0,2}}\right)\right) \frac{\ln\left(\frac{z}{0.09h}\right)}{\ln\left(\frac{0.3}{0.09}\right)} \tag{2.4}$$

- For $z > 0.3h$, the velocity profile is given by the original roughness parameter:

$$\bar{u}(z) = \frac{u_1^*}{k} \ln\left(\frac{z}{z_{0,1}}\right) \tag{2.5}$$

The friction velocities u_2^* and u_1^* are related to each other by matching the profiles at $z = h$. The relations presented above are part of the internal boundary layer (or roughness change) model and form the basis of the roughness procedure in WAsP.
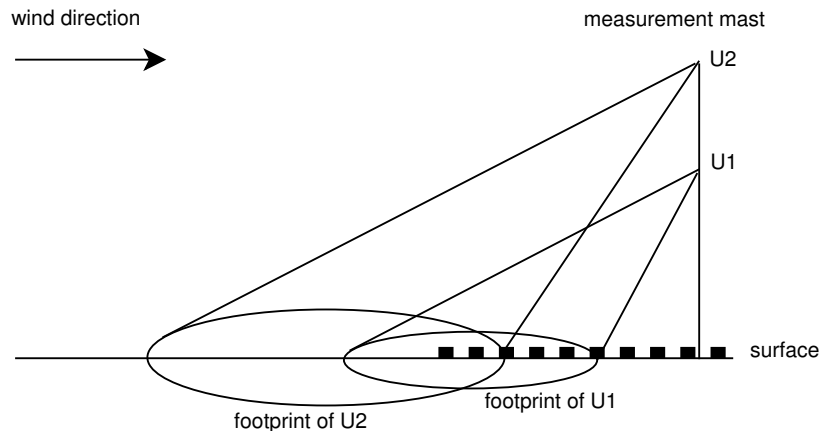
Figure 2.5: Conceptual visualization of the footprint model. Wind at height U1 is influenced by surface characteristics that lie within the footprint of U1. At a higher elevation, a larger footprint U2 influences the wind at U2.

Besides internal boundary layer models, there are other ways to deal with non-uniform roughness. J. W. Verkaik explains the use of a footprint model to obtain the effective roughness length at a certain height [53]. In the footprint model, the roughness over a certain upstream area (footprint) is averaged over the area. The size of the footprint increases with height; very close to the ground –around 10 m a.g.l.– the footprint area is limited to a few hundred meters but when the height is increased, the footprint area increases and a larger fetch of roughness should be included (figure 2.5). In Verkaiks application, an exponential weighing function is used to represent the decreased effect that a surface element has when it is located further away from the origin.

2.2.1.4   The Dutch mesoscale wind climate

The *Windkaart van Nederland* is one of the most recent wind maps produced for the Netherlands [29]. It aims at covering the wind climate at utility-scale turbine height over the entire country of the Netherlands. We can consider this atlas to represent the Dutch mesoscale wind climate, because at the height it was produced for, effects of roughness on the microscale are invisible and of far less importance than a mesoscale characteristic such as the distance to the sea.

The wind atlas was produced by the computer program WAsP –introduced in section 2.3– to vertically and horizontally extrapolate a measured wind climate and to account for surface roughness and orography. The production involved the following steps:

1. Derivation of long term statistics from the KNMI measurement station network

2. Production of a set of regional wind atlases, from a station wind climate, using a roughness database for selected stations

3. Division of the Netherlands in 10x10km blocks, and calculation of regional wind speeds per block by an interpolation method

4. WAsP calculation within the 10x10km block incorporating the roughness database

5. Merging individual blocks into a complete wind atlas

The roughness database used is a database created from land-use data LGN3+, developed by Alterra [5] . For the Netherlands, this database is available with a 100x100m resolution. Regarding urban terrain,
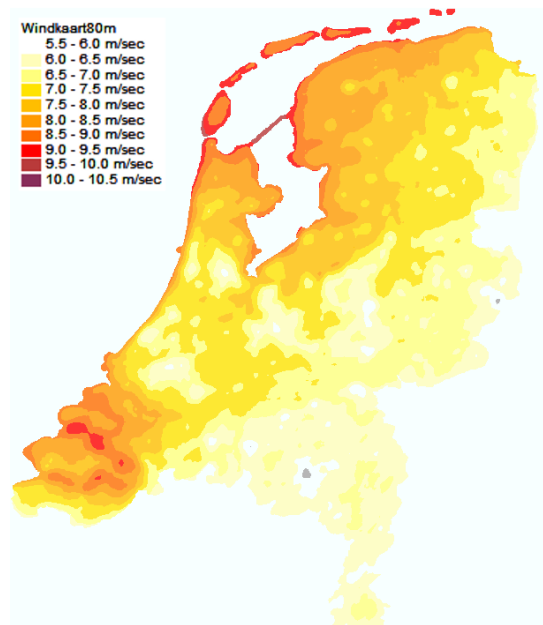
Figure 2.6: Dutch Wind Atlas for 80m height. Effects of meso roughness are visible such as large cities and distance to sea and lakes [29].

it distinguishes between four types, ranging from built-up area ($z_0 = 0.5$ m) to built-up area with dense forest ($z_0 = 2.0$ m). It does not hold a zero-plane displacement height value, as this becomes insignificant at the height of most utility scale wind turbines. The final map was produced with a 200x200m spatial resolution.

2.2.1.5 Velocity distribution and power in the wind

For wind energy purposes, the mean is not the only important descriptor of the energy content in the wind. It is in fact the full velocity distribution that determines the maximum available energy, because of the cubic relation between wind speed and power in the wind. The power available can be expressed as the product of the mass flow and the kinetic energy per unit time flowing perpendicular to the rotor area, giving:

$$\frac{P}{A} = \frac{1}{2}\rho U^3 \tag{2.6}$$

With P the power, A the rotor area, ρ the air density and U the wind speed. Modeling the wind speed distribution with a Weibull function is appropriate for most places on earth. It is the standard to express this distribution as a probability density function, in which the probability of a speed occurring in a certain range is given by the area under the curve in this range.

An intuitive method of binning can be applied to calculate the average energy available in the wind per year. This involves defining discrete regions below the Weibull graph, calculating the hours of occurrence by multiplying the probability with 8760 (hours per year), calculating the power by equation 2.6 and averaging outcomes over all bins. The book of J.F. Manwell, J.G. McGowan and A.L. Rogers gives a precise overview of this procedure [24].

Under the Dutch wind climate it is appropriate to assume a Weibull shape factor of 2. Some wind climates in other countries may not always be described accurately with a Weibull shape, one example is
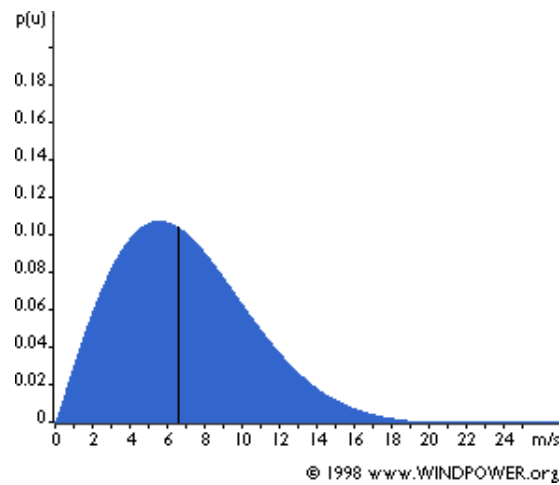
Figure 2.7: Weibull wind speed probability function for a site with an average speed of 6.5 m/s. (Courtesy of Windpower.org)

that there are two prevailing wind directions with each having a very distinct velocity distribution. In such cases the wind speed distribution could show two peaks and a poor Weibull fit.

Last note is that the wind speed probability function can be used to calculate the total available energy in the *mean* components of the wind speed. Turbulent structures also hold energy which may, or may not be, extractable by a wind generator. Turbulent power extraction eventually is determined by the scale of turbulent fluctuations and the turbines response to these fluctuations. This may be of particular importance of small wind turbines given their exposition to wind with turbulent energy and their quicker response times.

2.2.2   Microscale wind climate

In the previous subsection we have dealt with wind in a general atmospheric boundary layer. If we further zoom in in a specific region, the generalized relations presented in the section above have to be reconsidered, adjusted or tailored the particular microscale features. Complex (mountainous or urban) sites require a more detailed approach that includes microscale effect that local features have on the wind conditions.

The importance of the microscale for urban wind energy applications is emphasized by the report of resource assessment published by the Wind Energy Integration in the Urban Environment (WINEUR) work group. It was concluded that the rooftop wind climate depends more on direct local parameters than it does on larger landscape features or dominant regional wind regimes on the meso and synoptic scale [60].

Based on results from some CFD and wind tunnel experiments, it can be concluded that the behavior of wind on the microscale remains difficult to predict. Small changes on the layouts of the buildings, their dimensions, their roof configuration or the wind-direction, can lead to totally different flow structures. Because in reality, we find an unlimited variety of microscale urban forms, it has to be born in mind that part of the microscale flow can never be rightfully resolved without performing a thorough CFD or wind tunnel study for each configuration.

This is unsatisfactory, since much time and effort is required to accurately solve microscale urban flows. Therefore, as a pragmatic approach, this section has a focus on methods to derive approximate descriptions of the flow in an urban environment, using a similar but extended framework as was presented in the previous section.

2.2.2.1   Log-law in the built environment

Urban boundary layer wind is a type of boundary layer wind that is large affected by bluff obstacles. In terms of the log-law presented above, urban areas are among the roughest surfaces available, with z_0 values of several meters. This section deals with two important side marks one should make when discussing the log-law in the build environment.

First, urban surfaces often require the introduction of a new parameter called the displacement height. When more than 20-25% of the land cover is occupied with roughness elements, the apparent level of the ground of the flow, with regard to the logarithmic profile, is virtually raised by a length denoted as z_d. Simply extending equation 2.1 yields an altered equation for the velocity gradient, including this displacement:

$$u(z) = \frac{u^*}{k} \ln\left(\frac{z - z_d}{z_0}\right) \tag{2.7}$$

Which is valid for $z > z_d$. Note that z_0 now refers to the microscale roughness. The effective value of z_d can be crudely related to the three flow regimes in rugged environments (figure 2.8):

- Isolated flow $z_d = 0$

- Wake-interference flow $z_d = 0.1\overline{H}$ to $0.7\overline{H}$

- Skimming flow $z_d = 0.7\overline{H}$ to $1\overline{H}$

Where $\overline{H}$ is the average obstacle height. With isolated flow, obstacles can be treated as being individual as the wake re-attaches before the flow hits another building; with wake-interference flow, the wake of the first obstacle extends to the beginning of the second obstacle resulting in much turbulent mixing; with skimming flow, obstacles are packed so dense that the effective ground level is raised and single vortices are present between the obstacles.

Second, while the log-law facilitates a range of roughnesses, it is sometimes questioned whether the basic assumptions for a logarithmic profile, namely constant shear stress, are actually applicable for the urban environment. Particularly at heights just above the roughness elements, the individual effects that these elements create becomes noticeable. This counts for the roughness sublayer, the lowest part of the surface layer.

For very homogeneous elements, the extend of the roughness sublayer is minimized and a logarithmic profile can be found down to a height very close to the top of the elements, according to CFD studies over staggered arrays of cubes [15, 2]. In case of more heterogeneous elements with varying heights (real cities), the guidelines are ambiguous. Mertens [37] refers to the guideline from ESDU (Engineering Sciences Data Unit), in which the validity range is related to the displacement height: $z_{min} = 1.5z_d$; R.W. MacDonald [35] choses to relate the extend of the roughness sublayer to the mean building height by proposing z_{min} to be between $2\overline{H}$ and $3\overline{H}$; H. Cheng and I.P. Castro derive from the wind tunnel experiments over staggered and in-line cubes that z_{min} should be between $1.8\overline{H}$ and $1.85\overline{H}$ [14]; and finally, in a paper by E. Willemsen and J.A. Wisse [18] it is noted that if a building is higher than $1.5\overline{H}$, it is often not sheltered by surrounding obstacles, hence not in the roughness sublayer.

Concluding, it seems that z_{min} can best be related to the mean building height. In doing so, a larger z_{min} should be chosen for large variations in building heights, whereas a smaller value could be chosen for obstacles of the same height.

2.2.2.2   Urban surface parameters

Until now no focus has been laid on the actual determination of the surface parameters z_0 and z_d for different urban environments. The most common method is based on a visual assessment of the roughness classification, originally developed by Davenport and later revised by Wieringa [57].
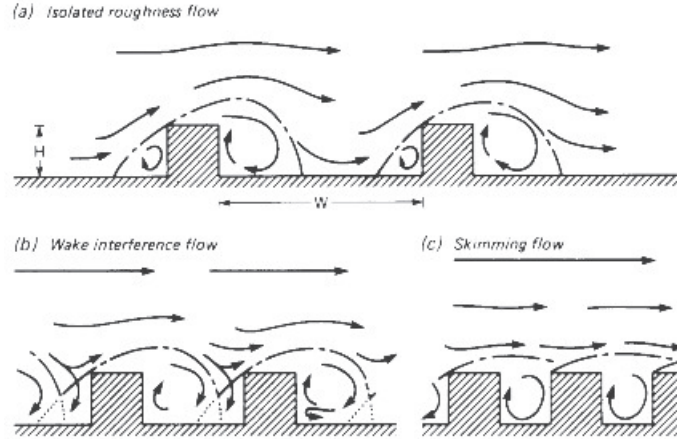
Figure 2.8: Sketch of three flow regimes in the urban environment. In isolated flow (above), the wake can re-attach the surface before a new obstacle is hit. In wake interference flow (bottom-left), a new obstacle is hit before the wake reattaches, causing a chaotic pattern. In skimming flow (bottom-right), the effective roughness is decreased by vortices that 'fill' the canyons [39].

In search for more objective methods, some researchers have worked on establishing an analytical form between the roughness geometrical parameters (or surface morphometry) and z_0 and z_d. The work of C.S.B. Grimmond and T.R. Oke [22] presents a comprehensive overview of these forms. Among them are the ones based on average building height; building height and plan area density; or building height and frontal area index. Plan area density λ_p and frontal area density λ_f are defined as:

$$\lambda_p = \frac{A_p}{A_T} \tag{2.8}$$

$$\lambda_f = \frac{A_F}{A_T} \tag{2.9}$$

Where the areas A_T, A_F and A_p follow from the definitions in figure 2.9.

Comparing the performance from various analytical methods with wind and turbulence observations from 60 field studies showed that some parametrization methods were more effective than others. This led Grimmond and Oke to prefer three analytical forms relating λ_p and λ_f to aerodynamic parameters. One of them, the form proposed by R.W MacDonald, R.F. Griffiths and D.J. Hall [36] (hereafter MacDonald), has shown to give good results for staggered and in-line arrays of cubicles. These relations are as follows:

$$\frac{z_d}{H} = 1 + \alpha^{-\lambda_p}(\lambda_p - 1) \tag{2.10}$$

$$\frac{z_0}{H} = \left(1 - \frac{z_d}{H}\right)\exp\left\{-\left[0.5\beta\frac{C_D}{k^2}\left(1 - \frac{z_d}{H}\right)\lambda_f\right]^{-0.5}\right\} \tag{2.11}$$

Where it is advised to use $\alpha = 4.43$ and $\beta = 1$ for a staggered array of obstacles. Nominally, the drag coefficient C_D for cubical building obstacles ($H = W$) is around 1.2, like a flat square plate in perpendicular flow, although it might also be 1.5 for buildings with a different aspect ratio.

A simpler relation between the surface characteristics of homogeneous obstacles and the effective roughness value was proposed by H. Lettau [34], relating the roughness only to the obstacle height and the frontal area density:

$$z_0 = 0.5H\lambda_f \tag{2.12}$$

14
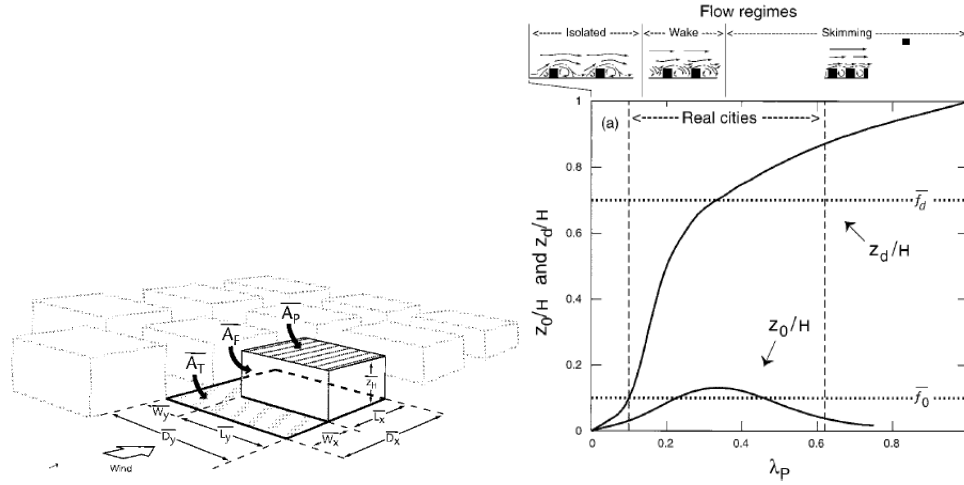
Figure 2.9: Geometrical measures used in urban surface parameterization (left), conceptual relation between plan areal density, surface parameters and flow regimes (right) [22]. Increased plan areal density decreases the roughness length because a transformation is made to a more skimming flow regime where the effective height of the roughness elements is decreased.

Table 2.1: Urban classes and wind profile parameters

Urban Class	$\overline{H}$ (m)	z_d(m)	z_0(m)
Low height and density	5-8	2-4	0.3-0.8
Medium height and density	7-14	3.5-8.0	0.7-1.5
Tall and high density	11-20	7-15	0.8-1.5
High-rise	>20	>12	>2.0

The relation of Lettau is known to work well up to a frontal area density of 0.2-0.3. For the cases where detailed geographical information is absent, a Davenport type of classification is proposed by Grimmond and Oke, again based on a visual assessment of urban classes (table 2.1).

The frontal area density is also a successful indicator for the determination of z_0 and z_d in forestry regions. It was for instance shown that the frontal area density can be related to the average width, height, and mutual distance of the trees [16].

2.2.2.3 Applications of frontal area densities in urban wind studies

Several applications are found in literature that rely on the use of frontal area densities. In a study at the effect of urban ventilation of Hong-Kong [61], frontal area densities have been produced from a Digital Elevation Model (DEM) of the city using a geographical information system. The authors were able to identify pathways through the city with a low frontal area density as well as blockages with high frontal area densities. Based upon these maps, they applied a least-cost method to predict the flow through the urban area. As part of the validation, some wind measurements were held, and the map outcome was compared with urban heat measurements taken over the city, which confirmed the usability of the analysis.

A similar DEM analysis was performed for three sites in Valle del Biferno, Italy [33]. Sonic anemometry was used to monitor the wind speed and friction velocities for four hours under neutrally stratified conditions simultaneously at the three sites. The authors could identify relation between the frontal area densities and the normalized friction velocity for the three sites.
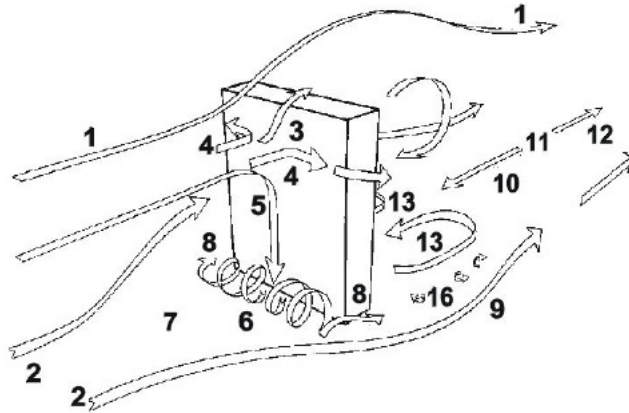
Figure 2.10: Typology of the air flows around a rectangular building positioned perpendicular to the wind [11].

In another study that focused on modeling the urban canopy wind climate in Lisbon, Portugal [46] a DEM was analyzed to extract the displacement height and the roughness length using the equations proposed by MacDonald. For an area of 450x450, λ_f was found to range between 0.07 - 0.36 for different directional sectors, λ_p=0.33 and $\overline{H}$=15.0 m. This led to an estimated zero-plane displacement of 8.8 m and a roughness length ranging between 1.05 to 2.25 m. A coupling was made between a mesoscale weather model and these micro scale variables.

2.2.3 Building scale wind climate

Up to now, we have mainly focused on wind resources models on scales in the order of kilometer(s). We will extend our analysis towards the building scale, as this is a very important scale for wind energy purposes. Wind turbines in urban environments will always feel a direct influence from building induced flows, because when mounted on roofs, their distance to the actual building is often only a portion of the building's height.

The first thing to consider is that in practice every building is characterized by very sharp edges that directly result in flow separation. That means that vortex effects in the wake and along the sides will be very pronounced. Also, due to the large blockage, a standing vortex often develops in front of the building.

A typological overview of the flow characteristics around a high, rectangular building is given in (figure 2.10). Some labels in figure 2.10 are: (3): upward flow from the stagnation point over building, (5): downward flow from the stagnation point, typically creating pedestrian discomfort, (12): restored region flow region and (13): recirculation vortex behind the building. A recirculation vortex above the roof might also be present but is not depicted in this figure.

2.2.3.1 Roof separation

Unless wind turbines are augmented or integrated in the building, the main point of interest for UWTs is the roof of the building. It is useful to consider typical rooftop wind effects found for most standard (rectangular) building shapes, to illustrate the processes that one could reasonably be expecting to happen above any roof.

A general typology of the average flow behavior is given in figure 2.10. An important flow is the rooftop shear layer flow denoted by (3) in figure 2.10. Citing P. Blackmore [10]; the shear layer can be

defined as the air layer that separates the turbulent recirculation region close to the roof's surface from the undisturbed flow above. 'Undisturbed' in this sense refers to unaffected by separation vortices emitted by the roof edge –obviously some other disturbances take place in flow above the shear layer, such as a mean speed and direction change due to a high pressure zone at the stagnation point on the building's frontal facade.

By distinguishing two regions, the shear layer practically defines a minimum height for the most successful application of rooftop wind turbines. Below the shear layer, there is a region of decreased wind speed, increased turbulence, in some cases even a clear vortex can be found with some backward flow towards the leading edge driven by the low pressure zone near that edge. Above the shear layer, no building-induced turbulence is found, and there typically is a slight increase in wind speed due to the streamline curvature, making it a most favorable spot for urban wind energy extraction.

From a dimensional analysis of a number of wind tunnel studies, an empirical relation was established between the dimensions of a 3D rectangular building and the approximate height of the separation streamline, independent of wind speed. A virtual dimension was introduced by N.L. Bagal et al. [7]:

$$D = D_{small}^{\frac{2}{3}} D_{large}^{\frac{1}{3}} \tag{2.13}$$

Where the two D_{small} and D_{large} refer to the smallest and the largest crosswind surface of the building. The height of the separation streamline can now be estimated by what is known as the Wilson equation (after D.J. Wilson [59]):

$$y = 0.28 D^{\frac{2}{3}} x^{\frac{1}{3}} \tag{2.14}$$

Which is valid for the domain $0.1 < \frac{x}{D} < 0.4$ [37]. Note that this relation does not include a dependence on the building length L parallel to the flow. Comparing this relation with his own CFD simulations, Mertens found that this shear layer height is correct for the middle of the roof but slightly overestimated for the roof parts closer to the side. He noted that it is important to include possible effects of a displacement height in the vertical dimension measure, so that $D_{vert} = H - z_d$. This is because a displacement height reduces the effective blockage of a building; when $H = z_d$ we are dealing with skimming flow and there is practically no blockage (c in figure 2.8).

S. Mertens also studied the dependence of the shear layer on various inlet velocity profiles, by varying the upstream roughness length in his CFD simulations. The Wilson equation aligned best with an urban roughness length ($z_0 = 1$m). Decreasing the upstream roughness led to a higher and steeper shear layer, which can be seen in figure 2.11. In this figure x is the coordinate in the direction of the wind, y the vertical coordinate, and b the building virtual dimension (D in this report).
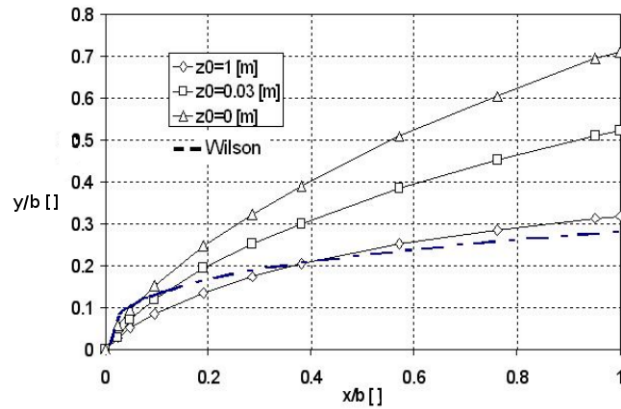
Figure 2.11: Comparison between Wilson's equation and results from CFD simulations on the shear layer development over a roof [37]. b is denoted by D in this report

17
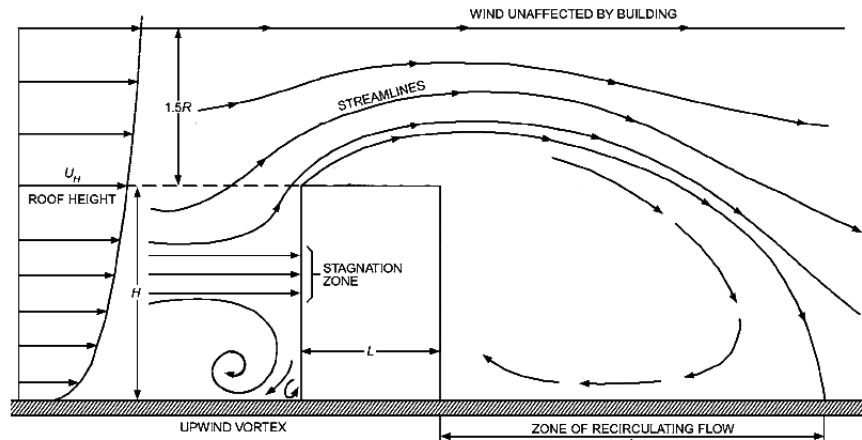
Figure 2.12: Sketch of the time averaged flow hitting an isolated building, without reattachment of the shear layer. R is the virtual dimension of the building (D in this report). Adapted from [3].

Blackmore recently studied roof flow over a number of scale models in the wind tunnel with different building dimensions [10]. His model building was placed in an urban boundary layer which he simulated with small blocks placed upstream. His results indicate that the height of the shear layer is indeed increased with increasing building heights. The shear layer development over the roof of his model building was below the Wilson's equation, this may be because of the increased upstream roughness or the definition of the shear layer that Blackmore applied.

Considering the definition of the shear layer, Blackmore noted that two criteria could be used, leading to diverging results. The shear layer could be defined as the region in which the velocity is within +/- 10% of the undisturbed wind speed. Alternatively, the shear layer could be defined as the height where the turbulence intensity is within +/- 10% of the undisturbed turbulence intensity.

His work leads to some practical rules of thumb for the minimal height of a rooftop wind turbine. At the windward edge, no building-induced turbulence was found, even at his lowest measurement points (2 m), indicating that the flow on the windward edge is indeed undisturbed. Further towards the leeward edge, turbulence intensity increases very rapidly. It was found that, using the turbulence criterion, rooftop installation height should be at least 12% of H for high-rise rectangular buildings (80m) to even 17% for low-rise rectangular buildings (20m) to be above the shear layer. Using the mean wind speed criterion, he notes that the minimum height may be lower, around 10% of the building height above the roof.

2.2.3.2 Speed up effects around single and grouped obstacles

The zone of high pressure in front of the building and the low pressure behind the building accelerates part of the flow around the building, such as depicted by 1 in figure 2.10. This speed-up effect is found with flows over smooth hill as well as flows over building-like obstacles. The magnitude of the speed up depends on the two absolute dimensions of the building, but also on their relative magnitude; if one size is very large as compared to another there is a 2D speed up, if they are similar there is a 3D speedup. 3D speed ups are always smaller than 2D speed ups because due to the extra dimension not all the flow is forced over the obstacle.

S. Mertens [37] showed that one can derive an upper limit for the speed up factor ($c = \frac{u}{u_h}$) based on potential flow around a sphere and cylinder. This limit is 1.5 for a 3D obstacle and 2 for a 2D obstacle. His CFD simulations for a free-standing building of 10x30x20 m (depth, width, height) subject to realistic flow separation yielded a speed up factor of 1 to 1.25, dependent on the the angle of the incoming wind and the location on the roof.

Other CFD simulations, such as those by M.A. Heath and J.D. Walshe [23], showed that the speed

18
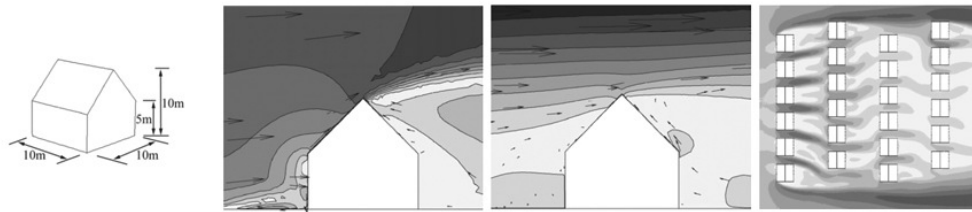
Figure 2.13: Results from a study at speed up factors around an isolated and embedded house. House dimensions on the far left, isolated and grouped CFD results in the middle and on the right a top view of the staggered houses (adapted from [23])
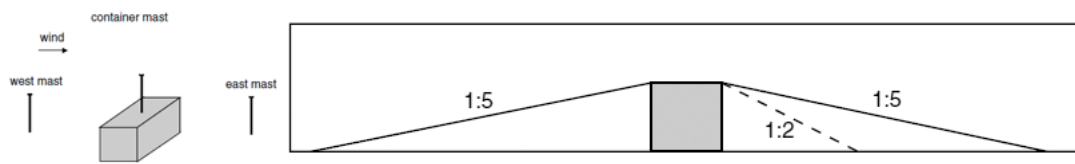
Figure 2.14: L. Landbergs experimental setup (left) and his proposed ´virtual hill´ above the container (right) (adapted from [32])

up factor can drastically decrease when the building is not isolated but part of a group of buildings. In the isolated case and under very smooth surface conditions ($z_0 = 0.001$) a 10x10x10 m building with an inclined roof created a speed up factor of around 1.3 - 1.5 just above the roof. Conversely, when these houses were grouped with 20 m. distance, the speed up became insignificant. Figure 2.13 shows the geometrical setup of this study. We can link this to a frontal area density of around 0.18. This corresponds to the wake-interference regime according to figure 2.9, where we can also see that there should indeed be a displacement height.

In a CFD study performed over an dense array ($\lambda_f = 0.25$) of staggered obstacles, no speed up above the building was found for the time-averaged flow [15]. The study did however indicate that the energy in the wind speed fluctuations reached a maximum near the building's roof, due to the important vortical structures that were present in the flow.

From a speed up study of a single shipping container located in a field, L. Landberg concluded that cup anemometers can measure speed up factors in the mean flow [32]. Combining the shipping container measurements with WAsP modeling, it was found that WAsP can indeed be used to calculate the speed-up above those isolated obstacles, given that a 1:5 slope around the obstacle is used. Prior attempts using the real buildings geometry and a slope criterion from literature (1:2 in front, 1:5 in back) were not successful.

For the present project, Landbergs results are important as they show that a potential model, which is essentially limited, can be in some cases still be used to model partially the complex separation flow that is present above buildings. The speed up effect in the potential flow model caused by this artificial hill is hence very comparable to the actual speed ups. It is possible that in reality, vortices present in front of and in the wake of a building effectively smoothen the building's rough edges and that the air flowing over these vortices behaves like a potential flow. In his study about wind energy in the built environment, Mertens concludes something similar as he writes that: "*the wakes smoothen the contours of bodies and virtually elongate them*" [37].

While Landberg studied only a simple geometry, his results are a proof of principles for the use of WAsP for speed up calculations outside its operational envelope. It is interesting to see whether, and under what conditions, this method also holds for other geometries.

2.2.3.3 Wind shelter from upwind obstacles

Downwind of a large obstacle, a wake region will be present in which the flow is disturbed. As can be seen in figure 2.10, there is a region of recirculation for isolated obstacles and a region where the normal wind direction is again restored. The wake can be subdivided in the following regions (again relating to D as the virtual dimension and x the downwind distance):

- Curved streamlines region $(x/D < 0.1)$

- Recirculating wake region $(0.1 < x/D < 1)$

- Near wake region $(1 < x/D < 3)$

- Far wake region $(x/D > 3)$

In most common cases a wind shelter is caused by obstacles closer than three building heights away. Walker, Wilson and Forest [55] provide a simple model for the velocity deficit present in the wake of a 3-dimensional shelter. This is based on the wake decay exponent of 1.5 as was found by earlier studies. It is proposed that:

$$\frac{\triangle U}{U} = \left(\frac{3.3}{\frac{x}{D} + 3.3} \right)^{1.5} \qquad (2.15)$$

for the centerline of the wake of a building like obstacle. Here, $\frac{\triangle U}{U}$ refers to the velocity deficit relative to the undisturbed wind speed. So an isolated building with a virtual dimension of 20 meters, will evoke a wake with velocity deficits of 57% at 30m distance, 43% at 50m and 25% at 100m. Given this relation, we can state that when the distance is further than 12 times the virtual building size, the deficit drops below 10%.

In reality, the decrease in velocity deficit is caused by wake expansion and mixing with the undisturbed flow. Wake expansion implies that the velocity deficit is divided over a region that becomes increasingly larger with distance from the obstacle.

2.3 The use of WAsP in wind climate studies

WAsP is a computer program for the vertical and horizontal extrapolation of wind climate statistics on the microscale. Its fundamental principle is to use the wind atlas approach, i.e. physical models to translate measurements on one location to estimates at another location. The program has proven its value in many European landscapes with smooth hills of moderate dimension. In fact it has been used to generate the European Wind Atlas, which is generally perceived to be reliable and accurate. The Dutch Wind Atlas, briefly discussed in section 2.2.1.4, was also generated with extensive use of WAsP.

Integrated in WAsP are three sub-models, the orographic model, the roughness model and the shelter model. A prediction through WAsP calls upon these models twice; first the models are used to remove orographic, roughness and shelter effects of the reference site, to create an universal atlas wind speed. Second, orographic, roughness and shelter effects are used to transform this atlas wind speed into a realistic target site prediction. Because WAsP follows the same procedure in two opposite directions, there is a chance that wind speed prediction errors, arising from imperfections in the sub-models of WAsP, partially cancel each other in the final calculation. The sub-models all have there operating limits and it is the collection of these limits that constrains the overall use of WAsP:

- Target and reference site should both have the same overall weather regime (i.e. the mesoscale climate should be similar)

- The prevailing weather conditions are close to neutrally stable
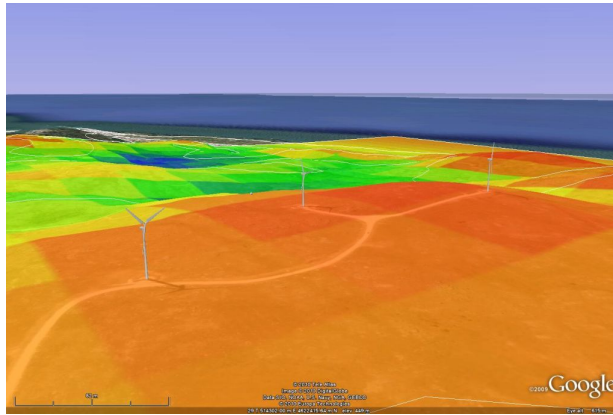
Figure 2.15: WAsP resource grid for a wind farm in Portugal integrated in Google Earth
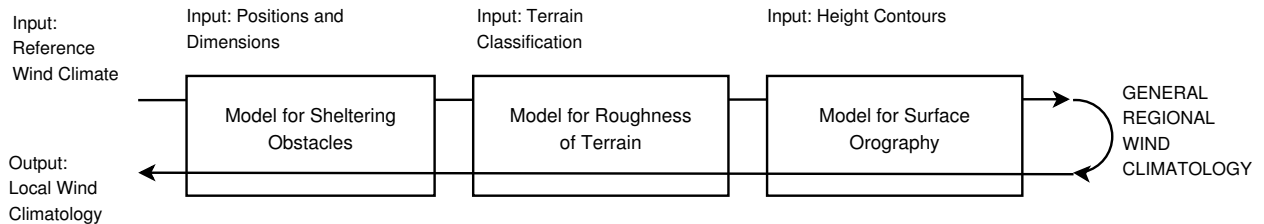
Figure 2.16: General outline of the Wind Atlas method used in WAsP

- The surrounding terrain is sufficiently gentle and smooth

- The reference data should be reliable

The foundations of WAsP are laid by the orographic and the roughness model. The roughness model calculates velocity perturbations caused by the spatial distribution of z_0 around the site of interest. It is totally independent from the orographic model, in the sense that the velocity perturbations predicted by surface roughness are unaffected by any orographic features. In fact, the roughness model is solved for a flat plate [51].

The remainder of this paragraph will be dedicated to the two sub-models, and the applications and its limitations of WAsP for complex sites studies.

2.3.1 The roughness submodel

WAsP has an advanced method of dealing with surface roughness. In essence, it is based on the theory of roughness transitions as was described in section 2.2.1.3. First, the reference roughness per sector is calculated by considering a large stretch of upwind surface and using an averaging method. This can be considered as the mesoscale roughness and is independent of height. Second, the effective roughness at a site and at turbine height is estimated by considering the deviations from this reference roughness due to smaller patches with other roughness lengths. These smaller patches constitute to the emergence of internal boundary layers within the original mesoscale profile. The effect of a patch decreases with increasing (turbine) height and increases if a patch stretches out further into the upwind surface.

WAsP reports to the user what the reference roughness is and also what the local roughness speed in- or decrease is due to patches of varying roughness. The speed in- or decrease is reported in percentages with respect to the speed of the unaffected terrain with constant reference roughness.

A displacement height is not included in the roughness sub-model of WAsP. Since WAsP is developed for large (utility sized) wind turbines, a displacement height of a few meters usually has a negligible effect on the energy performance of these turbines. Even so, for turbines at low heights, a displacement height can become significant.

2.3.2 The orographic submodel

The orographic sub model, or BZ-model, deals with the interaction between the neutral flow and the shape of the hilly terrain below it. It is based the assumption that the velocity and pressure perturbations can be represented by a velocity potential function which is related to the surface form. The integrals in this model are then numerically solved to obtain a solution on the middle point of a zooming polar computational grid. This grid is zooming and polar so that nearby geometries can still be treated with a good significance while at the computational efforts in regions far away from the point of interest are minimized. Geometries further away have a smaller influence on the velocity perturbation in the point of interest and the same counts for the errors in their computation caused by inaccuracies of some sort.

The smallest grid size of the mesh used in the BZ-model (located in the center) will be in the order of meters. In many cases, height data will only be available at a similar or lower resolution, so the BZ-model is often not the resolution-limiting factor. A choice left to the user will be to define the total domain size; the range at which geographical features are available or are expected to be influencing the perturbation. This length should minimally be 5 km.

Besides height-data, the orographic sub-model also incorporates the local roughness length. In solving the BZ-model there is a requirement to have knowledge of the vertical extend of the surface stress layer and this length is modeled using the local z_0.

2.3.2.1 Limitations of the orographic submodel

It is the linearity of the BZ-model that theoretically limits the application of WAsP for complex sites. While the linearized model is practical and fast, it is by itself not capable of accounting for phenomena that appear when wind flows over very rough elements such as separation of the boundary layer, wakes or the vortices that we have seen in figure 2.10. The mean wind speeds in build up areas are so largely affected by those phenomena that in principle a BZ-based wind speed prediction in a complex site comes with a large error.

The limitations of the orographic sub model were first studied by field measurements at 10 m a.g.l in rugged natural terrain Northern Portugal [41]. One of the conclusions was that speed ups due to the orography are over-estimated for very complex terrain, because flow separation effectively modifies the terrain to something that is less rugged and less hilly than the actual terrain.

The Portuguese study confirmed that prediction errors are related to the percentage of slopes in the neighborhood that exceeded a certain steepness criterion, and the authors propose that this orographic indicator criterion should be 0.3. Consequently, WAsP was extended with a ruggedness index (ΔRIX) calculation. The ΔRIX gives the percentage difference in ruggedness between two sites and is found to be directly related to the wind speed prediction error, see figure 2.17. Speed up effects of sites with much separation are overestimated while speed up effects of sites with little separation are underestimated.

There is some room for nuances about whether non-linear flow models should always be preferred above WAsP, for complex terrain. During a research study aimed at predicting the wind speeds in very rugged terrain around Gurskøy (western Norway), WAsP (including ΔRIX) was benchmarked against two industry CFD alternatives; WindSim and 3DWind [9]. The two CFD models were based on k-ϵ turbulence modeling without buoyancy terms and solved until a steady-state velocity and turbulence solution was reached. Comparing the model outputs with measurements (10 & 50 m a.g.l), it was found that WAsP actually performed much better than both CFD models in the precision of the vertical velocity profile and annual average speed.

In another study [56], WAsP was again benchmarked against WindSim to model wind speeds in rugged terrain, this time in Scotland. It was found that without a ΔRIX adjustment, WindSim outperformed WAsP, but by including the ΔRIX adjustment, the predict accuracy was increased to beyond that of WindSim.

It would be wrong to conclude solely on the basis of the Scottish and Norwegian study that WAsPs linear orographic flow model is sufficient in these terrains and that there is nothing to gain from a full CFD simulation. Rather, the studies emphasize that CFD simulations require a very careful operation as well as more precise data. Any model outcome is only as good as its input data is.

In these case studies, the constraining factors were for instance low-resolution height contours, non-neutral stratification and insufficiently accurate model boundary conditions. In the CFD simulations, turbulent closure can often be problematic. It seems that WAsP (including ΔRIX), currently remains a preferable method for wind energy predictions, from a practical and performance point-of-view, especially in the absence of high quality input data to impose boundary conditions for CFD simulations.
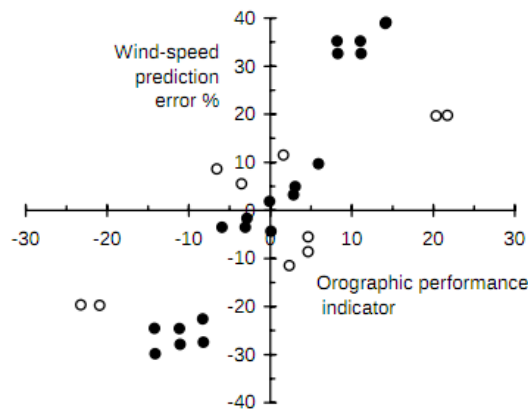
Figure 2.17: Example of the relation found between the wind speed prediction error and difference in percentage of steep slopes between predictor and target site[12]

2.3.3   Artificial orography in WAsP

In attempts to extend the use of the orographic model to difficult situations, alternations were made to orographic input in WAsP. We have already come across the study by Lars Landberg, in which he showed the possibility of simulating the speed up effect of a single bluff body by shaping a digital elevation model (section 2.2.3.2).

In another occasion, the use of WAsP for dense forest sites was studied [16]. Standard WAsP settings for forest, $z_0 = 0.4$, led to some alarmingly large errors (14-70%) in the annual average wind speed prediction and the authors noted that the inability of WAsP of including a displacement height was one of the main causes. By using tailored estimates of z_0 and z_d, obtained through formulas that used tree indicators (i.e. frontal area density, tree width, canopy height and distance between trees) they could reduce the errors down to 1.7-19%. To include a displacement height, the ground level of the forest was virtually raised by z_d in the orographic model, and along the sides of the forest, a gentle slope of 1:5 was applied.

Further tweaking was applied in two studies aimed at determining the wind conditions in an urban environment. First, WAsP was used for an initial investigation at the wind potential urban Portugal [45] and second, TU Delft graduate F. Yemer used it to model the wind potential in the Rotterdam-Zoetermeer-Delft region in the Netherlands [62] (the thesis project preceeding this work). Unfortunately, the Portuguese study did not include a validating measurement campaign, so the accuracy of their WAsP

prediction could not be evaluated. The Dutch study did include simultaneous measurements on top of a building and at nearby meteorological station. Omni-directional (sector-averaged) errors could be held very low, often around a percentage, although remarkably the errors per sector were often around 20 to 30%.

In both studies, the shape of the urban surface is represented by an artificial digital elevation model; a smoothened representation of the actual urban building geometries. According to the results from the Dutch study, this decreased errors in the prediction as compared to the use of unmodified building height data.

The general assumption is that the smoothened layer makes physical sense because it covers more or less those regions where normally flow separation occurs and non-linear effects prevail; around the edges of buildings and in canyons between clusters of buildings. By constructing an artificial digital surface, these regions are modeled as being impenetrable for flow, as it were mountain slopes.

Concluding, we can summarize several problems and notes to make, regarding the WAsP digital surface layer approach for rooftop wind climate modeling:

1. Both the Dutch and the Portuguese study gave little foundation on the geometry of the smoothened layer. How should the layer be constructed given a certain urban form? In the Dutch study, it is noted that the artificial layer corresponds to a skimming flow regime assumption. It was however not checked whether local building density or frontal areal density would indeed indicate a skimming flow regime at these spots.

2. The studies did not fully address the fact that an artificial surface can have two effects in WAsP. First, it can model a displacement height, as was seen by the study of WAsP for dense forest sites. This is achieved by virtually raising the ground level in WAsP around a site. Second, it can be used to model speed up effects of individual obstacles, as was seen in section 2.2.3.2. The speedup is governed by the steepness of the slopes around a roof. Measurements performed in the Dutch study indicated that the wind climate prediction was improved by the artificial surface. It is however unclear whether this improvement could be attributed to a better model for the displacement height, a better model for the speed-up, or both.

3. Importing the artificial surface in WAsP can only be done under the assumption that the flow displacement it represents is constant for different directions or speeds. The surface is not altered for different wind directions so it acts evenly on all sectors. Also, it may be the case that with higher wind speeds, the chance of eddies penetrating gaps between buildings is reduced (as was noted in [16]), leading more quickly to a skimming flow regime. This would mean the shape of the artificial surface layer should, in theory, be modified as a function of wind speed.

To conclude, we can state that the modified surface approach is a method with potential because of the speed and small computational efforts. However, the methods benefits and deficiencies are not well explored nor is were the outcomes extensively validated. There are no guidelines on how it should be used and what the operational limits are.

2.4 Conclusion

The main goal of this chapter was to present an overview about theories and techniques related to the assessment of an urban rooftop wind climate. It was found that the rooftop wind climate, can essentially be considered as the result of a meso, micro and building scale wind effect. Every wind resource estimation in the built environment should incorporate these three scales.

The wind atlas of the Netherlands at 100m (2.6) gives an indication of the different mesoscale wind zones that are present in the Netherlands, which differ mainly due to the distance to the sea or other large stretches of water. A correct mesoscale wind estimation should hence be made with consideration

of these zones. In practice, that means selecting the most nearby long-term measurement station for reference wind resource data. For the Netherlands, good quality long-term measurement data is always available within mesoscale distance through the KNMI measurement network.

The microscale is the second scale to be considered, most importantly for non-flat terrain. On this scale, complex wind effects from surface irregularities such as local roughness, local surface elevation and obstacle wakes are increasingly important. When the local surface is sufficiently well registered in a digital format, i.e. as height and roughness contours, WAsP can be used to successfully predict the wind climate in the inertial sublayer above most non-urban surfaces. For the Netherlands, roughness contours may be obtained through processing the LGN3+ land-use map.

The microscale is at least of similar importance for the wind climate above urban surfaces, but since many non-linear effects prevail, direct use of WAsP is dissuaded. Instead, assessing the urban wind climate involves at least consideration of the type of flow likely to be present (isolated roughness, wake interference or skimming), and the minimal height above which the average surface stress caused by urban obstacles becomes constant with height: the roughness sublayer - inertial sublayer interface. As a first approximation, the WAsP prediction may be extended by inclusion of a zero-plane displacement height (z_d), for instance by artificially raising the local orography.

The average obstacle height, plan area density and frontal area density are descriptive urban surface parameters that may be obtained by analysis of the local DEM. They can be related to the urban roughness length (z_0) and the zero-plane displacement height through different formulas, among which equation 2.10 and equation 2.12 are most simple in tunable parameters and are said to give good results for staggered and in-line arrays of cubes.

Finally, an assessment of effects of the building scale should also be performed. In some situations, wind shelters can be identified in the direct surroundings of a rooftop. When these are identified, their approximate effect on the wind speed can be assessed by empirical formulas that take as input the obstacle's porosity, its dimensions and the distance to the site. At last, it is worth considering zones of increased turbulence and zones of acceleration which are present above a roof. Until now, such a consideration is most practically based on a comparison with results from existing CFD studies or rules of thumb, such as those recently developed by Blackmore [10] and Mertens [37].

2.4.1 Positioning this project

This project is a follow-up of the project by F. Yemer [62], in which an artificial orography was used in WAsP to model the flow displacement over an urban surface. The current objective is to obtain a stronger foundation for the use of WAsP in urban terrain for urban rooftop wind climate prediction in the Rotterdam-Delft-Zoetermeer region. The central hypothesis is that the readily available AHN height data can be successfully be used for this purpose.

We limit the scope of this project to roofs that are located in the inertial sublayer, as this chapter shows, the wind climate in the roughness sublayer below it is difficult to predict and the research efforts in this layer are primarily limited to spatially and time-averaged velocities (see for instance [46, 43]) or to CFD simulations of idealized city models that mostly lead to qualitative conclusions about wind behavior in actual urban areas (see for instance [26, 15]). A spatially-averaged roughness sublayer wind climate is of almost no use for the UWT industry, since UWTs are small machines that derive their performance not from the spatially-averaged but from the direct local conditions at the rotor.

As a result of our project scoping, it needs to be clear under what circumstances the rooftop wind climate may be determined through a wind atlas method, and under what circumstances it may not and more thorough site assessment is required.

Chapter 3

Towards a new methodology

In the previous chapter, we have discussed some general methodologies for determining wind resources in an urban environment. Among other things, it appeared that a correct microscale consideration is important, and that there are difficulties on several levels to integrate the complex urban shape in a micro scale model like WAsP. This chapter is dedicated to presenting three new attempts to combine urban surface data with the wind atlas application program WAsP.

3.1 Three strategies

Based on the literature presented in the previous chapter, we come to define three possible extensions or strategies of combining the urban surface data in the current WAsP framework:

1. Inclusion of a zero-plane displacement height z_d, obtained by equation 2.10, included as a post-processing step to a WAsP prediction.

    (a) Omni-directional (similar for all directions)
    (b) Sectoral

2. Calculating the urban frontal area density λ_f per sector, and attempt to define and apply a wind speed correction factor based on this density.

3. Application of the effective microscale urban roughness z_0, obtained by equation 2.11 per sector, directly in WAsP instead of the land-use LGN3+ roughness.

The first part of this chapter is dedicated to an extensive overview of dealing with digital elevation model and extracting the parameters that are required for the extensions. The second part of this chapter is focused on the use of WAsP and the implementation of the three extensions given above. The chapter is finalized by some conclusions and notes regarding the necessity to calibrate the methods to a real urban wind climate.

3.2 Using the Digital Elevation Model

The digital elevation model available to us consists of a set of 5 km by 6.25 km laser altimetry datafiles. They were created around 2001 as part of the Actual Height of the Netherlands project (AHN1). The full dataset theoretically available covers the entire country with a horizontal resolution of 1x1 m. The heights are stored in centimeters and are relative to the Amsterdam Ordnance Datum (NAP), a fixed vertical datum related to the sea level.

For practical reasons, it was decided that for this project a 5 m horizontal resolution was most appropriate. Figure 3.1 depicts an intensity image of a datafile used in the project.

Processing the digital height data was needed to extract the plan and frontal area density and the average obstacle height parameters. It was chosen to follow the image processing approach for this purpose, as it was distinguished from GIS-based approaches in a paper by C. Ratti et al.[42].
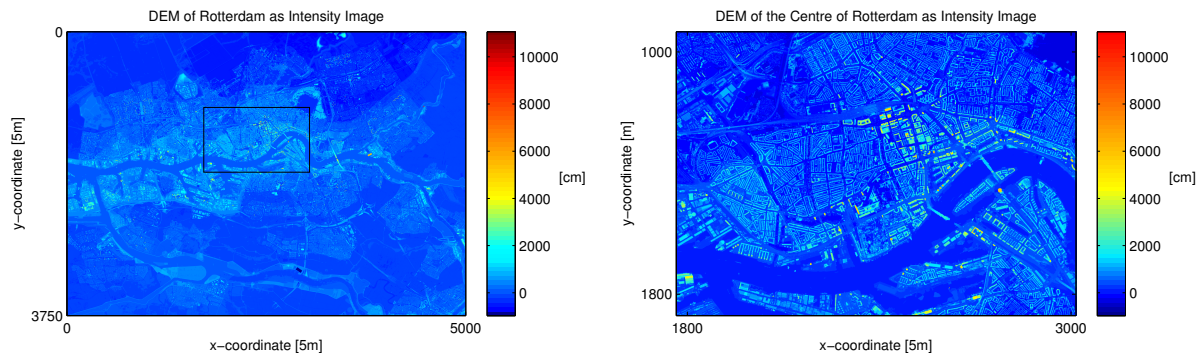
Figure 3.1: Digital Elevation Model as an intensity image: Rotterdam (left) and the center of Rotterdam (right)

3.2.1 Preparative steps and considerations

As a first preparative step, 15 or 20 data files are clustered to form new larger maps. Four of these large maps make up the complete region covering Rotterdam, Delft and Zoetermeer. Each large map overlaps another large map with one datafile; this is done because the filtering procedures fail near the borders of the maps due to border-effects; with this overlap these borders can be discarded.

The choice of dividing the region into four maps was made due to practical limitations in processing such large data. The complete region contains about 70 million data points (>1 GB) and, if it were processed at once, a very large RAM memory would be needed to store all this data. The maps currently chosen hold about 18 or 25 million data points (350 MB) and are considered to be a practical limit for most personal computers.

3.2.1.1 Ground and obstacle separation

Because we are interested in the parameters related to surface *obstacles*, we need to somehow separate the obstacles from the surface ground level which is more gradually evolving. A background removal procedure often applied in image processing is morphological opening[1]. Morphological opening is a procedure involving two non-linear filters that are applied to the image one after each other; the erosion filter and the dilation filter. The erosion filter generates an eroded version of the source image. Erosion can be defined by the following rule:

> In the eroded image, every cell has a value that is the minimum of all the cells that are neighbors of this cell in the original image

The dilation filter does the opposite:

> In the dilated image, every cell has a value that is the maximum of all the cells that are neighbors of this cell in the original image

The process of erosion and dilation is visualized in figure 3.2. The most top graph represents a cut-through view of a Digital Elevation Model (DEM) with a hill on which obstacles are located. By performing an erosion (one-dimensional in this case) a line is obtained which approaches the original hill now without the obstacles. The structuring element that defines the neighborhood is given by the red line and has a length larger than the obstacle; all features with a length smaller than this element are removed. The middle graph shows the result of the original DEM minus the eroded DEM. Indeed, almost only the obstacles are

---

[1]See for a step-by-step introduction *example 2* in the MATLAB image processing documentation, published on-line by Mathworks at: `http://www.mathworks.com/help/toolbox/images/f0-8778.html#f0-17842`
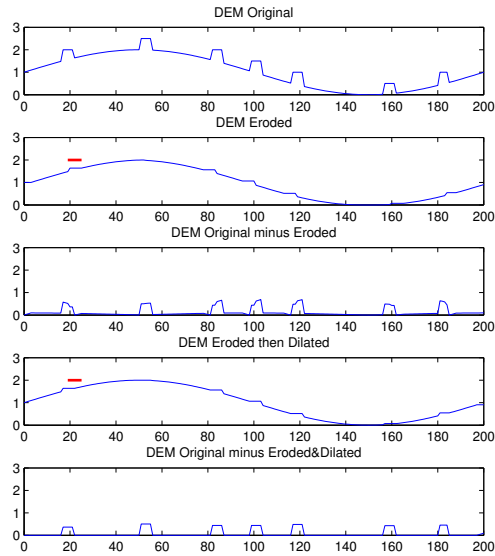
Figure 3.2: One-dimensional example of the erosion and dilation procedure that is used to separate obstacles from slowly varying ground level elevation. The red line (at x=20) represents the structuring element or neighborhood in the dilation and erosion procedure.

present, but their roofs are distorted and show to be affected by the local slope of the hill. The lowest two graphs show that the result can be improved by applying a dilation filter after the erosion filter, using the same structuring element.

The size or radius of the neighborhood should be used to fine-tune the background filtering for the present purpose. For small disk-shaped neighborhoods (smaller than typical roof areas), image erosion fails and the houses are not separated from the ground level. The minimum disk size is hence determined by the maximum size of obstacles that should be filtered out. On the other hand, very large disk sizes have the problem that they start to erode away landscape features. It was found that by using a disk with a radius of 10 cells (50 m.) in the erosion and dilation procedure, practically all obstacles could be separated from the ground level and typical structures in the ground level (dikes, small hills) could be preserved well (figure 3.3 left). Two grids can be derived from the original map; a ground elevation level grid and an obstacle height grid (denoted by h in the coming steps).

The surface analysis may now be proceeded by an omni-directional parameterization or sectoral parameterization. Section 3.2.2 and 3.2.3 will present both approaches seperately.

3.2.2 Omni-directional parameterization

A ground level-filtered DEM in grid format is the starting point for this analysis. A sequence of steps is executed to obtain the right result: (1) thresholding, (2) determining plan area density, (3) determining average obstacle height, (4) determining zero-plane displacement height.

3.2.2.1 Thresholding

A thresholding procedure is performed to the obstacle height grid to generate the threshold grid (denoted by t). Cells in the threshold grid are dependent on corresponding cells in the obstacle height grid and the
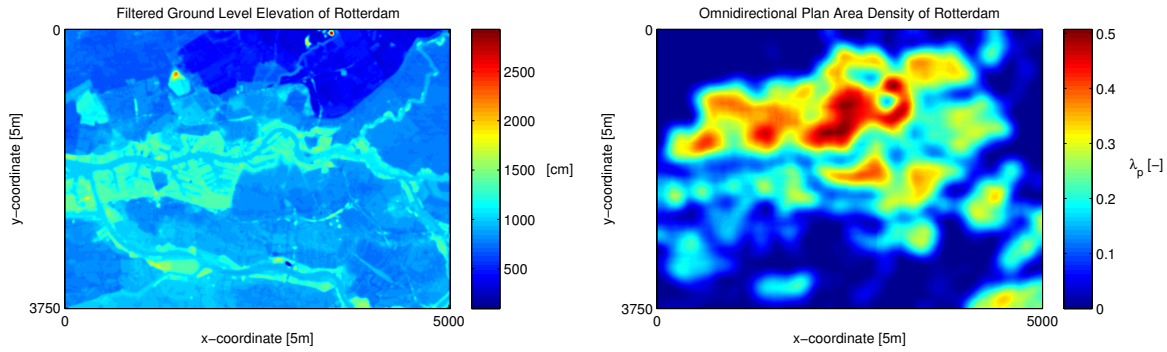
Figure 3.3: Left: Filtered ground elevation level grid through erosion and dilation processes. Heights have been raised by 10m to avoid negative values. It can be seen that the diked marshes (top) have a lower elevation than the built-up areas, roads and rivers. Right: Map of the plan area density λ_p obtained through filtering the threshold map with a 2D isotropic Gaussian filter.

threshold value:

$$t_i = \begin{cases} 0 & \text{if } h_i < h_{threshold} \\ 1 & \text{if } h_i \geq h_{threshold} \end{cases}$$

The tuning parameter here is the threshold value. It is related to the minimum height of what should be considered an obstacle. Visually and with the help of Google Maps it was checked at which threshold value an acceptable building plan overview could be recreated. It appeared that setting the value at 3.5 m. resulted in best recognizable pattern of obstacle plans.

The threshold grid shows clusters of cells with value 1, mostly rectangular, which can readily be identified as buildings. In between these structured shapes there are noisy clusters which are identified as vegetation. Some of the vegetation occurs in very small clusters (single trees) and can hence be distinguished from buildings simply by size. So, it was chosen to filter all clusters in the threshold by a minimum size criterion of 5 cells (125 m^2). Still, vegetation remains to cause noise in the threshold grid in cases of multiple trees located close to each other. To this point it appears that it could not automatically removed from the DEM.

3.2.2.2 Determining the plan area density grid

The plan area density of the map is obtained by a linear convolution procedure applied on the threshold map. In image processing, a linear convolution procedure is a simple filtering procedure that involves a source map and a filter kernel. Both are represented as matrices. The source map in this case is the threshold map obtained from the previous step, the filtering kernel is a user-defined matrix that can be tailored to a specific operation. For example, a 3x3 kernel with the value $\frac{1}{9}$ in every cell acts as a simple 3x3 averaging filter which smoothens the image or grid, other kernels can achieve other operations.

The plan area density is a neighborhood-averaged parameter, that can be obtained by summarizing the cells in the threshold map that are part of the build-up area for a certain region divided by the total number of cells in this region. Therefore, an averaging filter can be used for this purpose. It is initially decided to use a filter kernel with the following characteristics:

- 200 x 200 cells (600x600m)

- 2D Gaussian distribution of weighing factors having a standard deviation of 50 cells (250m)

- Isotropic (approximation)
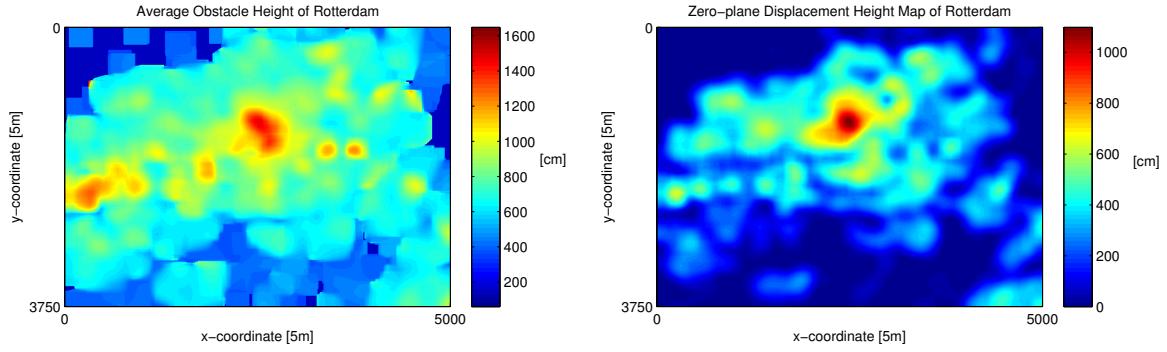
Figure 3.4: Left: Average obstacle height map. Notice the 'unsatisfactory' effects at the urban-rural border, where only very few buildings are included in the averaging. Right: Displacement height map as was generated by combination of the plan area density map and the average obstacle height map. Values appear to be in range of those proposed by Grimmond and Oke (table 2.1). The zero-plane displacement map for the entire area is given in Appendix C.

Filter isotropy implies it is rotationally symmetrical; this fits the current omni-directional analysis. In the simple 2D Gaussian filter, the standard deviation of the distribution acts as a distance constant. It is related to the relative importance of nearby surface features versus features that are further away. The choice of 250m currently is an arbitrary choice and will be fine-tuned later on. The result of this filtering procedure for Rotterdam is given in Figure 3.3.

3.2.2.3   Determining the average obstacle height grid

Intuitively, one would define the local average obstacle height as:

$$\overline{H} = \frac{1}{N} \sum_{j=1}^{N} H_j \tag{3.1}$$

With N the number of obstacles over the area and H_j the height of obstacle j above ground level. For the current DEM, this definition introduces the following two problems: (1) A single obstacle can have several heights, so H_j is not always clearly defined, (2) it is difficult to count or distinguish one obstacle from another. Furthermore, the above definition is counter-intuitive for situations where obstacles have varying plan areas; an obstacle with a very large plan area has the same effect on the average obstacle height as a very small obstacle.

It is therefore decided to use a slightly different definition for the local average obstacle height. Individual cells instead of individual obstacles are averaged over a region. This leads to an approximation of the average obstacle height. In a formula form this can be presented as:

$$\overline{h} = \frac{1}{\lambda_p n} \sum_{i=1}^{n} t_i h_i \tag{3.2}$$

Where n is the total number of cells over which is averaged, t_i is a logical cell from the threshold map and specifies whether cell i is built-up ($t_i = 1$) or non built-up ($t_i = 0$) terrain and h_i is the value in cell i. λ_p is the local plan area density and when multiplied with n yields the local total built-up area –number of cells– of the region. With a non-zero plan area density this definition works.

The spatial summation that is needed for this procedure is implemented with the same filtering kernel as the previous step.

3.2.2.4   Determining the displacement height grid

The zero-plane displacement height is determined from the parameter grids that were prepared in the previous steps. It was chosen to apply equation 2.10 for similar-sized cubical obstacles, recalling from Chapter 2:

$$\frac{z_d}{H} = 1 + \alpha^{-\lambda_p}(\lambda_p - 1) \tag{3.3}$$

The assumption is made that H can be replaced by the average height obtained in from the image analysis, $\bar{h}$, given that the variation in height is not too large. This could in theory be checked by the DEM but is not currently pursued. Figure 3.4 gives the displacement height as it was obtained from Rotterdam.

3.2.3   Sectoral parameterization

While the omni-directional approach is attractively easy, it is essentially incorrect because the important characteristics of the (urban) surface are always located upstream of –instead of around– a location of interest. Furthermore, the frontal area density could not be determined in an omni-directional analysis because it is directionally dependent. Hence, we pursue to analyze the same DEM, but now using a directional parameterization procedure.

While in literature several studies are found that apply a frontal area density calculation (see for instance [61, 33, 46]), no specific software was found to perform these kinds of calculations in this project. Therefore, continuation on this track required writing a tailored module to perform this calculation. This section describes the calculation methodology.

A consequence of the sectoral approach appeared to be that parameters can hardly be found for the entire area under consideration, without saddling ourselves with an enormous computational task. In absence of a better computer or more efficient algorithm, sectoral parameterization should hence be considered as a selective process to be executed once an initial selection of sites is known.

3.2.3.1   Determining the sectoral frontal area density

Building facades directly opposing the wind direction are often the most important sources of turbulence in the flow in the urban surface layer. The frontal area density parameter quantifies the amount of flow-obstructing surfaces A_F per unit ground area A_T, dependent on the flow direction. Recalling the definition equation 2.9 from 2:

$$\lambda_f = \frac{A_F}{A_T} \tag{3.4}$$

The frontal area density can be approximated by analyzing surface cross sections emitting from the point of interest at different azimuths. To illustrate the method, we chose to analyze 12 cross section lines, each being representative for a 30 degrees azimuthal window. A fictional DEM is used to test the analysis (figure 3.5). This fictional DEM is constructed of repeated patches of 100 x 100 meters, each with a 35 x 35 x 35 m obstacle located in the middle. It hence has a known frontal area density of 0.1225 for wind parallel to the x- or y-axis.

Twelve cross sectional height profiles are extracted, in different directions, with a shared origin and a length of 750m (figure 3.6). The frontal areal density for every sector is now approximated by analyzing these height profiles. This approximation involves three steps per height profile: (1) height difference transformation, (2) multiplication with a distance weighing function, (3) summarizing over total length.

The height difference transformation step involves the application of a simple difference function to the discrete cross section line h, where i refers to the cell number, which is zero at the origin and increases with distance from the origin:

$$d_i = h_i - h_{i+1} \tag{3.5}$$
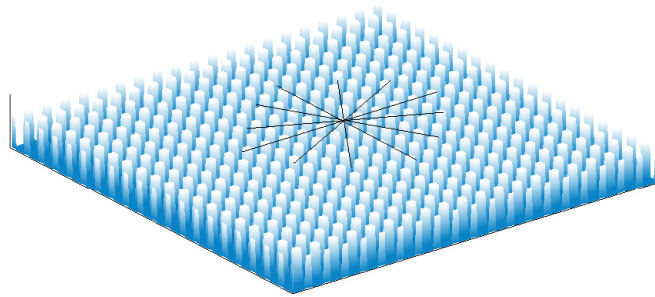
Figure 3.5: Fictional DEM to test the frontal area density analysis
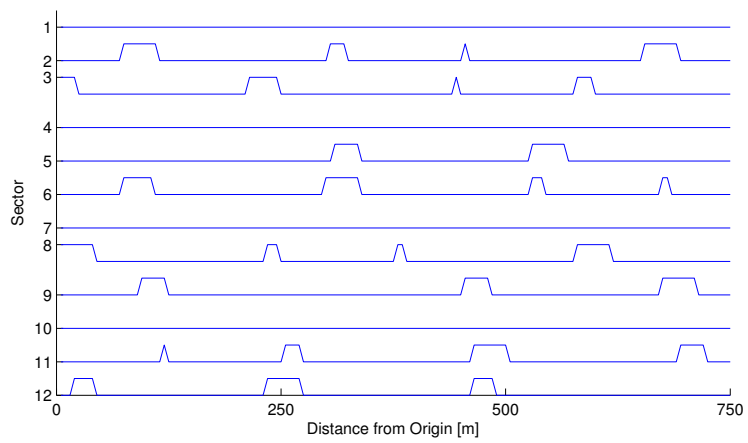
Figure 3.6: Extracted height profiles from the fictional DEM
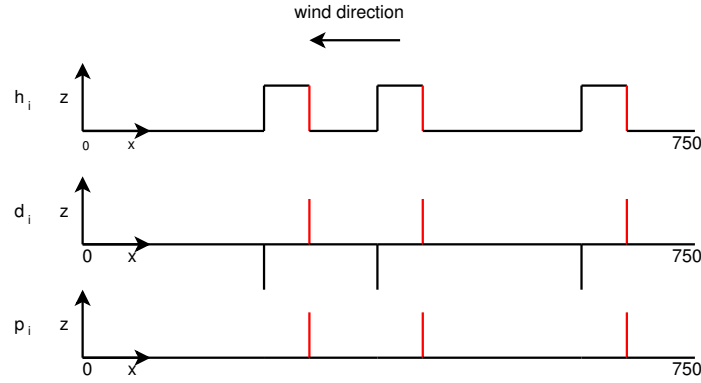
Figure 3.7: Conceptual overview of h_i, d_i and p_i in the frontal area density calculation for a fictional line of 750 length holding three obstacles.

This step is conceptualized by the top and middle graph in figure 3.7. Positive cells in d are now related to height decreases (seen from the origin) while negative cells are related to height increases. The frontal area density for wind blowing towards the origin is logically given by height decreases seen from the origin. All negative cells of d are hence made zero:

$$p_i = \begin{cases} d_i & \text{if } d_i > 0 \\ 0 & \text{if } d_i < 0 \end{cases}$$

To anticipate on the fact that a nearby frontal surface has a larger effect on the wind conditions at the origin than a surface further away, the peaks are multiplied with a distance weighing function (figure 3.8). A literature-based choice is made for an exponential weighing function characterized by a single distance constant D. The choice was based on considerations of the footprint model developed by Verkaik ([53], see also section 2.2.1.3).

$$W(x, D) = \frac{1}{D} \exp(-x/D) \tag{3.6}$$

A normalization of $\frac{1}{D}$ is applied to make the integral equal to 1. Verkaik found that a distance constant of 600m was appropriate for a footprint model at 10 m measurement height. Because the application in this project will generally be for other heights, finding a tailored distance constant is important and will hence be treated in the calibration phase (Chapter 4).

The weighing function is discretized over the length of the cross section line, leading to W_i. The frontal area density of a single line is now given by the summation:

$$(\lambda_f)_{line} = \sum W_i p_i \tag{3.7}$$

It appears quickly that the method is very rudimentary since the height profile analysis may just hit or miss obstacles, leading to much variation among sectors and positions. For the obstacles in the fictional DEM, this variation occurs on the scale of individual buildings and repeats itself. Because the frontal area density is in principle a neighborhood parameter, an averaging procedure may be performed over a relatively small scale to mitigate these unwanted fluctuations. For the fictional DEM, averaging over an area at least 100x100 m (repeating distance) is sufficient, yielding a frontal area density of 0.1213 for flow parallel to the x or y axis, only a percent different from the real known value. For wind at a 30 degrees angle, the frontal areal density is slightly higher: 0.1570, also close to the real value.
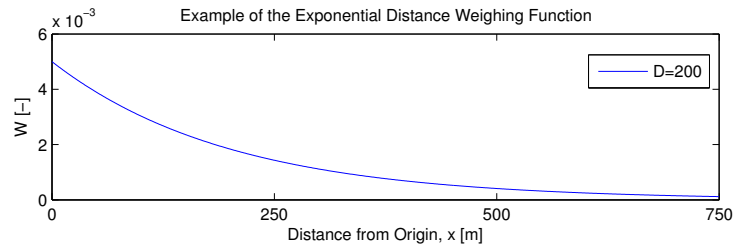
Figure 3.8: The exponential distance weighing function, here with a distance constant of 200m.
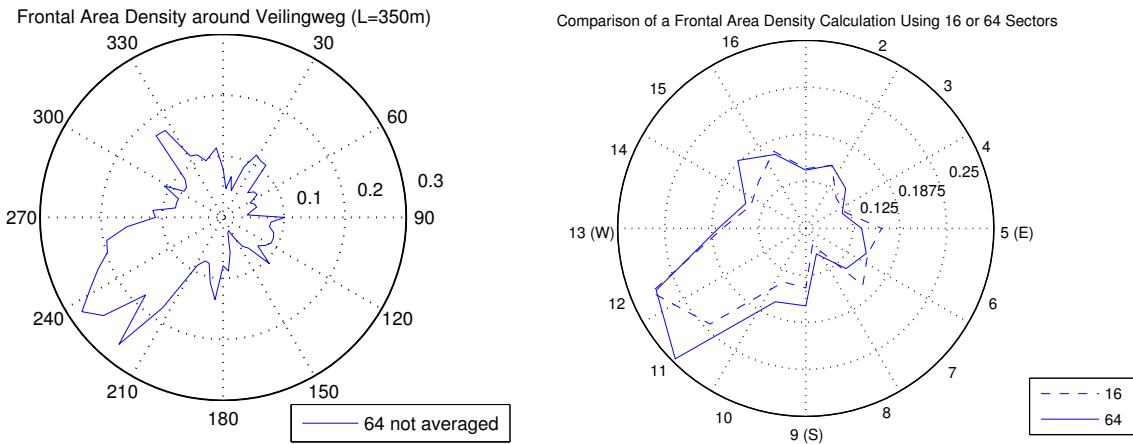
Figure 3.9: Left: Frontal areal density calculation of the Veilingweg in Rotterdam using 64 lines. Right: Difference between the use of 16 or 64 lines averaged to 16

3.2.3.2 Final modifications to the method

Further modifications were made based on tests at real urban surfaces:

- The use of 64 instead of 12 or 16 directional lines

- Finding solution for 11x11 cells (55x55 m^2) around a roof and averaging

- Shifting the weighing function 10 cells to the right, padding with zeros, to avoid effects of the building itself on the solution

The effect of using 64 instead of 16 lines was tested on a real urban DEM at the Veilingweg Rotterdam (figure 3.9). More lines means that the surface is analyzed more thoroughly. It was found that significant changes occur when analyzing 64 lines and then averaging back to 16 lines as compared to only analyzing 16 lines. Therefore it was decided to use 64 lines. To transform the solution from 64 to 16 sectors we decided to use a small weighted-averaging kernel: $\{0.15, 0.2, 0.3, 0.2, 0.15\}$, based on the idea of Verkaik [53].

No further modifications to the calculation method were tested because it was felt that doing so would be very time-consuming and would deviate too much from the main objective of this project.

The plan area density, average obstacle height, and displacement height are also determined per sector, using the height profile analysis and the same assumptions as in the omni-directional approach (threshold height at 3.5 m).

3.3 Using WAsP

WAsP is used to perform a wind atlas calculation for the region. It integrates the terrain classification, surface orography and observed wind climate in order to find wind climates at any height within the domain of the map. We chose a rectangular domain that widely covers Delft, Rotterdam and Zoetermeer and other nearby towns.

3.3.1 Roughness map input

Traditionally, WAsP roughness inputs are based on land-use data. The Royal Dutch Meteorological Office published a computer program that can generate roughness contour lines based on the LGN3+ land-use database. This program was developed under the Dutch Wind Atlas project. Appendix F gives an overview of the roughness classes used. Figure 3.10 gives an screen-shot of the roughness contours of Rotterdam.
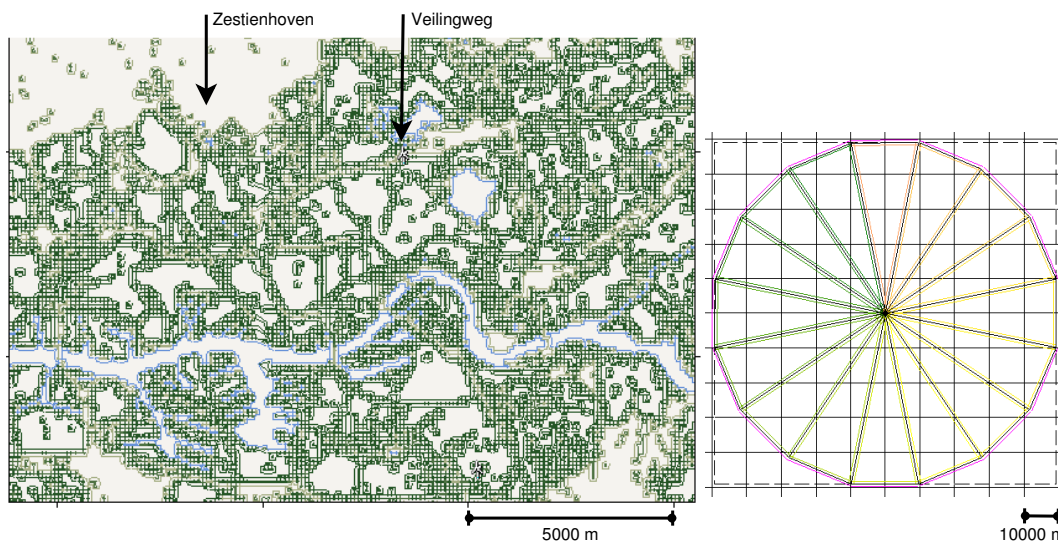
Figure 3.10: Left: Traditional Roughness map of Rotterdam based on LGN3+ land-use. The blue contours are assigned to water. Seven different roughness values are assigned by the green contours, differences are not visible in this map. Right: Roughness 'wheel' used in this project to directly manipulate the effective sectoral roughness length used in WAsP

3.3.2 Direct effective roughness input

The map editor of WAsP also allows the user to directly draw and specify roughness contours in a manual process. In absence of a detailed land-use database, this can be used to manually digitize existent maps or areal photographs of the surroundings.

For the current project, we also like to be able to directly manipulate the effective roughness per sector (extension 3). This cannot directly be done in WAsP. Hence, as a workaround, we have created a tailored roughness line structure, enabling direct dictation of the effective roughness used in WAsP per sector. The structure is shaped like a wheel of 50 km radius, with 16 spokes dividing sectoral roughness source areas of 22.5 degrees wide (figure 3.10 right). The spoke division is exactly equal to the sector division in the reference wind climate of Zestienhoven.

A wind generator positioned in the exact center of the wheel experiences far-extending homogeneous roughness within every direction, without any local roughness speed-ups, speed-downs or transitions that

36

are normally present in a land-use map. The wheel simply acts as a direct roughness input and is therefore a suitable tool to test extension 3.

3.3.2.1 Difference between a direct roughness input in WAsP and the blending height approach

The direct roughness input by-passes the roughness change model of WAsP since it defines a single homogeneous roughness for each sector. One may question why WAsP is still is to be used under these simple conditions, since in theory one could also consider using the blending height approach (which was presented in section 2.2.1.2) to derive logarithmic profiles from a single observation at 10m.

In fact, the question rises whether the invisible internal model of WAsP does actually perform a different calculation than the blending height model proposes, in case that we only provide WAsP with a single homogeneous roughness per sector. To test this, we define four wheel shaped roughness structures having the following values for z_0: $\{0.03, 0.1, 0.4, 1.5\}$ and find a wind speed prediction for distinct steps in height between 10 to 500m. We use a single observation at 10 m height and a roughness length of 0.03 as a wind speed input for WAsP. The results of the simulations are given in figure 3.11.

The figure clarifies a number of things. First of all, the resulting profiles are not completely logarithmic over the entire domain. They approximately follow a logarithmic profile, but a gradual kink seems to occur around 100m. Second, the development of the profile steepness $\left(\frac{\mathrm{d}u}{\mathrm{d}y}\right)$ is almost identical for all roughness values considered. Still assuming a logarithmic form, this steepness can be expressed as the derivative of the log law: $\frac{\mathrm{d}u}{\mathrm{d}y} = \frac{u_*}{kz}$, implying that WAsP uses something like an equal friction velocity (u_*) to translate one logarithmic profile to another profile. As a result of this assumption, the profiles never cross, indicating the fundamental incompatibility with the blending height approach.

Concluding, there are fundamental differences in the assumptions between the two approaches. The kinked profile predicted by WAsP is not well understood. At the same time, it is acknowledged that WAsP has proven its power in industry and research, also under various stability conditions. This leads to a natural preference over the roughness method employed within WAsP. Hence, in the remainder of this project, to directly manipulate the effective roughness per sector we remain to prefer WAsP in combination with the tailored roughness structure over the blending height approach.
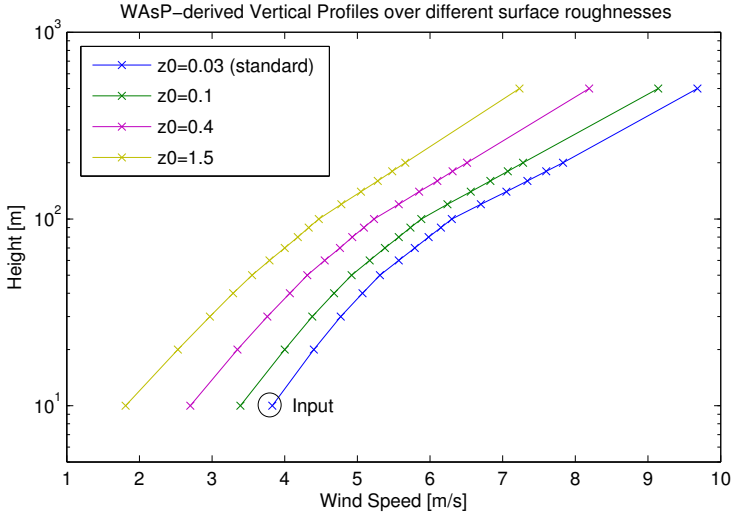
Figure 3.11: Log-plot of wind profiles using the same wind atlas (mesoscale climate) in WAsP. The circle indicates the input observed wind speed, from which WAsP derives all the other points.

3.3.3 Orographic input

A ground level elevation map of the area is obtained from the DEM by the erosion-dilation process. The surface is lightly smoothened using a Gaussian filter of 20x20m to minimize speed-up effects due to very abrupt transitions. Contours with a vertical resolution of 1m are calculated from the grid file by using the computer application SURFER[2].

Since the ground level evolves very smoothly in the Netherlands, minor wind speed effects are expected. Yet, since the maps are readily available, they are still included in the current project.

3.3.3.1 The effect of surface orography

The use of ground level surface orography, being essentially flat, is an important deviation from the previous study at developing a wind atlas for this region [62] in which a highly variable artificial surface was used. In our application, the surface is not used to directly model a displacement height. The choice was made on the basis of some small tests aimed at the effect of surface orography on the predicted wind profile in WAsP.

In the tests, two simplified hill models are imported as surface orography in WAsP. The first reflects a smooth step function, in which the elevation first remains constant, then gradually increases until a final value is obtained. The second reflects a smooth pulse, a quick increase followed by a decrease. The maximum slope steepness is in both cases 20%.

The surfaces are made constant in y-direction. The reference wind climate is constructed to have a wind rose with a 100% frequency in the positive x-direction, to force WAsP to only consider winds flowing over the hills. A constant roughness is used for the entire domain.
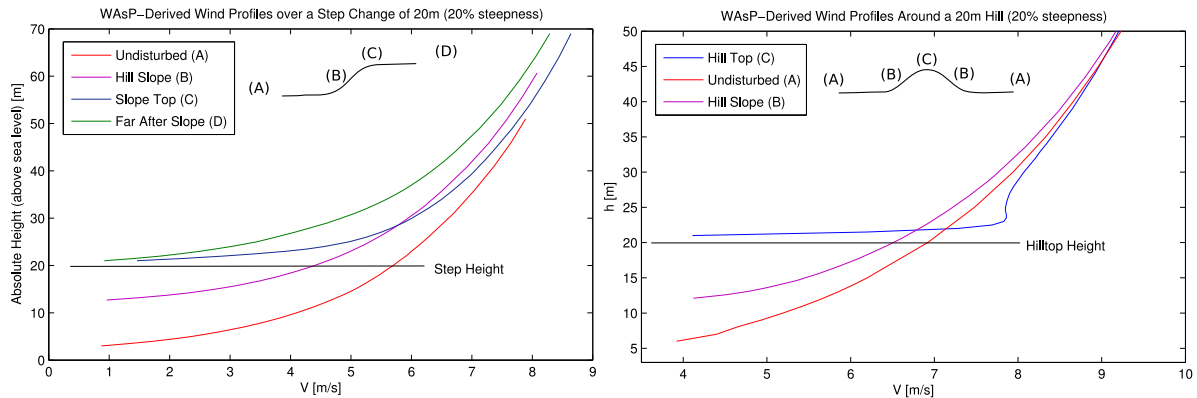
Figure 3.12: Wind profiles over a smooth step in height (left) and over a smooth hill (right) modeled in WAsP. Figures are meant to illustrate different effects a hill has on WAsP profiles.

We let WAsP predict wind speeds at different heights and different locations; before the hill, at the slope and at the top. The obtained wind speed profiles are plotted with respect to their absolute height (figure 3.12), hence they can be seen as profiles reacting to an artificial surface that models the displacement height for a flat urban area. The green line in the left figure is the profile far after the step, this profile is equal to the undisturbed profile but it is shifted upwards by 20 m. Again on the left, the blue line reflects the wind profile just at the slope top. Here two effects are present: the original profile is shifted upwards by 20 m, but this is partially counteracted by a speedup due to the vicinity to the slope.

A similar effect is observed on the right side of figure 3.12. Since this is a short hill instead of a step, no new log-profile can develop, but the speedup at the hill top is clearly visible. This speedup is maximum

---

[2]see: http://www.goldensoftware.com/

just a few meters above the hill, but even at h=40, WAsP predicts higher wind speeds above the hill than far away from the hill.

3.3.4 Wind climate input

KNMI station Zestienhoven was found to be the most appropriate weather station to use in the current project, due to its vicinity to Delft, Zoetermeer and Rotterdam. Hourly potential wind speeds over the period 1981-2011 were selected and binned into 16 directional sectors [31]. 16 directional bins was the best choice considering that the urban wind climate at the calibration location is only available in this format.

The potential wind speeds are exposure and roughness-corrected wind speeds to represent a 10 m measurement height and a WMO standard roughness length of 0.03 m. Roughness and height correction is typically performed by the blending height method (figure 2.3 in Chapter 2). The reference site can be freely positioned in WAsP. It is however important to define the surroundings of the reference site to have a standard roughness length of 0.03 m. This is ensured by manually digitizing the roughness lines around Zestienhoven.
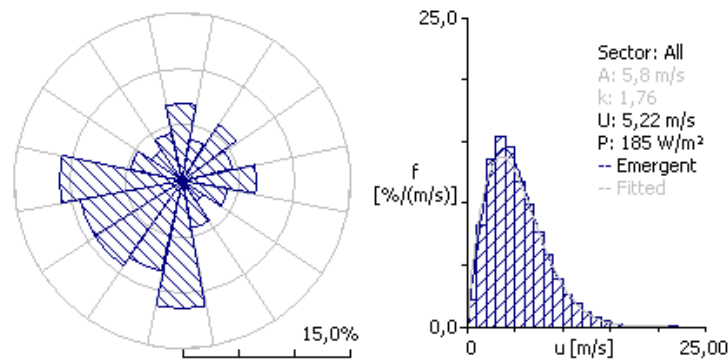
Figure 3.13: Observed wind climate of KNMI station Zestienhoven (1981 to 2011) binned in 16 directional sectors

3.3.5 Wind climate outputs

The output wind climate in WAsP is available in many different formats. Among them are Weibull scale and shape factors, power density and mean wind speed. Regarding the current project, a focus will be on the mean wind speeds exported by WAsP. When referring to the mean wind speed of a WAsP output, a distinction should be made between two definitions frequently used:

Mean wind speed (U) The mean of a fitted Weibull distribution to all-sector wind speed histogram consistent of 10-minute data.

Sector J mean wind speed (U^J) The mean of a fitted distribution to wind speed histogram of binned data in directional sector J.

For the modelling in the subsequent chapters, the sectoral mean wind speeds is most often used.

To produce a set of reference maps, we let WAsP predict the wind climate for 100x100 m grid cells covering the entire area, at heights 10,20,30 and 50 m above ground level. The output including sectoral mean wind speeds, power densities, etc. is stored in a WAsP project file, for later referencing. Appendix C shows contour maps of the mean wind speeds at 10 to 50m height.

3.4 Implementations

Attention was given to the practical implementation of extension 1a, 1b, 2 and 3, so that it could be used on a large scale in real projects. Now follows a conceptual overview of practice for each of the extensions.

For extension 1a, the inclusion of an omni-directional zero-plane displacement height, displacement height maps have been prepared in digital and printed format for the entire area under consideration (see Appendix C). The building height H is reduced to the effective building height $H - z_d$, which can then directly be inserted as the turbine height in WAsP. Running WAsP now yields an omni-directional displacement height corrected wind climate.

For extension 1b, a MATLAB module (*getparam64.m*) needs to be executed to calculate surface parameters around the site. For this, one needs to specify the exact coordinates in 5m precision, the size of the averaging area and the spatial weighing function distance constant (equation 3.6). The resultant zero-plane displacement height now varies with direction, as well as the effective building height $H - z_d$, requiring 16 different runs in WAsP. It is questionable whether the increased effort is justified by a better result as compared to the omni-directional approach; this will be checked in the following chapter.

Extension 2 will be based on the output of the same MATLAB module. The resultant frontal area densities of the surroundings are included by applying a correction function $f(\lambda_f)$ on the WAsP sectoral mean wind speeds. The form of the correction function is not known, and will be established in the trail campaign.

Extension 3 is implemented by calculating z_0 values from surface parameters generated by the MATLAB module. The DEM derived roughness can be assigned to the wheel-shaped roughness structure (figure 3.10) through a small command-line interface that was written. This interface generates a .map file, which is then loaded in WAsP. After positioning a turbine on the center of the wheel, and assigning a reference wind climate, WAsP quickly calculates the wind climate. This last extension is presented in more detail in Appendix A.

3.5 Conclusion

This chapter gave a more detailed overview of the processing steps required to analyze the DEM and to use WAsP. Regarding the DEM analysis, a distinction was made between omni-directional and directional parameterizing. The former can be applied with simple image processing techniques which enable a solution to be found for the entire region. The latter is required to fully extract *all* surface parameters, including the frontal area density, but is computationally not optimized therefore limiting its use in practice to only a few spots.

It was found that ground level elevation could successfully be distinguished from building-like obstacles by a standard image processing step (erosion-dilation). This led to the creation of a DEM with just obstacles, no ground level elevation. By applying a minimum height criterion of 3.5 m (threshold), this obstacle DEM could be used to create a plan area image of the entire region. By applying a minimum plan area criterion of 125 m^2, individual or small groups of trees could be removed, leaving primarily buildings. Only large groups of trees, such as those in parks, could not be removed from the DEM.

The plan area image was then used as the input of a 2D Gaussian filter, which is equivalent to a spatial averaging procedure, leading to a plan area density image of the region. Initially, this was done with a filter size (standard deviation) of 100 m, but due to arbitrarity of this choice, a further calibration of this filter size is required. The average obstacle height grid was created by averaging the height of the cells that are part of the built-up area (given the minimum height criterion). This led to reasonable results, except when approaching the borders of urban areas. There, a decreasingly smaller number of obstacles caused unsatisfactory results in the averaging procedure.

A directional surface analysis was developed to extract average obstacle height, plan and frontal area density from the DEM. It was tested in a block-model with known morphometry to see whether the analysis worked. A good solution was found if sectoral analysis was performed over a larger area instead

of a single position, this led to some small modifications in the procedure, which can be implemented as a MATLAB module.

Small tests were performed to investigate the behavior of WAsP depending on surface elevation and roughness. It was indeed found that surface elevation can be used to represent a zero-plane displacement height. However, the similar effect can also be implemented as a post-process; simply substituting $(z - z_d)$ for z. The advantage of this is that unwanted speed-ups due to the surface elevation are minimized. Furthermore, the calculated resource grids become less ambiguous since they are now solved for a constant height *above ground level* instead of a varying height *above surface level*.

A new method has been developed and tested to directly dictate the effective surface roughness that WAsP should use per sector. This involves defining a wheel-shaped roughness structure with a single homogeneous roughness per sector, and can be used to implement the third extension; combining a DEM-derived effective roughness length with a mesoscale wind climate.

Now that the theoretical methods have been defined to apply the three extensions, it is necessary to test and calibrate each extension for a real case study. In the following chapter, these attempts will be described for the Veilingweg police station in Rotterdam.

Chapter 4

Trial and calibration

The building of the police station at the Veilingweg in Rotterdam has recently been the subject of an urban wind resource study. Data was gathered at the rooftop for a period of almost a full year, at three heights above roof: 3, 6 and 9 meters. The data was checked, processed and correlated to a long-term dataset as part of a previous masters project of F. Yemer [62].

The surroundings of the Veilingweg could be classified as small to medium urban height and density combined with natural surfaces. Buildings are located in all sectors around the Veilingweg. The main exceptions are a small lake located in sector 1 to 3 and a small park with dense trees located in sector 7 to 9. To the east (sector 4 to 7), we mainly find industrial buildings with a low height and large plan area, while in the other sectors could be considered as residential areas. Figure 4.1 depicts the land-use around the Veilingweg (a map indicating the position of the Veilingweg with respect to the entire Rotterdam-Zoetermeer-Delft region is given in Appendix D)
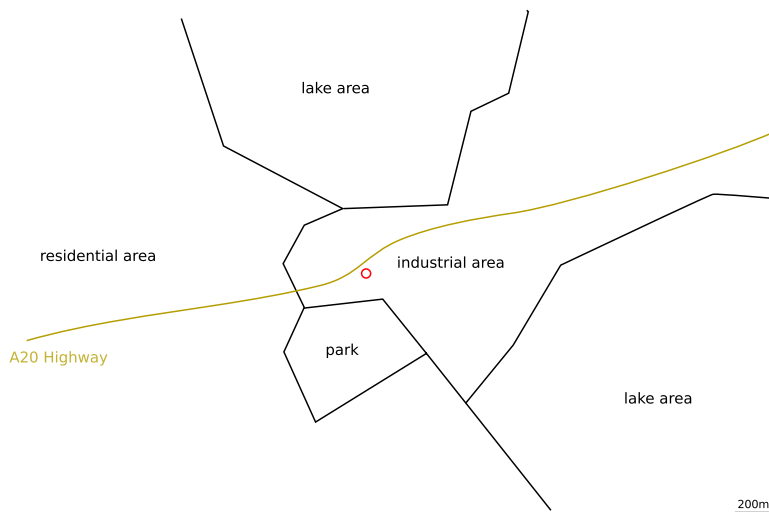
Figure 4.1: General surface coverage overview around the Veilingweg (indicated by the red dot)

The Veilingweg is one of the few urban rooftop sites with relatively reliable known rooftop wind climate in the region. Therefore, the site offers us a nice opportunity to test the three extensions developed so far. Most importantly, the question is which extension actually improves the prediction. Furthermore, we would like to see if the sectoral approach is to be preferred over the omni-directional approach, despite the increased effort. Regarding the distance weighing function, it is attempted to obtain some calibration material for the distance constant.
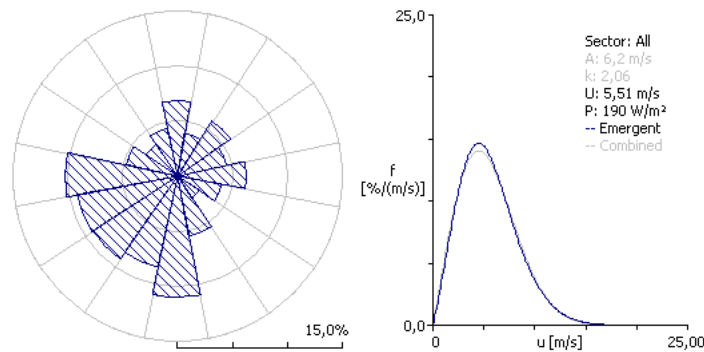
Figure 4.2: Predicted wind-rose and emergent wind speed frequency distribution. In the wind rose figure, sectors should be counted from the top, starting at 1 (N), increasing with clockwise direction. An earlier study indicated that there were no turning effects between the Veilingweg and Zestienhoven.

4.1 Direct WAsP prediction

As a first trial step, the WAsP output is taken at $H = 38$ m above ground level at the location of the Veilingweg using Zestienhoven as predictor with 30 years climate data. We will consider this prediction as the baseline prediction, since it is most straightforward. The 10-minute predicted mean wind speed is:

U_{wasp}:   5.51 m/s

The 10-minute observed mean wind speed at the Veilingweg is:

U_{obs}:   4.42 m/s

There is hence a 1.09 [m/s] over-prediction, which will be addressed later in more detail.

The predicted wind-rose and predicted omni-directional wind frequency distribution are given in figure 4.2. Sectors 9 to 13 can be considered as the prevailing sectors, which is a property of the general Dutch climate, also present in the Zestienhoven reference climate.

The long-term field study at the Veilingweg showed that the observed wind rose at the rooftop was almost identical to the predicted wind rose through WAsP ([62] page 63). Hence, the omni-directional error can not really be attributed to single sectors having a higher frequency than the reference climate (local turning effects). It therefore makes sense to distinguish between sectors and to investigate the sectoral means.

The deficiency of the direct WAsP prediction is most clearly noticed in figure 4.3, where the mean wind speed distribution is given for 16 directional sectors. The black line indicates the observed, long-term corrected mean wind speed, the blue line indicates the prediction as obtained through WAsP. The green line is also included as it illustrates the effect of a ΔRIX-correction made in a previous WAsP prediction for the Veilingweg [62].

Comparing the WAsP sector means to the observed means, it can be seen that the most problematic over-prediction occurs in sectors 10 through 16, from SSW to NNW. From an areal photograph, the impression is obtained that the most dense urban roughness is also located in these sectors, a point which is addressed in more detail further on.

The ΔRIX correction, made in the previous simulation, enhances the sector average mean wind speed of the WAsP prediction, although it should be noted that in this simulation artificial surface orography was also present. Furthermore, the WAsP ΔRIX line shows less resemblance in shape to the actual measurements than the WAsP line does. It seems that the ruggedness corrections are applied quite randomly and not in those sectors causing the vast majority of the over-prediction.
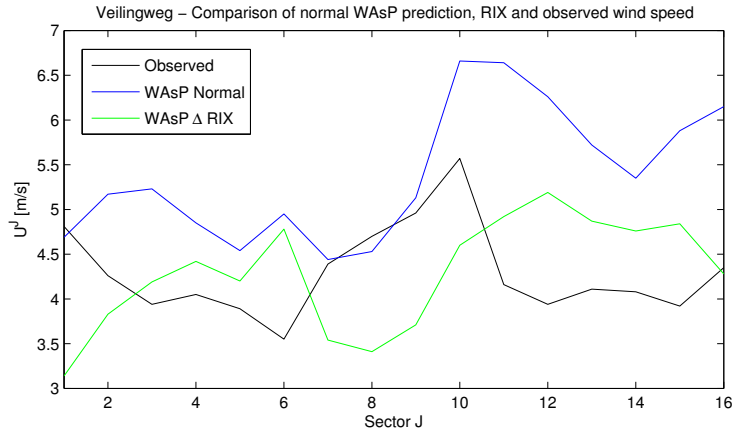
Figure 4.3: Comparison of the observed mean wind speed per sector (black) and predicted mean wind speeds, by running WAsP normally (blue) and by using an artificial surface that includes a ΔRIX correction based on slope steepness (green) as was performed in [62].

4.2 An omni-directional z_d correction

As a first extension, the effect of an omni-directional displacement height is tested. We apply the procedures presented in Chapter 3. The filter size is initially chosen to be 100 m, as rather coarse guess based on the some wind tunnel studies [28]. The filter size is then modified to see the effect on the zero-plane displacement height (table 4.1).

Table 4.1: Omni-directional surface parameters for the Veilingweg using different filter sizes.

Filter size σ [m]	$\bar{h}$	λ_p	z_d
100	8.0	0.41	5.4
200	7.3	0.38	4.8
300	7.1	0.37	4.5
400	7.1	0.37	4.5
500	7.1	0.37	4.5

The effect of the Veilingweg building itself on the surface parameters is reflected in diminishing parameter values with increasing filter size. The zero-plane displacement height settles on a value that is representative for the microscale: 4.5 m. Shifting the logarithmic profiles per sector by 4.5 m yields a WAsP prediction with omni-directional z_d correction (given by the dashed line in figure 4.4).
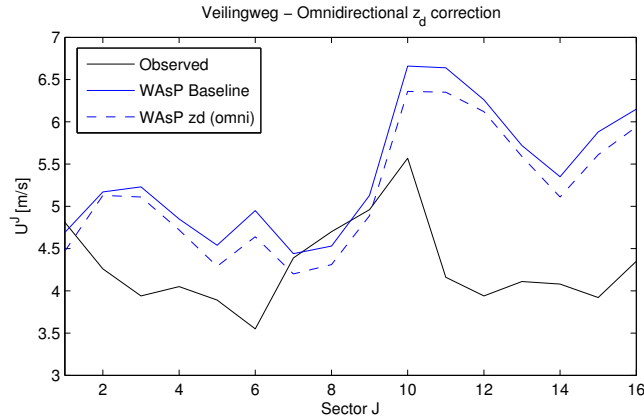
Figure 4.4: Effect of omni-directional zero-plane displacement height correction of 4.5m on the WAsP sectoral mean wind speed prediction.

4.3 A sectoral z_d correction

The sectoral zero-plane displacement height is determined from the sectoral plan area density and sectoral average obstacle height. This section test the effect of this extension in comparison to the omni-directional z_d correction.

4.3.1 Determining directional surface parameters

As a first step, we will investigate the sensitivity of the average obstacle height and the plan area density to the choice of the distance constant D in the weighing function 3.6, as we do not know the correct value for this constant. The original obstacle DEM is taken (no manual removal of vegetation) and the line analysis is performed for 10x10 grid points (50x50 m), centered on the Veilingweg. The weighing function is padded with 15 leading zeros (75m), to ensure we indeed calculate parameters of the *surroundings* without erroneously incorporating the height of the Veilingweg building *itself* in the parameters.

The lines in figure 4.5 show the average obstacle height for various distance constants. The average heights of most sectors fluctuates around 9 m or grows maximum 1 m with increasing D. Sector 11 to 13 indicate the largest increases if D is increased beyond 600 m.

It is peculiar that these results are almost 2 m different from the omni-directional average obstacle height calculated earlier. This raises questions about the correctness of the calculation methods. The true cause of this difference has not been identified.

The plan area density around the Veilingweg is given in figure 4.6. It indicates that this parameter averages around 0.3 with some exceedings towards 0.5 in the Southern sectors. Highest sensitivity with the distance constant is for the sectors around North.

The plan area density and average obstacle height combine through MacDonald's equation into the displacement height, yielding the lines in figure 4.7. On average, a distance constant of 400 m results in the lowest values, while a distance constant of 1000 m results in the highest values. Sector 6 to 10 vary less than 1 m between the different constants, other sectors may vary as much as 2.5 m (sector 2 and 3) or 4 m (sector 4).

The analysis is proceeded by looking at the sectoral distribution of z_d obtained, using a 400 m distance constant and using a 1000 m distance constant. Every profile is now shifted sector-wise by the corresponding displacement height value (figure 4.8). It becomes apparent that the sensitivity of U with
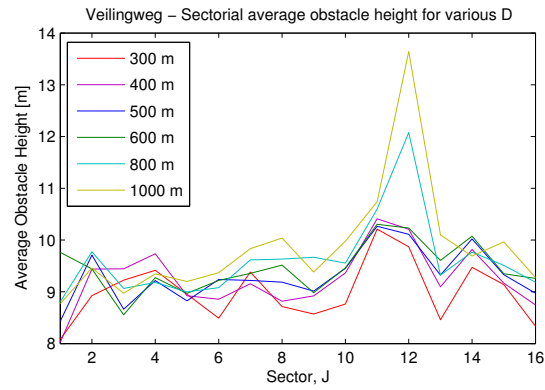
Figure 4.5: Effect of different distance constants on the average obstacle height parameter for the Veilingweg.
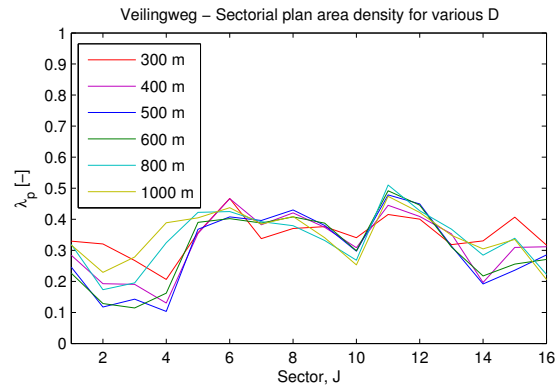
Figure 4.6: Effect of different distance constants on the plan area density parameter for the Veilingweg.
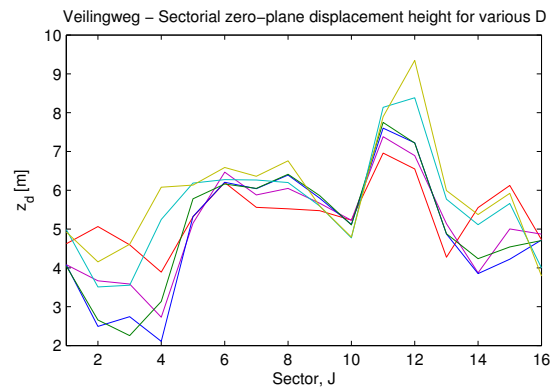
Figure 4.7: Effect of different distance constants on the sectoral zero-plane displacement height for the Veilingweg.

Table 4.2: Comparison of sector-averaged parameters using the two methods (length units in [m]).

Method	$\overline{h}$	λ_p	z_d
Omni-directional σ = 500 m	7.1	0.37	4.5
Sectoral D = 300 m	9.0	0.35	5.4
D = 400 m	9.3	0.32	5.1
D = 500 m	9.3	0.30	4.9
D = 600 m	9.5	0.31	5.0
D = 800 m	9.6	0.34	5.6
D = 1000 m	9.9	0.35	5.9
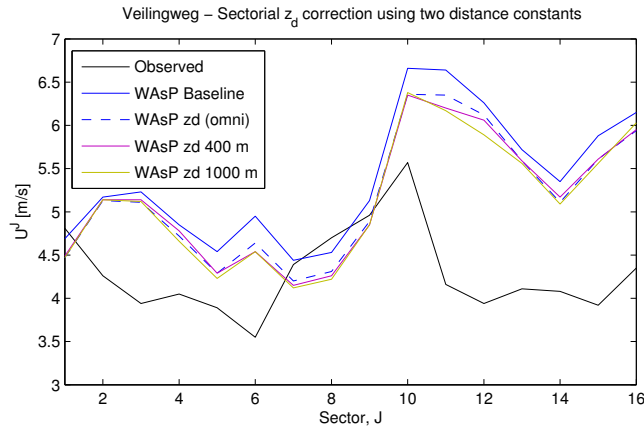
Figure 4.8: Effect of sectoral zero-plane displacement height correction on the WAsP prediction, indicating the low sensitivity of different filter sizes and surface calculation methods (omni-directional and sectoral).

respect to different filter sizes and surface calculation methods is very low. This is primarily caused by the log-profile of the wind, which becomes increasingly insensitive for steps in z with increasing height.

4.4 Inclusion of a sectoral λ_f correction

As a second extension, it is attempted to calculate the frontal area densities and transform those in a post-process correction factor for WAsP. Towards this end, the sectoral parameter is calculated, again using various distance constants.

The analysis is performed for the original DEM, that includes patches of dense vegetation and for a DEM with manually removed vegetation with buildings being the only source of frontal areas (figure 4.9 and 4.10, respectively). The latter is hence a better indicator of the surrounding *urban* morphology. In consideration to the different interaction of vegetation-like obstacles and building-like obstacles have with the wind (in terms of rigidity, porosity, seasonal influences) it is believed this distinction should be made. No effort was put in applying an automated procedure, because it was found that the horizontal resolution of the current DEM (5m) was likely to be insufficient (J.A. Berglund et al. [17] notes a resolution of at least 2 m is needed). Vegetation was also removed in consideration of MacDonald's equation, which was derived for bluff, non-porous building-like obstacles.

The bottom figure shows that for most distance constants, frontal area density due to urban obstacles peaks around sector 11 - 12. Sectors 1 to 8 are characterized by the lowest urban frontal area, around 0.1, while sectors 13 to 16 and 9 have a slightly higher frontal area density. There is increased variation with the distance constant in sectors 2 to 8, after removal of the vegetation.
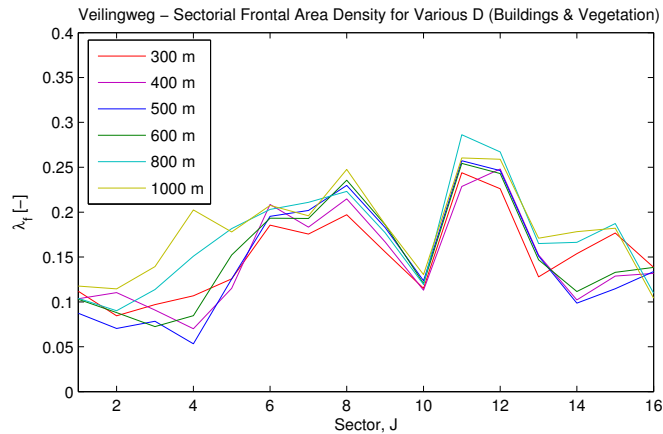
Figure 4.9: Effect of different distance constants on the sectoral frontal area density for the Veilingweg (buildings & vegetation).
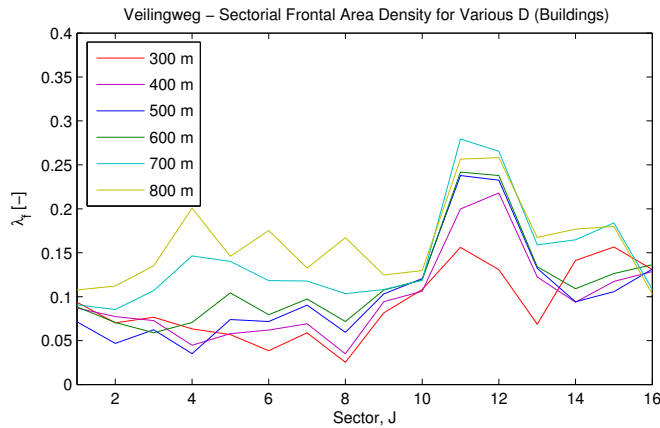
Figure 4.10: Effect of different distance constants on the sectoral frontal area density for the Veilingweg (only buildings)

We proceed by plotting the urban frontal area density and the WAsP (baseline) prediction error, to test the hypothesis that local surface parameter holds information about the local means wind speeds. Despite the large degree of scatter, it can be concluded that there seems to be some relation between the error through WAsP and the density of urban frontal area (figure 4.11). This figure is for D=800 m but similar (yet even more scattered) trends were visible for all distance constants.

It makes sense to draw a parallel to the ΔRIX correction discussed in (section 2.3.2.1). It is attempted to proceed in similar fashion with respect to implementation of a correction factor based on the frontal area density, hence the following steps could be made [12]:

- Calculation of wind speed error as a percentage to the observed wind speed

- Calculation of the frontal area density difference between target and predictor site

- Plot and finding a linear fit to these data, the linear fit can be used as a correction function

Because the predictor site is Zestienhoven and the data are potential wind speeds, these data are not
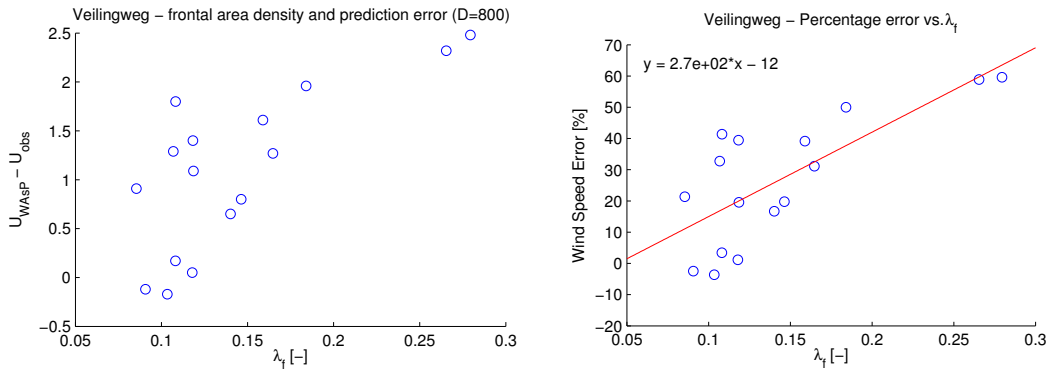
Figure 4.11: Frontal area density vs. WAsP over-prediction (left) and Frontal area density vs. WAsP percentage error (right) for the Veilingweg.

affected by urban obstacles. Therefore, it is proposed to find a relation between the absolute frontal area fraction and the percentage wind speed error. The choice for a linear fit is entirely based on the RIX implementation from literature [12] and the belief that a simple fit is more robust than a more sophisticated one, given the danger of over-fitting the data. The fit is obtained by a least-squares method in MATLAB. Distribution or residuals (not shown) appeared randomly.

Application of the model to the Veilingweg data can indicate the potential value of this correction. This is no validation, since we use the same data and site as to calibrate the model. Still it can serve as a first illustrative example. Per-sector, the percentage error is calculated by taking the frontal area density and applying the linear formula found in the fit (figure 4.11) to correct the baseline prediction. In figure 4.12 a plot is made of the observed, the baseline and the λ_f corrected wind speeds.
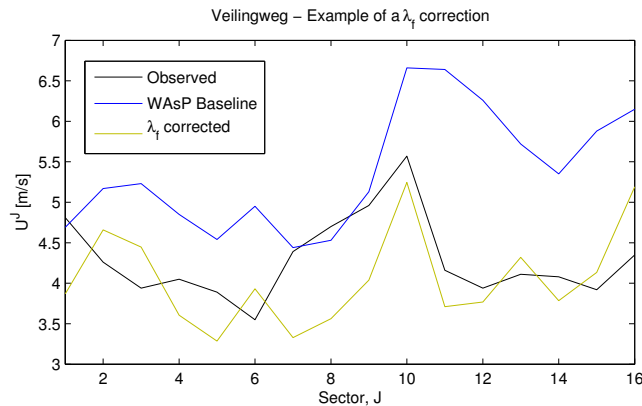
Figure 4.12: Improved prediction after application of a Veilingweg-calibrated model to correct for the amount of frontal areas around to the Veilingweg.

4.5 Wind climate prediction through DEM-derived z_0

As a third and last extension, it is attempted to directly substitute the LGN3+ roughness by the roughness lengths derived from the DEM. Since the plan and frontal area density and the average obstacle height are known, it is possible to estimate the sectoral roughness length through equation 2.12 or equation

2.11 or others (see [39] for an extensive overview). Recalling from Chapter 2:

$$\frac{z_0}{H} = 0.5\lambda_f \text{ (LE)}$$

$$\frac{z_0}{H} = \left(1 - \frac{z_d}{H}\right) \exp\left\{-\left[0.5\beta\frac{C_D}{k^2}\left(1 - \frac{z_d}{H}\right)\lambda_f\right]^{-0.5}\right\} \text{ (MD)}$$

In the last formula, $C_D = 1.2$ and $\beta = 1$. These relation of Lettau (LE) is chosen as it is most simple and the equation of MacDonald (MD) as it is reported to yield the best results for urban surfaces. Lettau's equation is simply based on the average obstacle height and frontal area density and a constant, whereas MacDonald's equation also uses the plan area density, the building drag coefficient and an extra constant. To obtain the surface parameters we choose a distance weighing function of 800 m.

Table 4.3: Surface parameters for $D = 800$ and corresponding roughness lengths (length units in [m]).

Sector	λ_f [-]	λ_p [-]	z_d	H	z_0 MD	z_0 LE
1	0.09	0.27	4.73	9.16	0.38	0.42
2	0.09	0.20	3.95	9.85	0.60	0.42
3	0.11	0.20	3.74	9.34	0.73	0.50
4	0.15	0.26	4.63	9.28	0.69	0.68
5	0.14	0.32	5.39	9.27	0.46	0.65
6	0.12	0.24	4.76	10.07	0.67	0.60
7	0.12	0.20	4.47	10.82	0.89	0.64
8	0.10	0.16	4.04	12.17	1.14	0.63
9	0.11	0.19	4.35	11.10	0.90	0.60
10	0.12	0.24	4.43	9.59	0.67	0.57
11	0.28	0.47	7.75	10.57	0.42	1.48
12	0.27	0.43	8.74	12.54	0.61	1.66
13	0.16	0.35	5.91	9.65	0.47	0.77
14	0.16	0.26	4.80	9.73	0.82	0.80
15	0.18	0.32	5.49	9.57	0.65	0.88
16	0.11	0.22	4.02	9.06	0.61	0.49
Average	0.14	0.27	5.08	10.11	0.67	0.74

Table 4.3 gives the resulting surface roughness lengths for the Veilingweg using MacDonald's and Lettau's equations. The values are in the expected range of roughness lengths for the low or medium urban class. On average, MD leads to higher roughness values than LE does and MD is more sensitive to plan area density.

It is chosen to select both LE and MD roughness lengths and create a roughness structure as in figure 3.10 to force WAsP to use a single effective roughness per sector. As turbine height, the height of the Veilingweg is taken and reduced with a zero-plane displacement height of 5 m, based on earlier results of the omni-directional z_d. The WAsP simulations are performed and the mean wind speeds per sector are plotted in figure 4.13.

In general, the simulation using Lettau's equation approaches the observed wind speed most closely, also considering the general shape of the plot and the positions of the peaks. Between sector 2 to 10, the observed, Lettau's and MacDonald's roughness lengths seem to align well as most wind speed prediction errors in that region remain limited. From sector 10 to 16, the simple equation of Lettau most clearly outperforms that of MacDonald, limiting the errors to within 1 m/s.

4.6 Conclusion

This chapter has presented the results of three possible strategies to combine WAsP with the digital elevation model. The Veilingweg functioned as a suitable testing and calibration case study, since for this
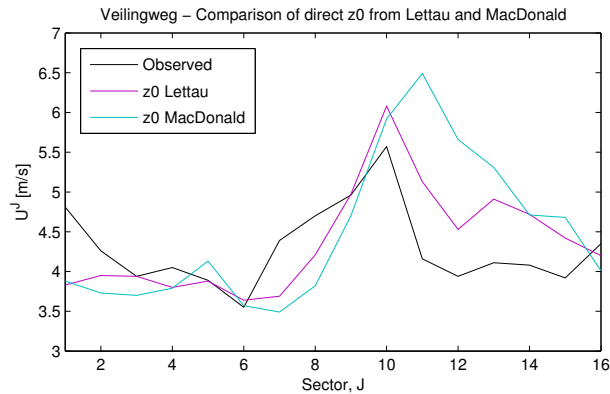
Figure 4.13: Comparison of observed wind climate and wind climate prediction with surface roughness obtained from the DEM using $D = 800$.

site a reliable long-term rooftop wind climate has already been determined.

All three extensions could be implemented without encountering any practical constrains of WAsP. However, the extensions vary in the extend they could improve the baseline (LGN3+) prediction. The most simple extension was to include an omni-directional zero-plane displacement height based on the DEM parameters. This adjustment could be made by simply consulting displacement height maps that were created for the entire region, see Appendix C. The improvement achieved with this correction is however very limited, which became apparent by plotting the sectoral predicted, observed and base line mean wind speeds (figure 4.4). A second attempt using the sectoral instead of omni-directional zero-plane displacement heights also showed little improvement. Buildings with a size like the Veilingweg or higher have a very limited sensitivity to a zero-plane displacement height. Yet, if a correction is to be made, it is preferred to simply make a z_d correction based on the omni-directional contour map, given the difference in effort between determining sectoral or omni-directional parameters.

As a second extension, it was attempted to find a correction based on the density of urban frontal areas of the surroundings. The basic idea of this correction relied upon the ΔRIX concept which is frequently used in WAsP for mountainous areas. It was argued that a frontal area may similarly as a steep mountain slope trigger flow separation and a loss of momentum of the mean wind speed. Removing vegetation in the DEM around the site gave a more precise value for the urban frontal area density around sector 6 to 8. Automated methods of removing vegetation found in literature could not be performed due to the relatively low resolution, so a manual approach was taken.

Despite much scatter, a relation could be found between the error in the baseline prediction and the frontal areas. Application of the linear fit to the Veilingweg baseline model logically improved the prediction but there's a real danger of over-fitting this model in general terms, since it is only based on a single location.

A more thorough approach was followed in the third extension, when the Veilingweg surface parameters were used to calculate surface roughness lengths using two established equations of MacDonald and Lettau. The sector-averaged roughness of both methods was quite similar (0.67 to 0.74), but each method led to a slightly different roughness profile, with MacDonald being affected by the sectoral variation in plan area density while Lettau was not. The found results were in range of the typical urban roughness lengths corresponding to the low, medium and tall urban classes reported in literature (table 2.1).

Directly implemented in WAsP, it became apparent that the equation of Lettau, being the most simple of the two, could deliver a wind speed prediction most similar to the long-term observed wind speed.

The results of this chapter can most concisely be summarized in a single table, listing the wind speed errors per sector and the mean absolute error (MAE) for each of the proposed extensions (table 4.4). The MAE is defined as the following relation between the observed wind speed U_{obs} and the model predicted

wind speed U_{pred} per sector:

$$\mathrm{MAE} = \frac{1}{n} \sum_{i=1}^{n} |(U_{obs})_j - (U_{pred})_j|$$

Table 4.4: The error with respect to the observed wind speed [m/s] for the extensions tested in this chapter.

Sector	Observed	LGN3+	z_d Corr	λ_f Corr	z_0 MD	z_0 LE
1	4.81	-0.12	-0.34	-0.94	-0.93	-0.98
2	4.26	0.91	0.87	0.40	-0.53	-0.31
3	3.94	1.29	1.17	0.51	-0.24	0.00
4	4.05	0.80	0.67	-0.44	-0.26	-0.25
5	3.89	0.65	0.40	-0.61	0.24	-0.01
6	3.55	1.40	1.09	0.38	0.02	0.09
7	4.39	0.05	-0.19	-1.06	-0.90	-0.70
8	4.70	-0.17	-0.39	-1.14	-0.88	-0.49
9	4.96	0.17	-0.07	-0.92	-0.26	0.01
10	5.57	1.09	0.79	-0.33	0.35	0.51
11	4.16	2.48	2.19	-0.45	2.33	0.97
12	3.94	2.32	2.18	-0.17	1.72	0.59
13	4.11	1.61	1.48	0.21	1.20	0.80
14	4.08	1.27	1.03	-0.30	0.63	0.64
15	3.92	1.96	1.69	0.21	0.76	0.50
16	4.35	1.80	1.59	0.84	-0.34	-0.15
MAE		**1.13**	**1.01**	**0.56**	**0.72**	**0.44**

This chapter shows that DEM derived surface roughness enabled us to obtain a more accurate wind speed prediction at the Veilingweg. The three surface parameters (λ_p, λ_f and $\overline{h}$) may not capture the full complexity of the actual urban surface, but it appears that they at least describe the local wind related characteristics better than the LGN3+ land use map. The predicted and observed wind speeds at the Veilingweg indicate that it is not a logic extension to model a speed-up above the roof in WAsP by the artificial surface model presented in [62], as we have found during the small WAsP tests that this 'hill' would further increase the speed predicted (see section 3.3.3.1).

4.7   Discussion

One should be cautious with binding too definitive conclusions to the final results of the Veilingweg (the improved prediction), given the number of choices made and the calibration done. Undoubtedly, we have to some extend 'overfitted' the methods to suit the data derived for this site. For instance the choice of the optimal distance constant or the relation between the surface and z_0. Regarding this last point, it is at least partially encouraging to see that the most simple roughness parameterization (Lettau) led to acceptable results. Under all the simplifications and the assumptions made it intuitively makes more sense to choose a simple formulation between the digital surface and z_0.

Regarding the choice for the most appropriate distance constant, $D = 800$ m best suited the data for this site, although margins are low. It may be that the range now considered (300 to 1000 m) was to narrow or it may be that the relatively slow-evolving surface around the Veilingweg generated only small differences (certainly from some sectors, including sector 10). A validation on a site with an abrupt surface transition may give more insight in the correct values.

It can be argued that the Veilingweg was not a totally ideal site to test the DEM analysis, given the moderate degree of urban obstacles and the portions of vegetation and natural areas. Yet, the well-

established rooftop wind climate through more than 12 months measurements still made it a location of preference, also considering the fact that it was known that negligible local turning was present.

Now that we have established evidence about the actual surrounding urban roughness, we will proceed in the following chapter by an attempt to measure those quantities directly using an ultrasonic anemometer.

Chapter 5

Roughness validation with turbulence measurements

High frequency sonic wind speeds measurements are the best experimental means to investigate a local wind climate, not only in terms of mean wind speeds but also in terms of vertical components, turbulence intensity and spectrum. It was chosen to re-investigate the local wind climate at the Veilingweg to attempt to validate the urban surface roughness found in the previous chapter. This chapter will describe in some detail the theoretical background, measurement setup, data analysis and results from the ultrasonic wind study at the Veilingweg.

5.1   Measurement objective

The primary objective of the 3-D ultrasonic measurements at the Veilingweg is to determine the sectoral turbulence characteristics. The sectoral turbulence characteristic is the standard deviation of the wind speed for observations within a selected directional sector. In theory, there is a link between the observed turbulence intensity and the effective surface roughness of the upwind source area, hence the turbulence measurements may give insight in the effective surface roughness around the Veilingweg.

We can distinguish several sub goals:

- Test whether realistic z_0 values can be derived from the acquired data.

- Test whether a sectoral dependency can be found on z_0.

- Compare sectoral z_0 values with sectoral parameters found in Chapter 4.

- Test the effect of a stability consideration on the results.

A parallel objective is to investigate the mean vertical velocity components which normal cup anemometers cannot register. Mean vertical velocity components may be present as a result of the high pressure zone on the windward facade which directs flow over the building.

5.2   Theoretical background

The link between effective surface roughness and turbulence, being the standard deviation of the horizontal wind components at a fixed spot, is discussed by a number of authors including R. Sozzi and M. Favaron [47], A.C.M. Beljaars and A.A.M. Holtslag [8], and S.M. Arens, J.H. van Boxtel and G. Sterk [25]. Wind speed variance at a fixed spot in the inertial sublayer is the resultant of a superposition of large and small eddies, which are, in the urban case, primarily caused by drag of the underlying upwind surface. As the eddies are carriers of momentum between different vertical air layers, they are strongly related to the shape of the logarithmic mean wind profile.

For neutrally stable conditions, several authors note the following similarity equation, which can be used between the standard deviation of the longitudinal mean wind speed and the friction velocity:

$$\frac{\sigma_U}{U_*} = 2.5 \qquad\qquad (5.1)$$

55
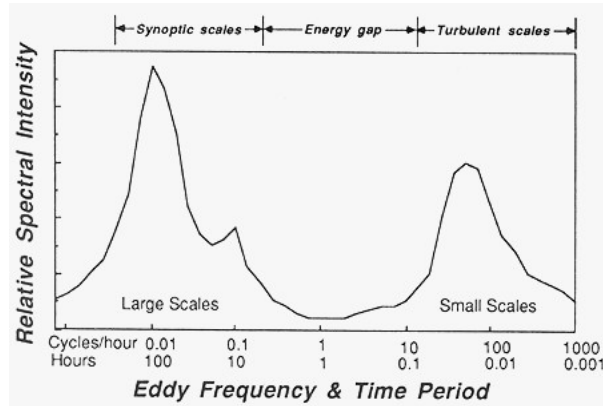
Figure 5.1: Relative spectral intensity of the wind [49]

It should be noted that this 2.5 is derived from a fit to experimental data and other experiments reported other values (see for instance the discussion by Verkaik [52]). Combining equation 5.1 with the equation of the logarithmic profile gives a direct relation between the standard deviation and the roughness length (the Von Kármán constant disappears due to multiplication with 2.5):

$$\frac{\sigma_U}{U} = \frac{1}{\ln(\frac{z}{z_0})} \tag{5.2}$$

The left size of this equation is the regular definition of the turbulence intensity. The standard deviation σ_U around the mean U for a block consisting of N individual samples denoted by u is defined as follows:

$$\sigma_U = \sqrt{\frac{1}{N-1} \sum_{i=1}^{N} (u_i - U)^2} \tag{5.3}$$

5.2.1   The turbulence spectrum

Not all the variance in the wind speed is related to actual turbulence, as part of the very low-frequency variance is related to changing weather patterns. Figure 5.1 depicts a typical relative spectral intensity of wind speed measurements. It can be concluded that there are large variations with a frequency of a few days, the synoptic scale, which can clearly be distinguished from fluctuations with a frequency of minutes or seconds, on the turbulent scale.

Since our measurement objective is to estimate the surface roughness, we are interested in turbulent eddies that drive momentum from higher air layers to lower air layers. While very large vortices may transfer much momentum at once, their occurrence is with a very low returning frequency (rare). On the other hand, very small vortices occur very often, but only carry small portions of momentum. Most of the momentum between vertical air layers in the inertial sublayer is transported by the vortices of intermediate size [25], right in the operational spectrum of anemometers. Currently, the choice is made for a 10 minute sampling time. This filters out almost all non-turbulent contributions to the wind speed variance, such as changing weather conditions, while still minimizing low-frequency loss of the turbulence that is related to vertical momentum transport.

The upper frequency losses are given by the measurement volume –or path-length– of the anemometer together with the data logging speed. J.J. Finnigan and J.C. Kaimal write that vortices can be measured as small as $\lambda = 2\pi d$, with d the path-length of the anemometer, which is for sonic anemometers equal to the transducer distance [27]. For typical path-lengths of sonic anemometers one can therefore resolve vortices
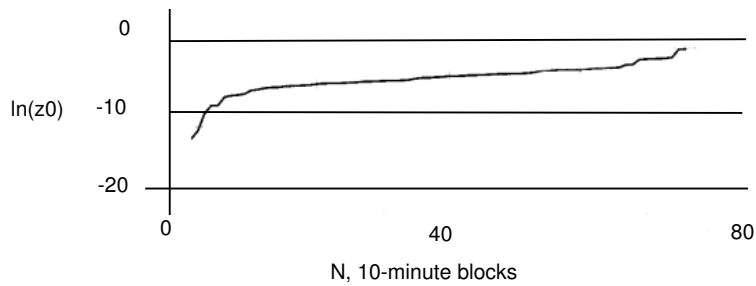
Figure 5.2: Example of a plateau of ranked y-values (adapted from [47])

sized 1 m and bigger. Based on the spectrum of uw-covariance, Van Boxtel and Sterk calculated that the high-frequency losses due to the path-length instrument limitation are around 1%, for anemometers installed at $z = 2$m [25]. As in the current study the measurement height is greater than 2 m, it can be assumed that turbulence measurement 'losses' due to vortices smaller than 1 m are negligible.

5.2.2 Measurement stochastics

Equation 5.2 should be interpreted as an estimator for the actual sectoral roughness length. When a large number of couples U and σ_U are collected, this equation can be used to determine a large number of z_0 estimates. For a several of reasons, we can expect much scatter in the estimator: on top of standard measurement errors, there may not be homogeneous roughness within a sector, stability effects may have influence on the measurements or there may be non-turbulent contributions to the variance during changing weather conditions within a 10-min block.

Sozzi and Favaron [47] propose to calculate the logarithm of the roughness length, which follows from rewriting equation 5.2:

$$y = \ln(z_0) = \ln(z) - \frac{U}{\sigma_U} \tag{5.4}$$

And then rank y-values and plot those in a graph. If the measurements are successful and enough data is collected, the ranking should indicate a clear plateau in the middle where y varies very little. The final y-value is then obtained by taking the median of the set.

5.2.3 Assumption of neutral stratification

In the equation between the standard deviation of the wind speed and the surface roughness length, it is implicitly assumed that wind speed fluctuations represent turbulence caused by shear effects of the mean wind speed profile –or momentum transfer between air layers. One can however distinguish two other sources of turbulence in the urban environment: convective turbulence and wake turbulence. Convective turbulence is caused by heat differences in the flow, wake turbulence refers to the direct effects of separation vortices emanating from an upwind obstacle. To guard this assumption, it is important to minimize both sources of turbulence as they can interfere with a correct estimation of z_0. Wake turbulence is minimized by optimal siting of the sonic anemometer clearly above the roughness sublayer, minimizing effects of convective turbulence requires a more thorough approach.

Convective turbulence can primarily be an important contributor to the total turbulence under unstable conditions; during light winds and significant heat flux. This may lead to an over-prediction of z_0. During stable conditions (clear skies, cooled surface) the logarithmic profile is formally not valid and turbulence can be suppressed leading to an under-prediction of z_0. Hence, the assumption of neutrally stable weather conditions is required to free the measured turbulence from non-neutral stability effects. This assumption

can be checked in different ways. One way is to refer to the simultaneous Pasquill stability scale value. The Pasquill stability scale ranges from A to F with the following significance:

- A: Very unstable

- B: Moderately unstable

- C: Slightly unstable

- D: Neutral

- E: Slightly stable

- F: Moderately to very stable
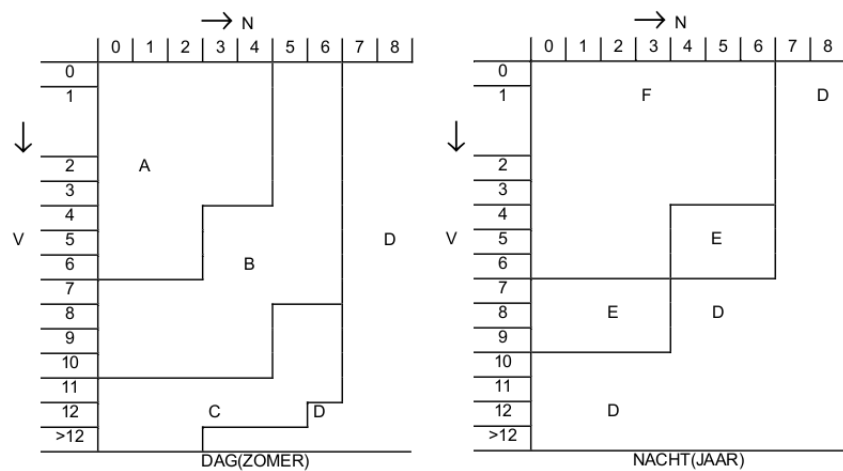
Figure 5.3: Guideline in diagram proposed by the KNMI to determine the atmospheric stability based on the cloud coverage (N) in octaves and the mean wind speed (V) in m/s. The region denoted by D refers to neutrally stable conditions. The left diagram is valid for summer days, the right diagram for nights (year-round).

The Royal Netherlands Meteorological Office published a guideline to determine the Pasquill scale on the basis of season, cloud coverage (in octaves), wind speed and day/night [30]. Neutral stability is generally valid during times of heavy overcast, 7-8 octaves cloud cover. During nighttime and strong winds (6 m/s), 4 to 6 octaves may also be sufficient. Figure 5.3 indicates the conditions for a neutral atmosphere.

5.3 Methodology

In this section the general methodology is outlined. The chosen instrumentation, measurement setup and data-analysis are presented in detail and the choices are substantiated.

5.3.1 Instrumentation

A fast response ultrasonic anemometer is the instrument of choice for wind measurements in the built environment. Unlike their cup counterparts, these instruments have a linear response to wind gusts, can measure at a higher frequency and can measure in a 3D format. The fast response wind measurement
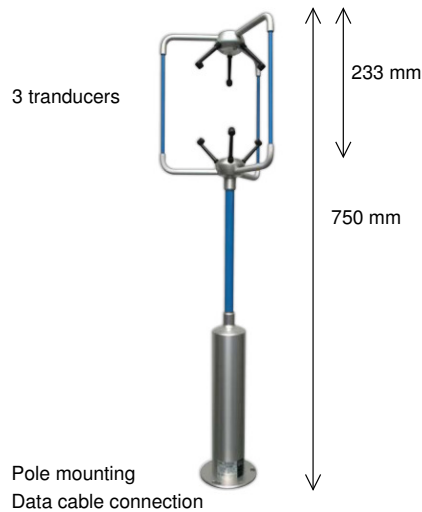
Figure 5.4: The Gill 3-axis ultrasonic anemometer (adapted from [20])

instrument in this study is the Gill Windmaster 3-axis sonic anemometer, which is mounted on a guy-wired pole in the center of the top roof. It is connected to a Guruplug[1] computer through the following subsequent steps: a 25m CAT6 shielded cable, a serial RS-232 connector and a serial to USB connector. The sonic anemometer is powered by a 12 Volt AC-DC adaptor with power lines running through the same CAT6 cable. For safety, we installed an additional 100mA fuse on the anemometer side of the AC-DC converter, in case anything would go wrong such as short-circuit in the outdoor wiring.

As a best concession between limitations posed by data storage and the benefits of acquiring higher frequency data, it was chosen to let the script log and store the wind speed at 10 Hz in u, v, w format (although the instrument was capable of 20Hz). 10 Hz is often taken as the standard for turbulence measurements [54]. The data logging was achieved by design of a tailored Python script that would initiate the readout at steady intervals and store the parameters on an external flash drive.

Table 5.1: Gill Windmaster Pro specifications as supplied by the manufacturer [20]

Specification	Value
Range	0-45 m/s
Accuracy	<1.5% RMS m/s - 2 deg @ 12 m/s
Resolution	0.01 m/s - 0.1 deg
Internal Sample Rate	20 Hz
Sample Path Length	15 cm

After some initial failures, a stable measurement system was obtained that could run autonomously and error-free as long as the data storage could handle. The designed system logs 10 Hz u, v, w data for 59 seconds, then holds for 1 second to write these 590 data points to an SQLite database. This cycle runs for 11 hours and 50 minutes and is automatically restarted every 12 hours to minimize the loss in case of crashes. Since the restarting step was introduced the data loss has been minimized to only 3 hours in a total of 10 weeks.

---

[1]A Guruplug is a light and energy efficient computer (5W), capable of high speed customized data logging in this case by means of a Python script

59

5.3.2 Measurement setup

It was chosen to mount the anemometer 7 m above the top roof, see figure 5.5. The primary criterion for this height was to minimize the turbulence due to the direct (own) roof separation present at this height. A reference was made at a collection of CFD simulations performed by P. Blackmore [10]. One of his summaries is that, for standard rectangular buildings, the average turbulence intensity above roofs tends to converge to within 10% of the free-stream turbulence at a height of 0.12 to 0.17 H. This translates to 3.6 to 5.1 m for the Veilingweg ($H = 30$). A photo of the setup is given in Appendix D.
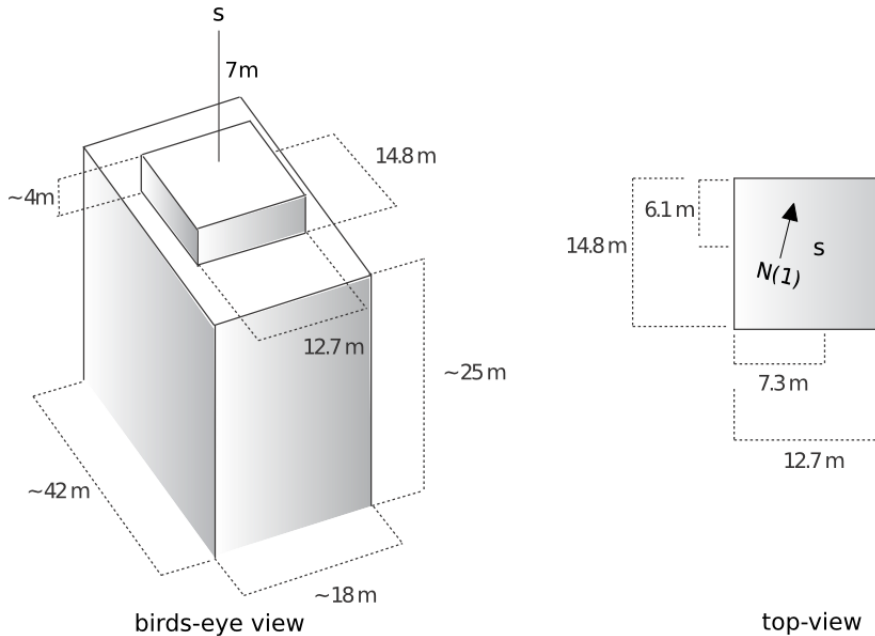
Figure 5.5: Building geometry and location of the sonic anemometer (denoted by s)

5.3.3 Data analysis

This measurement project required a streamlined data analysis, due to the total number of data points. A single week results in more than 6 million data points, which should be grouped together in blocks, selected or thrown away based on atmospheric stability and analyzed per sector. For this to go smoothly, the analyses are ran from an SQL-based system. The complete processing included the following steps:

1. Spike removal

2. Grouping of the data points, based on their 10-minute time stamp

3. Within group, calculation of the following components:

    (a) Time-averaged horizontal wind speed $U = \overline{\sqrt{u^2 + v^2}}$
    (b) Standard deviation of U by equation 5.3
    (c) Time-averaged vertical wind speed
    (d) Azimuth (1-360) -> sector (1-16) -> median sector of all points in the 10-min block
    (e) y-value ($\ln(z_0)$) by equation 5.4

4. Per group, lookup of the Pasquill stability class as was recorded KNMI station Zestienhoven

5. Filtering to only allow blocks obtained during Pasquill D conditions

6. Binning the blocks based on the median sector

7. Per sector, ranking the y-values, plotting the ranks and identification of a plateau

   (a) If a plateau is found, the median is taken as the most likely value of $\ln(z_0)$
   (b) If no plateau is found, more data points are required or if a large number of data points are taken the roughness may not be homogeneous

Spike removal is one of the first steps to ensure the quality of the data. A spike in a time series is a sudden big change of the output signals, which does not reflect any meaningful change in the measured meteorological variable. Some causes of spikes in sonic measurements are electrical surges from the power supply or moisture, dust or insects on the transducers. A possible spike removal algorithm is to define a maximum wind speed change between two data points, for instance 3 m/s [40]. By analyzing the current Veilingweg data it was found that most spikes could be removed using a maximum step size of 5 m/s and by defining a maximum absolute wind speed of 30 m/s.

A Pasquill stability class lookup was made by analyzing the hourly meteorological datum at Zestienhoven. Although this is an hourly instead of a 10-minute observation, it is assumed that cloud cover does not variate too much within an hour so the class is rightfully assigned. The data are downloaded from the climatology website of the KNMI [2].

5.4   Results

After some startup issues, data was successfully gathered between the 1st and 29th of August 2011 at the Veilingweg using the setup described above, resulting in a little more than 25 million data points. This section will present the results from the data analysis of this period.

5.4.1   Data selection

For the measurements in August, 66 % of the data could be accepted due to neutrally stable atmospheric conditions. This was primarily a lucky side-effect of a notoriously bad Dutch summer month, which was characterized many days of heavy overcast. Figure 5.6 indicates the partitions that were rejected and accepted for every sector.

5.4.2   Local turning of the wind

As one of the first things, a check is made for local turning effects of the mean wind speed by comparison with KNMI station Zestienhoven. Local turning may be caused by the building, blockage or by the surrounding surface, and is unwanted since it complicates clear definition of what is the upwind source area.

We assign sectors to simultaneous hourly data of Zestienhoven and calculate the number of times the observed 10-minute Veilingweg sector is higher or lower in clockwise manner (figure 5.7). Given the large number of data points, we conclude visually that negligible local turning is present. Among other things, this implies that the anemometer is mounted correctly, no systematic sector distortions are present in the data, and the turbulence characteristics from a wind in a specific sector can be assumed to be affected by the upwind source area of that sector.

---

[2]http://www.knmi.nl/kd/uurgegevens/selectie.cgi
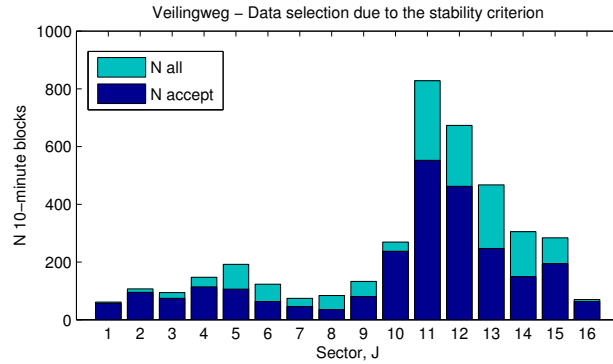
Figure 5.6: Data rejection per sector due to non-neutral stability at Zestienhoven meteorological station.
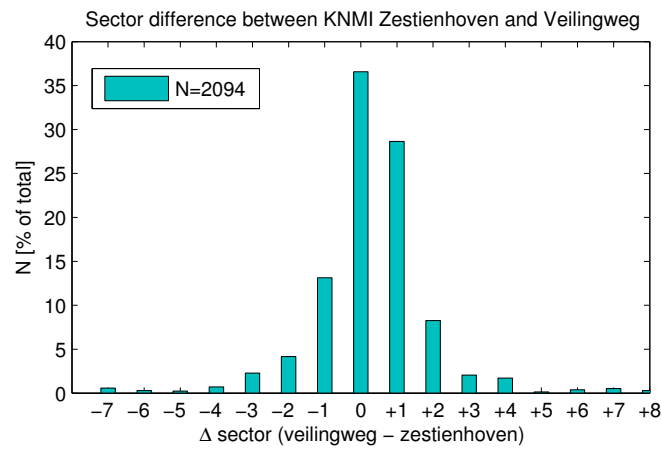
Figure 5.7: Histogram of the wind direction difference between Veilingweg and Zestienhoven based on 2094 10-minute data points (sectors are counted clockwise)

5.4.3 Sectoral roughness using neutrally stable conditions

Estimates of the sectoral roughness were obtained by application of equation 5.4. It was found that the histogram of the sample was not normally distributed but skewed towards the left, in some cases to $\ln z_0 = -10$. Hence, it can be confirmed that the median should be preferred over the mean as the most appropriate measure of the distribution. Although the mode could also be suitable measure, as it is the most probable value of the random variable.

For most of the sectors, a clear plateau could be found, which indicates that it is meaningful to talk of a single roughness at that sector. Exceptions were sectors 1, 6, 7, 8 and 16, that showed a relatively steep plateau without a clear inflection point. For these sectors, the limited number of data points seemed the primary cause of this. Generally, it appears that at least around 100 10-minute blocks are required before a reasonably good plateau and inflection point could be identified. The shapes of ranking for no plateau, a poor plateau and a good plateau are given in figure 5.8.

The sectoral roughness length was calculated by finding the median of $\ln z_0$. A 95% confidence interval on the roughness length is calculated using the method described by D. A. Altman [6], to indicate the precision and to convey the effects of sampling variation on the actual turbulence-related roughness of the sector, see figure 5.9 and the table in Appendix Chapter D. For about half of the sectors, the roughness length can be determined with an accuracy of ± 0.1 m. For the other half, the accuracy is
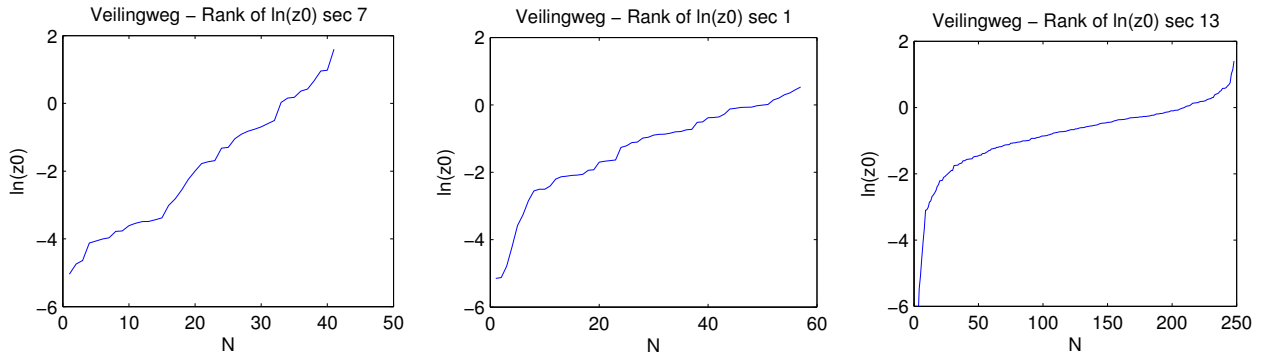
Figure 5.8: Results of ranking $\ln z_0$ for sector 7 (left) sector 1 (middle) and sector 13 (right) indicating no plateau, a poor plateau and a good plateau.
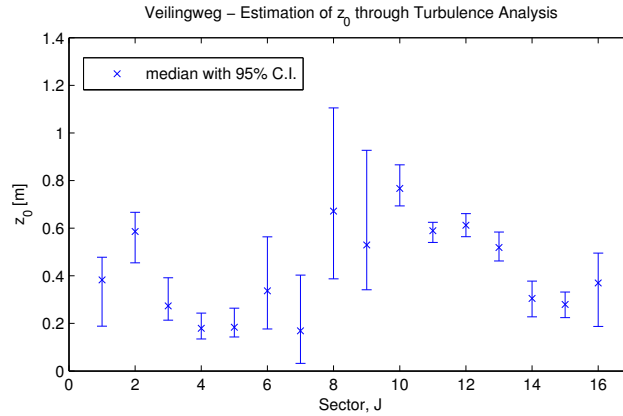
Figure 5.9: Estimates of z_0 through turbulence measurements including a 95% confidence interval.

decreased, with sector 6,7,8 and 9 being the four sectors with the widest confidence intervals. It is not only the sample size that determines the accuracy of the z_0 estimate, also the variance within a sample varied between sectors. This can most clearly be seen by comparing the confidence intervals of sector 3 and sector 9, both having a very different accuracy, but a fairly equal sample size (74 to 77).

5.4.4 Sectoral roughness including non-neutrally stable conditions

As was argued before, there are strong reasons to only focus on neutrally stable conditions when measuring the turbulence caused by the upwind surface roughness. For the present campaign, the stability criterion implied discarding one-third of the observations because of insufficient cloud cover. For some sectors, such as 8 and 9, this meant about half of the data points could not be used.

Despite these good reasons, the actual effect of the stability criterion is for our location and our weather conditions is not known. Therefore it is decided to re-analyze the data including all stability classes. The result of this re-analysis is given figure 5.10 and in table 5.2.
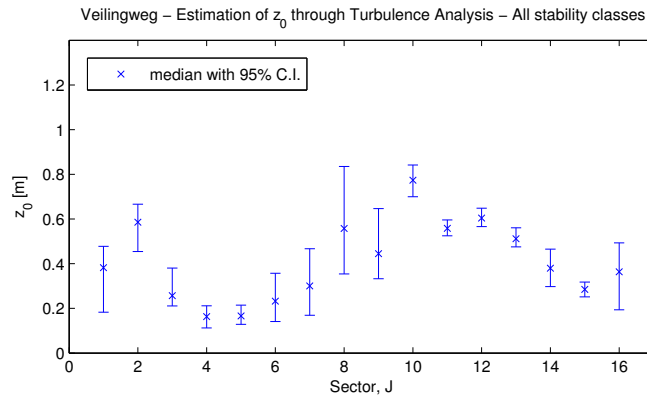
Figure 5.10: Estimates of z_0 through turbulence measurements including a 95% confidence interval, including non-neutrally stable conditions.

Table 5.2: Sectoral roughness lengths found through turbulence measurements using all stability classes. For comparison we include the roughness extracted by the DEM using Lettau's relation.

sector	N	plateau	z_0 [m]	l.b. [m]	u.b. [m]	z_0 LE
1	61	poor	0.38	0.18	0.48	0.42
2	107	good	0.59	0.45	0.67	0.42
3	94	good	0.26	0.21	0.38	0.50
4	147	good	0.16	0.11	0.21	0.68
5	191	good	0.17	0.13	0.21	0.65
6	123	good	0.23	0.14	0.36	0.60
7	74	poor	0.30	0.17	0.47	0.64
8	84	poor	0.56	0.35	0.84	0.63
9	133	good	0.44	0.33	0.65	0.60
10	269	good	0.77	0.70	0.84	0.57
11	839	good	0.56	0.53	0.59	1.48
12	717	good	0.60	0.57	0.65	1.66
13	485	good	0.51	0.48	0.56	0.77
14	306	good	0.38	0.30	0.47	0.80
15	286	good	0.29	0.25	0.32	0.88
16	70	poor	0.36	0.19	0.49	0.49

It appears that fair results are obtained when comparing the new graph with the previously obtained graph in figure 5.9. Including non-neutrally stable cases does not increase the error margins in the sector which have so far been characterized by the smallest errors (10 to 13). On top of that, the increased number of data points for sector 6, 7, 8 and 9 actually led to lower margins in these sectors without radically changing the positions of the medians. For sector 7, the plateau after ranking y values improved largely.

5.4.5 Vertical wind speed components

Although it is not the main focus of this chapter, the Veilingweg enabled easily measure the inclination angle of the incoming wind –a building scale effect. There are several reasons for knowing this angle:

- Turbine performance and loads may change under titled inflow

- The inclination angle may give some hints on the location of the shear layer

Above the shear layer one should expect some vertical components. From the complete dataset, the medians of the 10-minute mean vertical components as a fraction of that 10-minute mean horizontal are calculated for each sector, resulting in figure 5.11.
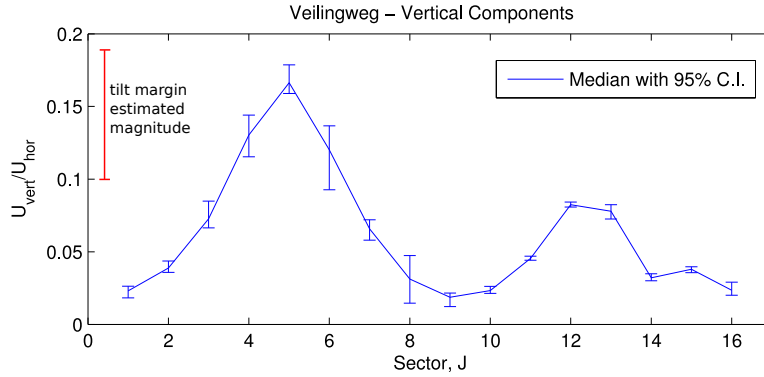
Figure 5.11: Vertical component divided by the horizontal component of the wind speed for each sector, based on 4-weeks of sonic measurements during neutral stability. The red line indicating the margin estimated due to a 5 degree tilt of the sonic anemometer.

It can be concluded that there is a clear positive mean vertical component for all sectors, indicating that the anemometer is indeed located in the curved streamline region above the shear layer, a region where there is an increased velocity due to the building-induced blockage. Comparison with literature points to two likely explanations for the peaks around sector 5 and sector 12-13: differences in cross-sectional area and differences in distance to the roof edge.

5.4.5.1 Comparison with shear layer model

As an illustration of the effect of increased blockage and increased distance to the roof edge on the measured wind tilting angle, we refer back to Wilson's equation on the shear layer growth as a function of the downwind distance and the virtual dimension of the building. Recalling equation 2.13, the virtual dimension of the Veilingweg can be estimated as:

$$D \approx \begin{cases} 30 & \text{for sector } \mathbf{5} \text{ and } \mathbf{13} \text{ (long edge)} \\ 20 & \text{for sector } \mathbf{1} \text{ and } \mathbf{9} \text{ (short edge)} \end{cases} [\text{m}]$$

where the small technical building on top has been neglected.

As an approximation for the separation streamlines for the long and short edge, we apply equation 2.14 resulting in figure 5.12. The two dots indicate the horizontal position of the sonic anemometer from the leading edge, which is 9 or 20 m, dependent on the wind direction. This is an approximate position, and may differ +/- 1 m. The figure clearly indicates that both a decreased distance to the leading edge, as well as an increased virtual dimension, lead to a steeper profile and therefore a higher relative vertical velocity component in the mean flow. For the Veilingweg, the shear layer model predicts a local $\frac{\mathrm{d}y}{\mathrm{d}x}$ of 0.2 [-] for wind perpendicular to the long edge and 0.09 [-] for wind perpendicular to the small edge.

The measured mean vertical velocity components are smaller than the steepness of Wilson's shear layer model would predict. Assuming the theory is correct, an explanation for the results currently found is that the streamlines have somewhat decreased in steepness, because the mast height is well above shear layer height from the model. Furthermore, the mast was located not on the main roof but the roof of a technical building with extended height.

The vertical wind components also show a difference in peak height between sector 5 and 12-13. It is not unlikely that this is a measurement error caused by a mast with a small fixed tilt; a five degree
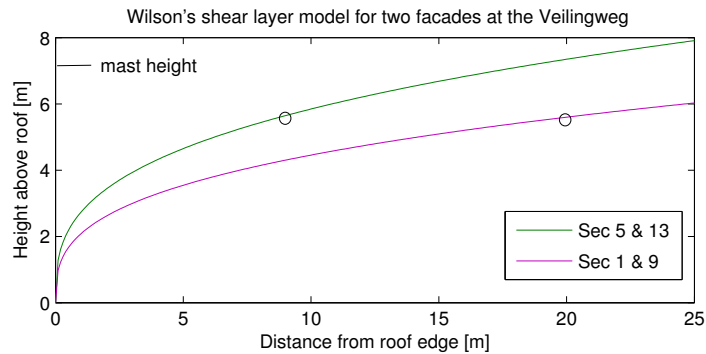
Figure 5.12: Application of Wilson's shear layer model for two wind directions at the Veilingweg. The two dots indicate horizontal positions of the sonic anemometer

tilt creates a rather large margin, as the red line in figure 5.11 indicates. Other explanations may be related to an increased roughness in sector 12-13, causing a flatter shear layer, but we refrain from this explanation considering the large potential error margin in the measurements.

5.5   Conclusion

This chapter has presented the results of an ultrasonic measurement campaign at the Veilingweg police station in Rotterdam. For four weeks, a sonic anemometer mounted at 7m above the roof registered 3-Dimensional wind speeds at a frequency of 10Hz. The data were analyzed according to a method described in literature to obtain estimates for the sectoral roughness length of the surroundings, which led to roughness lengths in the range of 0.18 (Sector 4) to 0.77 (Sector 10). Those values are in-range of the typical roughness lengths for the urban class.

It is an encouraging finding to see a clear sectoral dependence of the roughness length combined with relatively small error margins for the sectors with sufficient data points. However, on the basis of these results, we do not obtain strong evidence to validate the surface roughness determined in the previous chapter. First, regarding the sector average, the measured surface roughness is smaller than the DEM-derived surface roughness (0.42 compared to 0.67 for LE and 0.74 for MD). Second, the general measured roughness profile (figure 5.9), with a small peak around sector 2 and a bigger and wider peak around sector 10 is also not fully compliant with the DEM-derived roughness or fraction of frontal area, which only shows a thinner but more abrupt peak at sector 11-12.

We may obtain an explanation for the more diffuse roughness profile that is now found, by looking more carefully at two mechanisms inherent to this experimental setup. Suppose there is indeed a large surface roughness peak in sector 11-12. Then, it may well be possible that this peak 'smoothens out' to neighboring sectors in the observation at the Veilingweg through two mechanisms. In the first physical mechanism, air layers upstream of the Veilingweg may have mixed horizontally, so that in fact wind coming from sector 10 may have collected part of the turbulence emitted from sector 11-12, from which we may conclude there is an larger roughness in sector 10 than there actually is. The second mechanism is relates to the data analysis in this campaign. To assign a wind direction to our 10-minute block, we take the median of the angle. Yet, it may well be that for parts within these 10 minutes, the actual wind direction varies several sectors around this median. Due to this slow variability, the observations inside the 10-minute bin are likely to be 'contaminated' with minutes from other sectors than the median sector. Concluding, there are different plausible causes of sectoral diffusivity of the upstream surface roughness that may have affected our current results, although there are currently no means to confirm these causes.

Considering this limitation, a better objective of this campaign should have been to validate the general trend in the relative sectoral roughness, instead of validating the actual roughness for each isolated sector. Such an objective would have led us to conclude that we could indeed measure an increased urban surface roughness centered around sector 11.

Regarding the vertical wind speed components, it is concluded that there is a very clear sectoral dependency, which is –given the symmetry in the results and what is known from CFD studies– caused by building scale effects. The 10-minute averaged vertical component is always positive, and shows peaks of around sector 5 and 13. The sectoral distribution of the vertical components corresponds to the expected distribution based on Wilson's shear layer model above the roof, in which a higher frontal blockage comes with an increased vertical angle.

5.6   Discussion and recommendations

The data analysis uncovered some practical insights for sectoral roughness measurements and some points of discussion. First of all, it seems that at least around 150 10-minute data points are needed per sector to determine the surface roughness with an accuracy of ± 0.1 m. For 16 sectors, this may often take more than one month, depending a bit on the wind climate. Merging sectors (16 to 8) increases the number of data points per bin and may help to obtain a good accuracy with a shorter measurement time. At the Veilingweg, surface roughness was not homogeneous enough between the sectors, so that the increased number of data points per bin was canceled by a steeper plateau, effectively leading to a less-accurate z_0 estimate.

Second, we have found that the stability criterion did not improve our results. In fact, for some sectors, the increased number of data points outweighed possible distortions that convection may have caused. We presume that most of the observations that were discarded due to the stability criterion were in fact obtained during near-neutrally stable conditions, given the scarcity of clear skies in August 2011. The data suggest that, for an urban situation at relatively low heights, convective turbulence does not weigh up to shear turbulence caused by the high surface friction which is present. It is hence recommended to also include observations obtained during Pasquill class C and E (near-neutral stability).

Third, we would like to make the point that in case of high roughness, it may be increasingly difficult to define the upstream wind direction, because of rapid wind direction changes which are represented in the data. Currently, the median of all high frequency measurements was taken to define the wind direction. The wind direction difference plot between the Veilingweg and Zestienhoven indicated that this worked to a satisfactory degree, although improvements may be possible to reduce the sectoral diffusivity in the z_0 data. One of those improvements could be to reject all data below a certain mean wind speed, as during low wind the definition of the wind direction (and hence the upwind fetch area) is increasingly ambiguous.

The fourth point we would like to make, is that in this data analysis, we have chosen to study the fluctuation of the horizontal wind speed as a measure for the surface roughness. There are two other possible approaches to relate wind speed measurements to a surface roughness length. Verkaik describes and compares in detail two methods that include the gustiness (U_{max}) besides the standard deviation and the mean wind speed [52]. He also calculates the errors involved from a theoretical analysis. We have currently not used this method, for the primary reason that it was only found at the end of the project and involves a more advanced and time-consuming data analysis. Besides these two methods, an approach that could also be used is to measure the uw-covariance as an estimate for the friction velocity $u*$ directly [25]. The reason why the fluctuation of the horizontal component is preferred over the uw-covariance is that the uw-covariance is very sensitive to tilted inflow. Since it is known that the mean wind speed induces vertical components due to the building blockage, the covariance between the two will be increased substantially simple by the building induced tilt, probably making this method incompatible within the current setup.

Fifth, no attempts were made to study in detail the effect of the actual wind conditions on the

measured $\frac{\sigma_U}{U}$ distribution. This ratio $\frac{\sigma_U}{U}$ is known to vary to some extend over different mean wind speeds, which explains the variance found in the ranking plots. Manwell, McGowan and Rogers note that the highest ratio is found at the lowest wind speeds [24]. They also note that there is a lowest limiting value of $\frac{\sigma_U}{U}$ which depends on terrain features and surface conditions.

The last point noteworthy is that in our method it was chosen to use $U = \sqrt{u^2 + v^2}$ as a definition for the longitudinal wind speed, from which both the time-average and the standard deviation are calculated. In fact, this definition of the longitudinal wind speed is incorrect, since a lateral component will also contribute to this speed. No clear guideline is found for this, but it could be checked in future work whether using the 'pure' longitudinal component in formula equation 5.4 leads to roughness values which are more representative for the surface.

This sonic measurement campaign marked the end of the urban wind resource study at the Veilingweg. The following chapter a focus is laid on a new urban location in the city of Zoetermeer, for which we will try to validate the wind climate prediction method developed so far.

Chapter 6

Study of a second urban site

All the experimental results and experiences so far are based on data collected at the Veilingweg in Rotterdam. So far the two main conclusions are that we can improve the rooftop wind climate prediction using DEM-derived roughness and that it appears possible, to some extend, to measure the roughness lengths in the surroundings. This chapter present the result of a study at a second urban location in the same region; the Witte Dame in Zoetermeer. This location was chosen from a set of locations which were proposed by the housing cooperation De Goede Woning for two reasons. First, the Witte Dame extends well above the surrounding urban canopy and second, the roof enabled relatively easy installation of a measurement pole. The most important difference with the Veilingweg is that we do not know the rooftop wind climate a priori for this site, since it has not been measured in an earlier campaign. Also, no reliable LGN3+ prediction is available, due to the fact that the surroundings are under heavy development.

   This chapter will present the following: First, the results are presented from the surface calculation method to derive surrounding parameters. Then follows a description of the ultrasonic measurement campaign held at the Witte Dame between August 30th and the 2nd of October 2011. During this period, the mean wind speeds and turbulence characteristics have been recorded. The mean wind speeds are of interest because they describe a short-term wind climate, which can be compared with a short-term prediction made by WAsP using the DEM-derived surface roughness and a wind climate at Zestienhoven recorded over the same period. In addition, the turbulence characteristics will be analyzed according to the method presented in the previous chapter so that measured sectoral roughness lengths can be extracted, which can then be compared with the DEM-derived roughness.
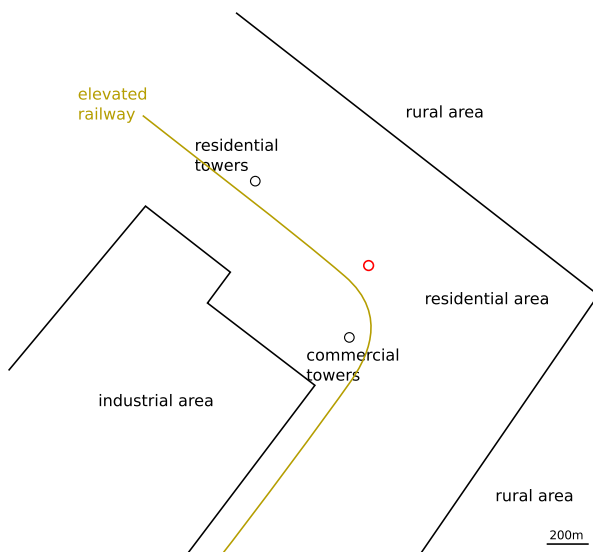
Figure 6.1: General surface coverage overview around the Witte Dame (red dot)

6.1 Site description and surface parameters

De Witte Dame is a residential tower located in the newly built area Oosterheem in Zoetermeer. This area spans around 1 km^2 and lies at the Northeast side of Zoetermeer, adjacent to a rural area (see Appendix D). The Witte Dame is 40 m high and extends for most sectors well above the surrounding urban coverage, which could be classified as a low height but high building density. Major exceptions are found around sector 9, where a set of larger commercial towers are currently in construction within around 300-400 m distance. Some of these buildings extend in height above the Witte Dame. Towards sector 14 (NW), we find two smaller residential towers of 30m height within about 500-600 m distance. In figure 6.1 a general sketch is given of the surrounding land-use.

6.1.1 DEM-derived parameters

In calculating the surface DEM-derived parameters, a particular difficulty was that most of the buildings in Oosterheem were only recently constructed or still under construction. On the AHN-1 Digital Elevation Model, it was found that the entire neighborhood was missing. AHN-2, the successor of AHN-1, was produced more recently and indeed showed almost the entire neighborhood in full form. This DEM originally had a 1x1m resolution but we reduced the resolution to 5x5m so that we could easily integrate the new neighborhood in the original AHN-1 DEM of the region. Only a very limited amount of manual digitization was necessary, primarily to include a commercial center currently under construction in sector 9.

We calculate the surface parameters using the exact same settings which were found most appropriate for the Veilingweg ($D = 800m$, 16 sector division). The frontal and plan area density, average obstacle height, displacement height and roughness lengths (using Lettau) are given in table 6.1.

Table 6.1: Surface parameters calculated for the Witte Dame, using the method proposed in this report and a distance constant of 800 m (length units are in [m]).

Sector	λ_f	λ_p	z_d	$\overline{h}$	z_0 LE
1	0.07	0.19	3.3	10.9	0.40
2	0.02	0.04	1.3	13.4	0.18
3	0.04	0.06	1.6	16.1	0.31
4	0.09	0.16	3.5	10.4	0.47
5	0.10	0.18	4.1	11.3	0.57
6	0.12	0.21	4.2	10.1	0.60
7	0.11	0.21	4.3	10.3	0.57
8	0.11	0.18	3.9	10.8	0.58
9	0.12	0.27	6.9	14.1	0.82
10	0.08	0.30	4.3	7.9	0.35
11	0.09	0.24	4.7	10.7	0.51
12	0.08	0.18	4.2	12.5	0.52
13	0.07	0.15	3.3	13.8	0.47
14	0.08	0.13	3.1	12.4	0.51
15	0.11	0.19	3.9	10.4	0.57
16	0.09	0.26	4.0	8.1	0.34
Average	0.09	0.18	3.8	11.5	0.49

6.2 Roughness validation with turbulence measurements

The ultrasonic measurement campaign that started at the Witte Dame has two main goals: determination of the short-term wind climate and determination of the sectoral turbulence characteristics. Again, since the setup allows it, vertical components are also investigated.

6.2.1 Measurement setup

We use exactly the same instrumentation as on the Veilingweg; the Gill Windmaster Ultrasonic anemometer. The data acquisition setup and the connections are unchanged. Instead of a 7 m pole, a 6 m pole is initially used for practical reasons related to structural integrity and safety. In a later stage, the mast was extended by 1.3 m. The connection point on the roof was an existing safety ladder which was not designed to be loaded by the wind, so the choice was made for a lower mast and the use of additional guy-wires. Figure 6.2 depicts a top-view of the Witte Dame, where *s* indicates the location of the anemometer. The anemometer could not be installed right in the middle of the roof due to practical constraints. A photo of the setup is given in Appendix D.
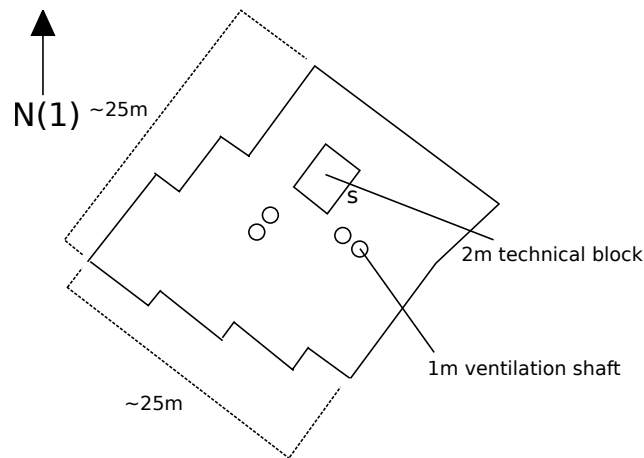
Top-view sketch of the Witte Dame (H=40m)

Figure 6.2: Top-view of the floor plan of the Witte Dame and the location of the ultrasonic anemometer.

6.2.2 Wind direction distribution

The data are processed in identical way as for the Veilingweg, only with the exceptions that all Pasquill stability conditions are included in the analysis. Figure 6.3 indicates the distribution of the wind direction over the measurement period. Relative to the Veilingweg, the distribution is more uneven. On the basis of this graph the choice was made to include all stability classes since some sectors have become very sparsely populated if this criterion is maintained. This decision was supported by the results from the Veilingweg, in which it became clear that the effect of non-neutrally stable conditions on our z_0 estimator was minimal.

6.2.2.1 Local turning of the wind

Local turning of the wind may be caused by the building, by blockage or by the surrounding surface. Similarly to the Veilingweg, sectors are assigned to simultaneous hourly data of Zestienhoven and a frequency plot is made giving the number of times the observed 10-minute sector at the Witte Dame is higher or lower (in clockwise manner) than Zestienhoven. The distribution of the wind sector differences for 4588 10-minute data points is given in figure 6.4.

On average, no turning could be identified of more than a sector, while the distribution appears to be slightly broader than the Veilingweg, with about 70% of the sector differences within -1 or +1 sector. The increased sector 10 frequency (figure 6.3) as compared to the KNMI raises the presumption that some
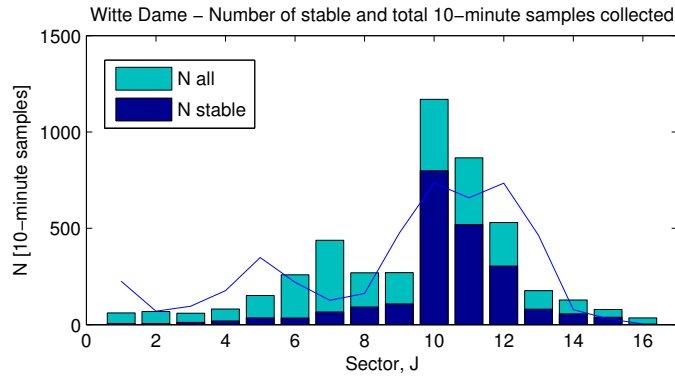
Figure 6.3: Wind direction distribution of the accepted data. The blue line indicates the direction distribution measured at Zestienhoven and is included to show effects of wind direction changes. It appears that the region between sector 10 and 14 are susceptible to most directional differences.
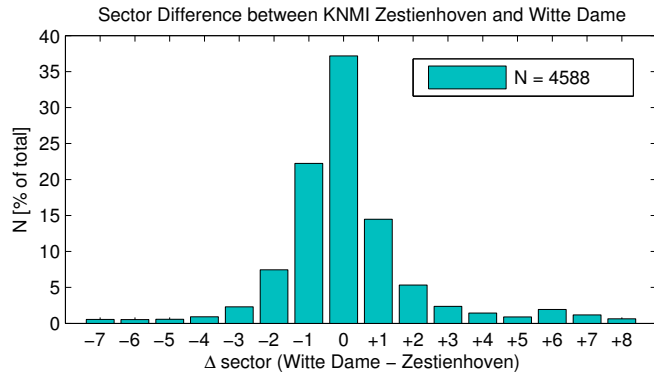
Figure 6.4: Histogram of the wind direction difference between Witte Dame and Zestienhoven based on 4588 10-minute data points.

turning effects may be present that distort our data. Sector 12,13 and 14 are relatively underpopulated and could as well be susceptible to direction change effects.

To investigate further, the data is binned per sector recorded at the KNMI weather station (this is a reliable mesoscale wind direction). Then for each bin, the percentage is calculated of observations at the Witte Dame that are turned clockwise and anti-clockwise. In case of no local direction changes, we can expect the directional error to follow a normal distribution centered around zero, which obviously implies that the clockwise percentage and anticlockwise percentage would be approximately equal.

The result for the Witte Dame is plotted in figure 6.5 (left), in which it can be seen that the two cannot be considered as comparable for all sectors (the sample size on which these percentages are based is given by the blue line in figure 6.3). Most alarming is that more than 50% of the data collected in sector 11 to 15 has been rotated one sector or more sector(s) backwards, while only a small part rotated forwards, causing a significant net average rotation towards sector 10. At the same time, there appears to be a smaller net average rotation also from lower sectors towards 10.

Given the absence of observable, nearby causes in the surroundings that could trigger a wind direction change towards sector 10, we strongly suspect building scale effects causing this turning. Figure 6.5 (right) indicates the assumed building scale effect.

In the remainder of this chapter, we prefer to use the KNMI sector over the Witte Dame sector as the most reliable estimate for the actual angle of the wind hitting the building. Hence, from now on, x-axes
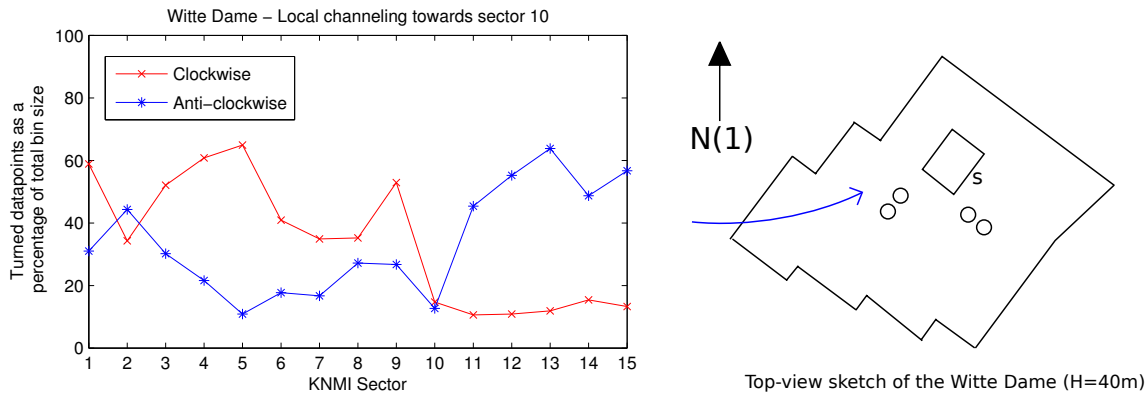
Figure 6.5: Left: Local turning effects for each wind direction. Right: The most important assumed building scale effect causing wind from W to align with SW direction.

denoted by *Sector, J* imply that the data point shown is the result of sectoral binning based on the KNMI direction. This also allows us to have a better populated sector 13 and 14, but also forces us to discard sector 16 as it only holds four 10-minute samples.

6.2.3 Spike removal

As opposed to the Veilingweg data, the Witte Dame data showed significant spikes; sudden, short-lasting increase in horizontal wind speed without any identifiable physical causes. Figure 6.6 depicts a period of spikes found by the maximum wind speed criterion.
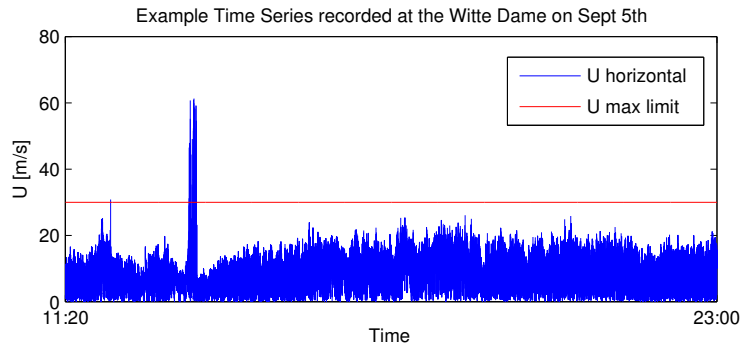
Figure 6.6: Unexplained sudden increase in the horizontal wind speed measured at the Witte Dame.

Besides the maximum wind speed criterion, our algorithm detected an increased number of spikes due to the maximum step difference set previously (5 m/s). In some cases, up to 72% of the 10-minute sample would be identified as a spike. With visual inspection, no real irregularities could be detected besides very gusty conditions. The question hence rose whether our criterion set earlier was to strict for the new location.

To test this, we first maintained the maximum step at 5 m/s and set the maximum number of spikes per 10-minute sample at 1%, leading us to reject 10% of the total samples. Second, we increased the maximum step difference to 8 m/s, remained the maximum number of spikes per 10-minute sample at 1%, leading us to reject 2% of the total samples. Upon comparison, it was found that both datasets did not lead to different roughness results so we maintained the original maximum step criterion.

6.2.4 Results 6 m pole length

We will now present the measured sectoral roughness lengths and the vertical wind speed components measured at the Witte Dame in the original setup (6 m pole length). In Appendix D one can find more detailed measurement results such as measured average wind speeds and extremes.

6.2.4.1 Measured sectoral roughness

The sectoral roughness is again determined using the ranking method with visual identification of a plateau and calculation of medians. Again, the distribution shape of measured roughness lengths differs largely between sectors. Generally, for sector 1 to 6, the z_0 distribution did not really show an inflection point and a clear plateau. These are labeled as a poor plateau. Yet, we maintain to use the median as the most appropriate measure and proceed by calculation those medians including a 95% confidence interval. The results are given in figure 6.8 and in a table in Appendix D.
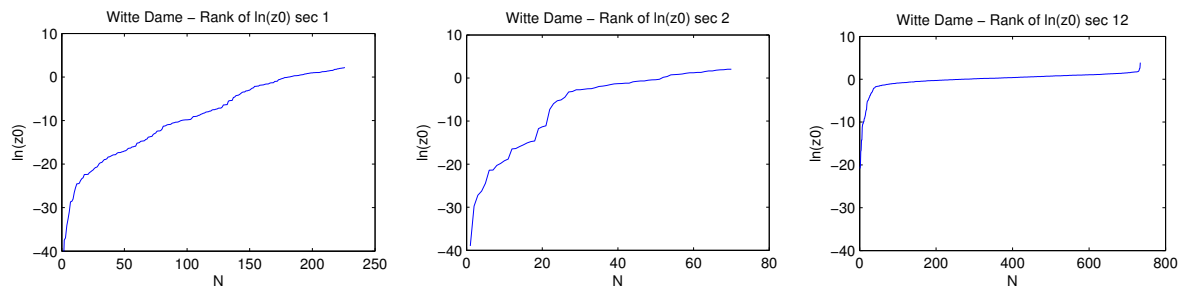
Figure 6.7: Different shapes after ranking $\ln z_0$ for the Witte Dame. Despite the sufficient number of data points, *sector 1* does not level off into a single plateau. *Sector 2* levels off slightly better, although it does not show a clear inflection point like *Sector 12* does. Note the difference x-scales used.
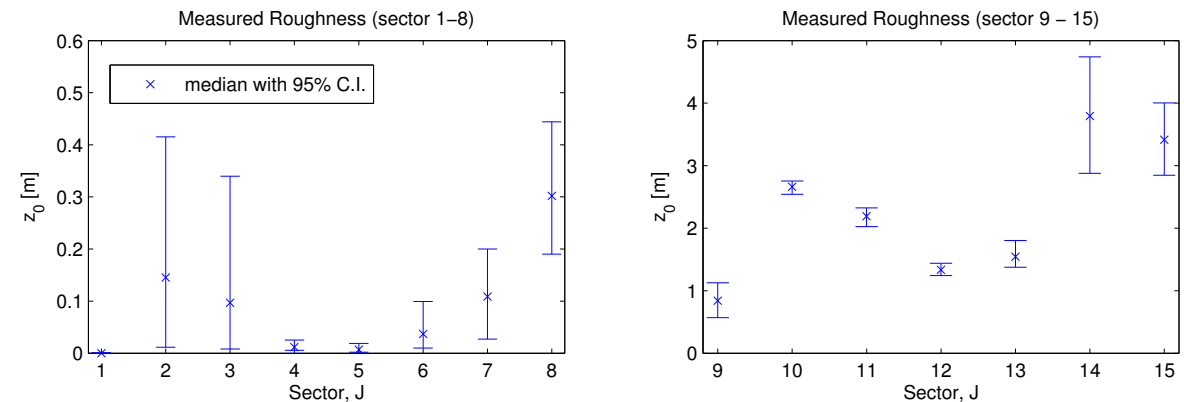
Figure 6.8: Estimates of z_0 through turbulence measurements including a 95% confidence interval (low setup). Two scales are used for better readibility.

The derived roughness lengths from the measurements are not as expected. In particular between sector 1 and sector 5, the resulting estimates are so low that they even include a zero (or 0.01) roughness length within the confidence interval. This is particularly striking since we cannot directly explain these results because of insufficient data points.

The Western wind directions (sector 10 to 15) also show quite unexpected roughness lengths, with sector 14 and 15 even above three meters. A three meter roughness length is one which would normally

be assigned to a high-rise urban class surface. Clearly, upon visual inspection, the surface does not qualify for that class.

6.2.4.2 Vertical wind speed components

Based on the KNMI sectoral binned data, we derive the vertical components as a fraction of the horizontal wind speed, see figure 6.9. Unlike the Veilingweg, we do not obtain a shape which has a clear symmetry, instead it can be seen that there exists a rather abrupt 'dip' in the average inflow angle between sector 8 and 14.

Based on these results, and the large tilt margin, currently no strong conclusions are drawn. In section 6.2.6.2 we reach a more definitive conclusion by comparison with vertical components measured in a new setup.
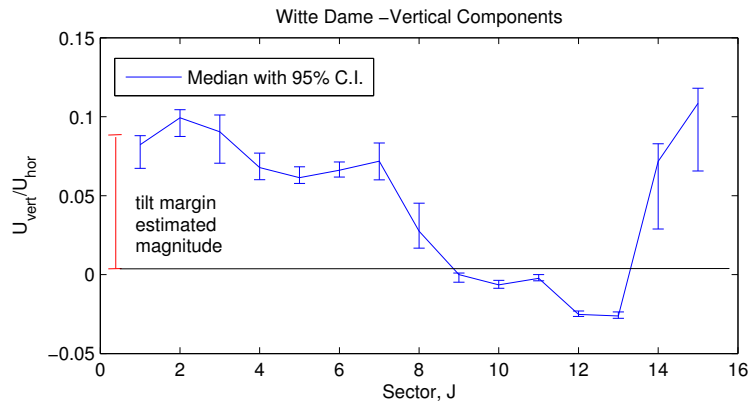
Figure 6.9: Vertical components recorded at the Witte Dame (low setup), also indicating the estimated (5 degree) error which could have been caused by a titled pole.

6.2.5 Interpretation of the measurement data

The measured roughness lengths (figure 6.8) do not compare well with the ones derived from the surface model (table 6.1). Furthermore, the measured results are not in-range to what would have been expected given the urban classes surrounding the site. For sector 1, 4 and 5, the values are between those found at calm sea (z_0=0.0002) and at flat terrain (z_0=0.03), the values for sector 2 and 3 are those found at terrain with low to high crops and for section 10, 11, 14 and 15 they are close to those found at a real high urban class.

First focussing on the small lengths that are found, a logical explanation lies in the fact that the Witte Dame is located close to a clear rural/urban boundary. This may imply that at a height of 46m, the sonic anemometer is still located in the original -rural- boundary layer instead of the internal -urban- boundary layer or the transition region between the two (see 2.2.1.3 for a definition of those layers). This appears a feasible explanation, given the relatively small distance to the rural surface transition. Still, assuming the flow indeed carried rural turbulence characteristics, the found values are relatively small to what one could expect given the actual rural environment around Oosterheem, which is covered by trees, a high-speed train track, an elevated road and several buildings. There should hence be other mechanisms surpressing the measured turbulence. After presenting the remaining results, this issue is further addressed in the discussions section.

In regard to the high roughness lengths between sector 10 and 15, the most feasible explanation is that these data points have been affected by roof edge separation effects. Referencing to Blackmore [10], the hypothesis is that the current setup is too low for the assumption that the turbulence intensity

is within +10% of the free-stream turbulence intensity. The sectors in the West may have been more severely affected than those in the East, either due to an increased distance to the roof edge, or due to separation caused by the small technical block on the roof (see figure 6.2). In any case, these effects seem to distort a proper assessment of the surrounding surface roughness, which is the primary reason to increase the mast and do a second 10-day campaign.

6.2.6 Results 7.3 m pole length

For a second 10-day measurement campaign, the mast is increased by 1.3 m in order to check whether building-scale separation vortices affect the surrounding turbulence, thereby distortion the roughness measurement originally intended. We anticipate on the expectation that we can lower the measured roof separation by increasing the mast, while the microscale roughness remains unaffected. A mast of 7.3 m is 0.5 m above the upper boundary of Blackmore's guideline. A higher increase would be advisable but was not possible due to potential rigidity and safety issues of the setup.

The new measurement collects data between the 7th and 17th of October. The weather during these 10 days was more variable leading to a better overall distribution of data points.

6.2.6.1 Measured sectoral roughness with the longer pole

Table 6.2 gives the measured sectoral roughness lengths for the increased mast. It can be seen in the third column that the found values in region 10-15 have decreased towards values that are certainly in-range of what the land-use criteria would predict. It is therefore strongly believed that the current setup leads to more representative values of the micro scale, implying that indeed the low setup was affected by building scale effects. To easify comparison, figure 6.10 depicts the estimated roughness for both mast lengths and indicates a large decrease in case of the higher pole length.

Table 6.2: Sectoral roughness lengths found through turbulence measurements at the Witte Dame (new setup). The column on the far right gives the DEM extracted roughness lengths.

sector	N	plateau	z_0 [m]	l.b. [m]	u.b. [m]	z_0 LE
1	30	poor	0.04	<0.01	0.11	0.40
2	30	poor	<0.01	<0.01	0.04	0.18
3	40	poor	0.03	<0.01	0.07	0.31
4	108	good	0.05	0.03	0.09	0.47
5	254	good	0.04	0.02	0.08	0.57
6	80	good	0.22	0.07	0.42	0.60
7	24	no	0.02	<0.01	0.23	0.57
8	64	poor	<0.01	<0.01	0.01	0.58
9	116	poor	0.24	0.10	0.37	0.82
10	24	no	1.58	0.92	2.23	0.35
11	40	good	0.75	0.52	1.01	0.51
12	288	good	0.73	0.67	0.78	0.52
13	82	poor	0.79	0.59	1.08	0.47
14	64	good	1.69	1.33	2.08	0.51
15	152	poor	0.74	0.67	0.96	0.57
16	58	poor	0.89	0.56	1.26	0.34

Considering the new results to be a more valid measurement, a comparison is made with the DEM-derived roughness which is repeated in the right column of table 6.2. Between sector 1 and 9, the turbulence-derived roughness is still low, mostly comparable with grassland. A better alignment is found in sector 10 to 16, where the final values also correspond better to the values expected due to the land-use. The two peaks found, one in sector 10 and one in sector 14, align quite well with the commercial and the residential tower located nearby. The first peak, now around sector 9, also results in a local high roughness value in the DEM.
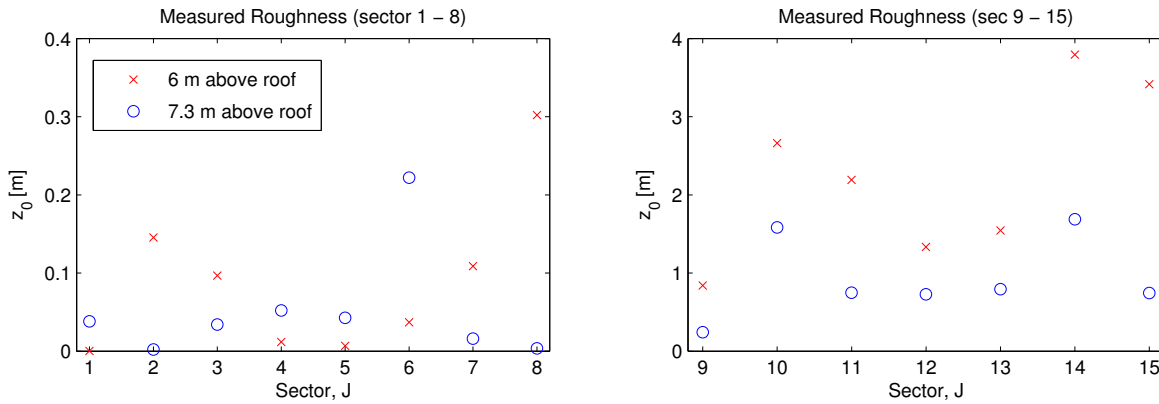
Figure 6.10: Estimates of z_0 through turbulence measurements (high setup). A large decrease of the estimated roughness was obtained in sector 8 to 15 by slightly increasing the anemometer height. Note the different scales used. Confidence intervals are given in table 6.2.

6.2.6.2 Vertical components with the longer pole

The increased measurement height also enabled re-analysis of the vertical components. In figure 6.11, it can be seen that the mast increase has not led to a large changes for most sectors, although the new medians do not always overlap with the original confidence intervals.

The strong similarity between the new and the old profile is striking in positive sense because the complete mast setup was put down, increased in length, put up and remounted at a steady and approximately straight position by tensioning the guy-wires. This result therefore gives us an increased confidence that the vertical components indeed reflect the actual flow situation and that the error margin stated earlier was too conservative.

Therefore, we can state that the long stretch of roof in the sectors 9 to 13 diminishes the vertical components so that the average flow is practically parallel to the roof. Furthermore, it is positive to see that a good picture on the vertical components is obtained after only 10-days of measurements.
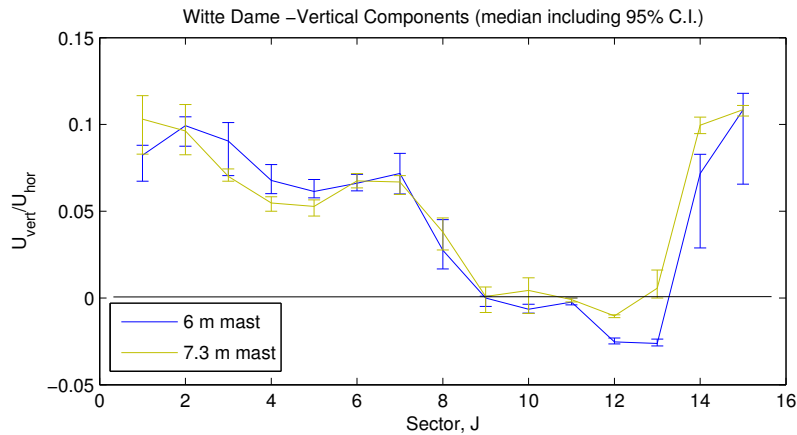
Figure 6.11: Vertical components recorded at the Witte Dame (low and high setup). Line indicates medians including a 95% confidence interval for two measurement heights. The mast was removed, increased in length, and re-mounted on the same position.

6.3 Observed wind climate compared to model prediction

Now a comparison is presented between the observed wind climate at the Witte Dame and the prediction obtained from the method proposed in this report (third extension). Lettau's roughness lengths derived from the surface parameters around the Witte Dame (table 6.1) are integrated in a roughness structure to enable direct use of WAsP to make a wind climate prediction. As a reference wind climate, we strictly select observations at Zestienhoven corresponding to the measurement period, which runs from Aug 30th to Oct 2nd. The height is set at 42 meters to compensate for a small displacement height which has been estimated at 4 m. Running the simulation now yields a predicted wind climate for the Witte Dame. Figure 6.12 depicts this prediction in comparison with the observed 10-minute means per sector.
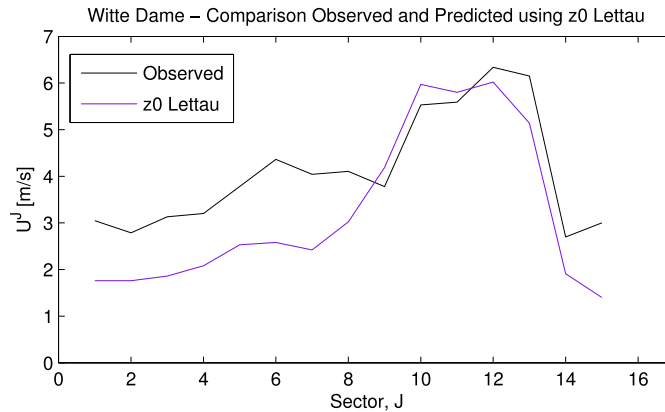
Figure 6.12: Model application ($D = 800$m) and comparison with observed wind climate at the Witte Dame (1 month data, low measurement height). Sector 16 is omitted since only 4 data points were available.

Again, the black line above the purple line could imply that the model roughness has been estimated too high. This is most clearly the case in sectors 1 to 7 and 15, where there is a 1 to 1.5 m/s under prediction compared to the observed wind speed. The satisfiable accuracy in the other sectors indicates that the urban surface roughness was well extracted from the DEM.

6.3.1 Under prediction and choice of distance constant

There is a clear under prediction for the region between sector 15 (NNW) to 7 (SW). This coincides generally with the sectors that hold a nearby rural/urban boundary (see figure 6.1). One possible hypothesis is therefore an under prediction occurs due to a 'defect' of the distance weighing function –which we defined in Chapter 2 and calibrated in Chapter 3. It could be that too much weight is attributed to the nearby surface instead of the surface further away, and the Witte Dame in fact experiences a rural boundary layer while the extracted roughness is primarily sub-urban. This explanation seems supported by the minimized turbulence levels experienced in the flow from these directions, even lower than those found at the Veilingweg.

As a test, a standard rural roughness length (0.03 m) is integrated in the WAsP model and the calculations are performed. As expected, an increased wind speed is obtained, however it is still well below the measured sectoral means at these sectors, see figure 6.13. This implies that an improved distance constant could only partially improve the prediction. No attempts are currently made to find new tailored substitute for the 800 m distance constant. Given the consistent difference between the rural boundary layer prediction and the observed wind speed, it seems most likely that a building-induced speed-up plays a role in these sectors.
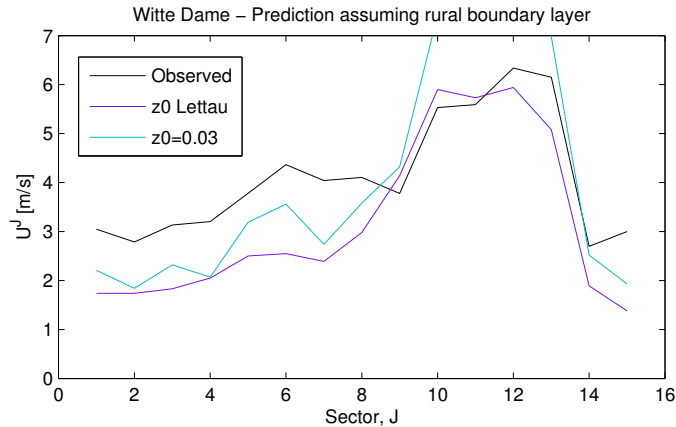
Figure 6.13: Limit of the wind speed prediction in sector 15 to 7 assuming a standard rural roughness length.

In Appendix E a long-term prediction of the wind climate at the Witte Dame is presented, also indicating the potential effects of a localized speed-ups on the energy density. This shows a potential increase of 32% on the annual average power in the wind.

6.4 Conclusion

After developing and calibrating the general surface processing method on the Veilingweg data, this chapter could be seen as a validation for the chosen approach. For this new site, two analyses were performed. First, the roughness lengths derived from the DEM were compared with those from turbulence measurements; second, the wind climate measured at the Witte Dame was compared to a WAsP prediction using this same DEM roughness and zero-plane displacement height.

Initially, it was found that turbulence measurements using the low mast were largely affected by roof separation with wind from sector 8 to 15. This was suspected given the high levels of fluctuations and could finally be confirmed by the reduced turbulence after increasing the mast by 1.3 m. Although the new roughness lengths are more in-range of those expected, it is still unknown whether these sectors are still contaminated to some extend by roof separation.

Despite the remaining uncertainty regarding building-induced turbulence, peaks in measured surface roughness for sector 10 and 14 correspond to the approximate sectors holding a commercial high-rise building and a large residential building. The first peak is also found in the DEM, around sector 9, corresponding to the same high-rise commercial building. The large residential building towards sector 14 show up with a peak in the average obstacle height but its contribution to the DEM roughness length is minimized due to a small frontal area density in that sector.

The measured surface roughness is very low in sectors 15 to 8. This could partially be explained by the rural surface transition which occurs in those sectors. The initial hypothesis was therefore that this difference was caused by a shortcoming of the distance weighing function. Initially, this seemed confirmed by the under prediction in sector 15 to 8 from the WAsP simulations using DEM roughness. Yet, when the WAsP simulation was ran using a standard rural roughness length, this under prediction was largely sustained. The final conclusion is therefore that the boundary layer may hold strong rural characteristics, but on top of that, building-induced speed-ups from those sectors are the most important contributor to the under predicted wind speed. As will be discussed in the following section, this building effect could in return also caused distortions in the roughness measurements.

The sectoral profile of vertical components was obtained with an increased confidence after re-

installation of the mast. Very similar profiles before, and after re-installation show that the results are less likely distorted by a mast tilted error, but rather really representing the actual average streamline shape. Furthermore, it was found that only a limited amount of data points were required, approx. 30 per sector, to obtain a rather good estimate for these vertical components. Depending on the variability of the weather, local building-induced effects may be known after measuring for about 10 to 20 days.

6.5 Discussion

The results from this case study show that the wind atlas modelling may result in an under prediction for an urban location. For about half of the sectors, measured velocities are higher than expected using any kind of surface roughness. We therefore tend to attribute this result to effects not in the microscale but in the building scale, in particular to building-induced speed-ups. While there is no easy way at hand to confirm that it is this building scale rather than a microscale or model peculiarity, two additional observations support the building scale hypothesis. First of all, the vertical components around 0.1 [-] indicate the presence of an inclined shear layer, and this occurs in exactly those sectors having a strong under prediction. Second, the turbulence levels are very low, indicating that the anemometer is indeed above this shear layer.

Still there are several points open for discussion. To fully attribute WAsP's under prediction to building scale effects, it has to be assumed that a speed-up with a magnitude of 40 to 50% has occurred. This seems too close to the theoretical speed-up limit of 50% which was calculated by S. Mertens and certainly not in-line with his CFD simulations on wind over buildings, which showed a speed up of no more than 25% [37]. Other studies, such as the wind tunnel experiments of P. Blackmore indicate a speed-up ratio of around 20% for rectangular buildings [10] in urban boundary layers. M. A. Heath and J. D. Walshe report CFD results showing a larger speed-up, 30 to 50%, for smooth upstream surface ($z_0 = 0.001$ m), but their inclined roof geometry makes comparison with the current case difficult [23].

Another point of discussion why the results do not give an under prediction for all sectors, also including 10 to 13. May we not, given the approximately symmetrical geometry, expect a similar blockage and thus a similar speed up for all sectors? In general, this should be the case, but for this site a number of conditions are such that they could potentially block a measured speed up.

First of all, sectors 9 to 13 do not show a positive vertical component which could indicate local curvature of the average streamlines. Again in reference to the results by Blackmore, a acceleration often coexists with a vertical component. His results also indicate that an acceleration may initially exist near the roof edge, but gradually diminishes when moving away from the edge, as the average streamlines settle more parallel to the roof. Because parallel flow has indeed been measured, and the distance to the roof edge is longer for those sectors, this would be the first feasible explanation.

Second, as S. Mertens has clearly shown (figure 2.11 in this report), the surrounding microscale roughness has an effect on the steepness of the separation shear layer and thereby also on the induced speed-up. In case of an increased rough upstream surface, the total momentum in the wind profile between the ground and the rooftop may be decreased, resulting in a decreased amount of momentum that is forced over the roofs edge. This corresponds to the conclusion of M. A. Heath and J. D. Walshe that the speed-up may diminish if the building becomes part of a dense group [23].

Probably the second most preculiar result of this measurement campaign is the low surface roughness found in sector 1 to 8, with values more in range of calm sea. No measurement errors could be detected or errors due to the data treatment. Yet, the coexistence of the decreased turbulence with a consistent vertical component and a local mean wind speed, revealed some similarity with results of decreased TI measured above hilltops.

In a number of field experiments, reduced turbulence intensities were measured in coexistence with a local flow acceleration at the hilltop (D. Founda et al. gives an overview, see [19]). Some of these observations were attributed to a rapid distortion effect. Rapid distortion theory states that eddies with a larger typical length scale of the hill, are advected over the hill sufficiently rapidly that the turbulent

fluctuations observed at the hilltop are modified by compressing and stretching of eddies as they are suffer from changes in the mean flow. The reduction of turbulent fluctuation is not yet compensated by additionally produced turbulence due to the distortion, as these large eddies do not react quickly. This may lead to an effective reduction of the $\frac{\sigma_U}{U}$ ratio, even as high as -30%, in a case presented by Founda et al. [19].

Obviously, the current setup is not totally comparable with a hilltop, so this explanation should serve mainly as an illustrative case how the current results may have been affected by these mechanisms. Yet, given the high sensitivity of the roughness estimates to reductions in the turbulence intensity, even a slight TI reduction has big effects on the present results. A simple sensitivity analysis on this effect is given in Appendix D.

A final point of discussion is whether we can or cannot consider turbulence measurements from sector 10 to 14 obtained at 7.3 m above the roof to be free of building-induced effects. Following the rule of thumb by Blackmore, the minimum height to reduce separation induced turbulence to below 10% is between 4.8 to 6.8 m for a 40 m building, meaning the current measurements are reliable. The maximum z_0 values are around 1.5 m, which is probably not too far off, given some high-rise buildings around the Witte Dame. Yet the wind speed measurements indicate otherwise, namely that the DEM-derived roughness from those sectors is most appropriate; we did not measure a momentum loss corresponding to a surface roughness of 1.5 m.

A final point of remark is that it would be very interesting to further untangle the building scale from the microscale, for instance by installing a second anemometer closer to the Southwestern roof edge which should measure simultaneously. This could shed light on the relation between speed-up effects and the microscale, and flow development over the stretch of roof. More ideally, CFD simulations of this Witte Dame setup are included for comparison. If this is done, the DEM-derived surface roughness and displacement height extracted in this study could be used to help setting the boundary conditions for this simulation.

Chapter 7

Conclusion

For urban wind energy, selecting a site with an advantageous rooftop wind climate is crucial. Yet, this climate often has to be predicted. Obtaining a reliable rooftop wind climate prediction is challenging as it should be made in consideration of the mesoscale, microscale, and building scale effects. This project is an attempt to improve the prediction methodology of urban rooftops.

In general, this project shows that the wind atlas approach remains a suitable framework for wind climate prediction during site selection or performance estimation processes. Yet, its application for urban (rooftop) sites is controversial, which was confirmed by some initial modelling results of the Veilingweg performed in this study and a previous project.

For this project to be innovative, efforts were made to implement high-resolution digital elevation data within the wind atlas framework, either as a complement to the land-use map or as a complete substitute for the land-use map, with the primary goal to improve the wind atlas prediction for urban rooftops. Let us recall the main problem definition as stated in the introduction:

> In what way(s) could a Digital Elevation Model of the surroundings be used to better predict the rooftop wind climate for urban locations using the wind atlas approach?

After a literature review, it was concluded that such method would only make sense for rooftops clearly above the roughness sublayer - inertial sublayer interface. This is the first delimitation of the project. In the inertial sublayer above the interface, it is assumed that the wind profile can be described in terms of an urban roughness length and zero-plane displacement height. It became apparent that there are existing empirical relations between those terms and parameters of the upstream surface, such as the plan area density, average obstacle height and frontal area density.

The project was further outlined by defining three possible extensions which justified further investigation:

1. Inclusion of a zero-plane displacement height correction to the LGN3+ prediction (omni-directional or sectoral)

2. Inclusion of a frontal area density correction to the LGN3+ prediction (inspired by the ΔRIX adjustment)

3. Application of DEM-derived surface roughness length instead of LGN3+ roughness

Extraction of the zero-plane displacement height, frontal area density and urban surface roughness was obtained with the use of MATLAB scripts. These procedures essentially all involved the use of a certain distance weighing function, which in this project was chosen to be exponential with distance constant D.

The Veilingweg acted as a suitable testing location for the three extensions given the established long-term rooftop wind climate. This resulted in the following general conclusions:

- The original LGN3+ prediction led to erroneous results in some sectors

- A zero-plane displacement height correction appears to primarily make sense for rooftop extending just above their surroundings. At the height of the Veilingweg (30m), a z_d correction could reduce the mean absolute sectoral error by only 10%.

- The best improved prediction was obtained by implementing DEM-derived urban surface roughness directly in WAsP

At the Veilingweg, there were large differences in the calculated frontal area density between different sectors. In particular, the Southwestern sectors indicated a high density, probably due to a nearby high-rise residential area. The formulation of Lettau appeared to most successful in summarizing the complex upstream surface into a single value for each sector. This was checked by comparing the observed wind speed with the predicted wind speed using DEM-derived roughness. An optimal value for D was established: 800 m.

More trust in the third 'roughness' extension was gained after it was found that again a satisfiable prediction could be obtained for a second urban rooftop, the Witte Dame in Zoetermeer. The prediction was not as good as the Veilingweg, but encouragingly enough it was good for the most urban sectors. Most notable errors were under predictions, which, upon further inspection, seem to indicate some building-induced speed-up may be present. This is noteworthy since these have not been measured as such at the Veilingweg.

In search for additional validation for the urban roughness lengths, two 10 Hz turbulence measurement campaigns were held, first one at the Veilingweg (5-weeks) and then one at the Witte Dame (7 weeks). The Veilingweg campaign was most successful, as a clear sectoral roughness distribution could be determined. The measured surface roughness was in-range of what could be expected given the urban surroundings and the sectoral distribution showed similarities with the distribution from the DEM. On average, the measured surface roughness was lower than the roughness obtained from the DEM analysis (0.47 as compared to 0.67 m).

As opposed to the Veilingweg, the anemometer at the Witte Dame appeared to be measuring within or below the shear layer for some sectors. This was concluded given very high roughness estimates (>2m), turbulence intensies, and no or slightly negative average vertical components for some sectors. After removing the mast, increasing it in length, and remounting it on the original position, more sensible roughness values were obtained. However, it cannot be said with confidence that the new measurement results are indeed unaffected by building-induced separation. The primary reasons for this is that there no average vertical components were measured from these sectors and that the roughness lengths were still rather high as compared to the mean wind speeds.

Some Northern and Eastern sectors at the Witte Dame indicated a very low estimated roughness, even below what could be expected from a rural terrain. It has been argued on theoretical grounds that this may have been caused by a rapid distortion effect; a reduction of the perceived TI which may occur at a local speed up. If this would indeed be the case, it could mean that roughness measurements in urban terrain may be an even more delicate undertaking than initially expected.

We finalize with the most important general conclusions from this project:

- Urban height data can indeed be implemented to yield a good wind resource prediction for the two rooftops in the region; although a more profound basis of experimental evidence can further substantiate the chosen approach.

- For optimal turbine siting, building scale effects remain important to consider, given the regions of variable TI and speed-ups.

- Urban surface roughness measurements are possible using a sonic anemometer, although effects of the building should be minimized as outcomes are highly sensitive to distortion.

Chapter 8

Recommendations and final remarks

This final chapter presents some recommendations for further study, regarding the use of WAsP, the use of Digital Elevation Models, and rooftop measurements. Furthermore, some remarks are given about the choices made in this project.

Urban roughness parameterization

There is an inherent danger for over-simplification when the urban surrounding, in its full complexity, is only reduced to two variables; z_0 and z_d. It is known that individual obstacles may interact with each other and do not simply contribute in a linear sense to the effective perceived surface roughness downstream. For example, a large building upstream may shelter smaller buildings, thereby reducing the effect these smaller buildings have to the actual roughness. These 'interaction effects' cannot be accounted for in the present analysis, which is an important shortcoming.

Further on this topic, it has to be admitted that only neighborhoods consisting of buildings with equal size and spacing, form a coherent urban texture which is comparable to the experimental setups from which the formula's of z_0 and z_d were derived. In using these parameters for real heterogeneous urban surfaces, it has to be assumed that deviations from this homogeneity lead to minimally different results in the eventual wind profile which develops. While results in this study prove the principle works, a remark has to be made that study of more rooftop wind climates and DEM parameters is advised.

More studies could also further shed light on the choice for an appropriate distance weighing function. In theory one could expect the distance constant D to vary with height; a higher rooftop will experience a larger effect of roughness located further away. The shape of the weighing function now used could be improved to be more similar to the footprint model (figure 2.5). It could for instance reflect in better way that very nearby roughness elements with low height do not influence the perceived roughness at the roof.

Digital Elevation Model

The Digital Elevation Model used in this project, AHN-1, was produced before 2003 and had a resolution of 5x5 m. Since 2008, digital height data in the Southwest of the Netherlands has been made available at a 1x1 m resolution, under the name AHN-2. This opens up more advanced possibilities, for instance more accurate separation of buildings from vegetation. For the current project, this higher resolution has not been used due to a bad trade-off between computational time and expected improvement, but this may change in the future when AHN-2 becomes the standard.

At a final stage in this project, it was found that there exists a filtered and a non-filtered AHN. The non-filtered AHN represents the actual ground level of the Netherlands. This discovery makes the erosion-dilation task presented in Chapter 3 not necessary. Yet, as it is still used in the further project, this part was not removed from the report.

Computational Methods

More time can be spend on optimizing the extraction of surface parameters from the DEM. As this project was illustrative for only two urban sites, we have not pursued to do so. Yet, if the same analysis would be continued for the entire region under consideration, optimization is essential. Currently, the most time consuming process is rotating the grid. Smarter programming can greatly decrease the loads.

It would be interesting to compare our computational method for the extraction of frontal area densities with methods proposed in literature, such as by Ratti et al. [42].

The use of WAsP

When producing the WAsP resource grids, based on LGN3+ roughness, they can only be solved for a constant height above ground level. Full integration of a zero-plane displacement height map in WAsP is therefore difficult, because in case this map is integrated as surface orography, WAsP will produce a resource grid for a constant height above this (fictional) orography. A possible improvement would be to enable integration of two separate maps is WAsP: a ground level map, which fixes the resource grid, and a zero-plane displacement height map, which shifts the log profile according to the local z_d.

The LGN3+ roughness land-use database was produced in 1997 and starts to get outdated. Especially in the West of the Netherlands, newly built residential and commercial neighborhoods continue to replace rural landscapes, which for instance became obvious in Oosterheem, the region of the second case-study. In this light, the rather new AHN-2 may be used in some way to update the LNG3+

The proposed implementation of urban roughness in WAsP –the wheel-shaped structure– largely by-passes the roughness change model of the program. We have retained WAsP for the purpose, but we should note coupling a roughness length to a known mesoscale wind climate may easily be performed without WAsP, for instance by assuming a blending height.

Optimal turbine siting

Regarding optimal turbine siting, this project has mainly focused on mean wind speeds as an indicator for the available energy in the mean wind speed distribution. The remark has to be made that, in practice, the technical success of an UWT is also highly dependent on selecting a site which minimizes loads. This criterion is not inferior to the mean wind speed criterion and should be considered with similar attention.

The actual position on the roof, and the height above it, are important determinants for turbulent loads. During the project, we have come across several examples of insufficiently positioned turbines. Mostly, installation heights were too low to assume the turbine extended above the separation shear layer –considering all directions, or the roof was too low to consider it in the inertial sublayer. In some cases it is suspected that one or more turbines positioned on the Northeast side of the roof were exposed to a turbulent shear layer coming from the Southwest side of the roof. This may be particularly harmful since extreme wind conditions occur often from those sectors.

We would like to propose the following sequence of steps to be followed for optimal turbine siting and performance prediction:

1. Visual assessment of the site, estimate of the surrounding roughness sublayer height and identification of possible shelters.

2. Estimation of the rooftop wind climate by the method proposed in this report. Establish an AEP prediction based on this climate.

3. Short (10-day) sonic measurement campaign at the proposed turbine position to investigate building-induced effects.

A short measurement campaign is still advised as it yields to a better understanding of the building-induced effects than simplified rules-of-thumb supply us with. In general, zones with consistent measured vertical components and a TI which is lower than expected may indicate flow acceleration. Zones with increased TI (higher than 30% at 5 m/s) may indicate localized shear layer effects. The real bottleneck in such a measurement campaign is the (non-) variability of the weather.

Current measurements at the Witte Dame have indicated that slightly changing measurement height may reduce the TI from 35 to 25 % for some sectors. This also indicated that rules-of-thumb from literature do not always apply. Better knowledge of local beneficial and harmful conditions can reduce the costs that come with turbine under performance or damage. A short measurement campaign, if done efficiently, does not weigh up to turbine (re)installation costs, repairs, and initial investment which may be at risk. Furthermore, as the results of the Witte Dame have shown, power density can be increased up to 32% by in the speed-up regions. A correctly located turbine can reap significant benefits of both a mean wind speed increase and minimized turbulence.

An important cost driver in the measurement campaigns was that a tailored measurement structure had to be created for every studied site. A standardized and more professionally designed measurement mast may greatly reduce those costs. At least, smart solutions should be found for guy-wire attachment and structural rigidity on various roofs.

Sonic measurements, when more structurally performed in industry, also help to build up a broader knowledge base. Every roof that is studied contributes to a gradual increase in expertise and can be used for comparison with future site assessments. An innovative logging system as used in this study can be inexpensive and energy-efficient, and should be used as the basis for a streamlined data analysis.

Sonic Roughness Measurements

As with any field study, the turbulence measurements in this campaign where susceptible to uncontrollable circumstances. Practical constraints often limited positioning the mast in the exact middle of the roof or high enough to reduce building induced effects. At the Veilingweg, a very rigid roof structure was available so that the high mast could be installed without problems. Furthermore, it was positioned on top of a smaller technical building (4m), so that the effective height above the main building was further increased to around 11m. This may explain the success of these measurements.

   At the Witte Dame, no rigid structure was available on top of the small technical block, so improvisation was necessary. After reviewing all the measurement results, the conclusion drawn is that the urban roughness measurement generally failed in its purpose, although the vertical component and wind speed measurements yielded expected results. It was found that zones of largely varying TI above a roof make a distinction between the microscale and the building scale TI very difficult. In this sense, the higher the mast, the lesser these unknown effects and the more likely it is that a better roughness measurement is obtained. The criterion by Blackmore can be seen as the minimum anemometer installation height, but a preference would have been to install longer masts.

   For similar roofs studied in the Dutch climate, the effects of atmospheric stability on the results are considered small and not very important to correct for. This may change for different climates and higher roof heights. As stated before, the bottleneck in the field measurements are the varying weather conditions. Results from the 10-day campaign and the 4-week campaign are largely comparable because the 10-day campaign had a more variable wind rose.

Bibliography

[1] *European Wind Atlas*. Risø National Laboratory, 1989.

[2] *Small-scale Wind Energy Technical Report*. Meteorological Office UK, 2008.

[3] *ASHRAE Handbook of fundamentals*. Chapter 24 Airflow around buildings, 2009.

[4] Francis Allard. *Natural Ventilation in Buildings*. James & James (Science Publishers) Ltd., 1998.

[5] Alterra. Land Gebruik Nederland 3+ database, 1997.

[6] Douglas A. Altman. *Statistics with Confidence*. BMJ Publishing Group, 2000.

[7] N. J. Bagal, B. Singh, E. R. Pardyjak, and M. J. Brown. Implementation of rooftop recirculation parameterization into quic fast response urban wind model. *5th Symposium of the American Meteorological Society on the urban environment, Vancouver, BC, Canada*, 2004.

[8] A.C.M. Beljaars and A.A.M. Holtslag. Flux parameterization over land surfaces for atmospheric models. *American Meteorological Society*, 30:327–341, 1991.

[9] Erik Berge, Arne R. Gravdahl, Jan Schelling, Lars Tallhaug, and Ove Undheim. Wind in complex terrain. a comparison of WAsP and two CFD-models. *EWEC conference paper*, 2006.

[10] Paul Blackmore. *Building-mounted micro-wind turbines on high-rise and commercial buildings*. BRE Press, 2010.

[11] Bert Blocken. Lecture slides introduction to CFD in building engineering, 2010.

[12] Anthony J. Bowen and Niels G. Mortensen. WAsP prediction errors due to site orography. *Risø National Laboratory*, 2004.

[13] Tony Burton, David Sharpe, and Nick Jenkins. *Wind Energy Handbook*. John Wiley & Sons Ltd., 2004.

[14] Hong Cheng and Ian P. Castro. Near wall flow over urban-like roughness. *Boundary Layer Meteorology*, 104:229–259, 2002.

[15] O. Coceal, T.G. Thomas, I.P Castro, and S.E. Belcher. Mean flow and turbulence statistics over groups of urban-like obstacles. *Boundary Layer Meteorology*, 121:491–519, 2006.

[16] Ebba Dellwik, Lars Landberg, and Niels Otto Jensen. WAsP in the forest. *Wind Energy*, 9:211–218, 2006.

[17] Judith A. Berglund Donald E. Holland and Joseph P. Spruce. Derivation of effective aerodynamic surface roughness in urban areas from airborne lidar terrain data. *Journal of Applied Meteorology and Climatology*, 47:2614–2626, 2008.

[18] Jacob A. Wisse Eddy Willemsen. Design for wind comfort in the netherlands: Procedures, criteria and open research issues. *Journal of Wind Engineering and Industrial Aerodynamics*, 95, 2007.

[19] D. Founda, M. Tombrou, D.P. Lalas, and D.N. Asimakopoulos. Some measurements of turbulence characteristics over complex terrain. *Boundary Layer Meteorology*, 83:221–245, 1997.

[20] Gill Instruments Ltd. *WindMaster 3D Ultrasonic Anemometer Technical Information*, 2011.

[21] Todd S. Glickman. *Glossary of Meteorology, Second Edition*. American Meteorological Society, 2000.

[22] C.S.B. Grimmond and T.R. Oke. Aerodynamic properties of urban areas derived from analysis of surface form. *Journal of Applied Meteorology*, 38:1262 – 1292, 1998.

[23] Malcolm A. Heath and John D. Walshe. Estimating the potential yield of small building-mounted wind turbines. *Wind Energy*, 10:271–287, 2007.

[24] J.G. McGowan J.F. Manwell and A.L. Rogers. *Wind Energy Explained*. John Wiley & Sons Ltd., 2002.

[25] S.M. Arens J.H. van Boxtel, G. Sterk. Sonic anemometers in aeolian sediment transport research. *Joint Conference International Center for Arid and Semiarid Lands Studies, Texas Tech University*, 2002.

[26] Yuguo Li Jian Hang, Mats Sandberg. Effect of urban morphology on wind conditions in idealized city models. *Atmospheric Environment*, 43:869–878, 2009.

[27] Finnigan J.J. Kaimal, J.C. *Atmospheric Boundary Layer Flows, Their Structure and Measurement*. Oxford Univ. Press, New York, 1994.

[28] Susumu Karita and Manabu Kanda. Characteristics of boundary layer over a sequence of small localized urban canopies with various heights obtained by wind-tunnel experiment. *Journal of the Meteorological Society of Japan*, 87:705–719, 2009.

[29] KEMA. *Windkaart van Nederland*. Senter Novem, 2005.

[30] KNMI. *Toelichting Stabiliteit van Pasquill (uurgegevens)*. KNMI Klimaatdata en Advies.

[31] KNMI. *Dataset Zestienhoven*. KNMI Klimaatdata en Advies, 2011.

[32] L. Landberg. The mast on the house. *Wind Energy*, 3:113–119, 2000.

[33] Laura S. Leo, Silvana Di Sabatino, Rex E. Britter, Carlo F. Ratti, A. Dallman, and Harindra J.S. Fernando. Parameterisation of in-canopy and exchange velocities based on the morphometric analysis of real urban canopies. *The Seventh International Conference on Urban Climate, Yokohama, Japan*, 2009.

[34] H. Lettau. Note on aerodynamic roughness parameter estimation on the basis of roughness element description. *Journal of Applied Meteorology*, 8:828–832, 1969.

[35] R.W. MacDonald. Modelling the mean velocity profile in the urban canopy layer. *Boundary-Layer Meteorology*, 97:25–45, 2000.

[36] R.W. MacDonald, R.F. Griffiths, and D.J. Hall. An improved method for the estimation of surface roughness of obstacle arrays. *Atmospheric Environment*, 32:1857–1864, 1998.

[37] Sander Mertens. *Wind Energy in the Built Environment*. Multi-Science, 2006.

[38] F.T.M. Nieuwstad. *Turbulentie*. Epsilon Uitgaven, Utrecht, 1998.

[39] T.R. Oke. Street design and urban canopy layer climate. *Energy and Buildings*, 11, 1988.

[40] S.P. Oncley. Flux parameterization techniques in the atmospheric surface layer. *Phd. Dissertation University of California, Irvine*, 1989.

[41] Ole Rathmann, Niels G. Mortensen, Lars Landberg, and Anthony Bowen. Assessing the accuracy of WAsP in non-simple terrain. *Paper presented at the BWEA18 conference*, 1996.

[42] C. Ratti, S. Di Sabatino, E. Britter R Solazzo, M. Brown, F. Caton, and S. Burian. Analysis of 3-D urban databases with respect to pollution dispersion for a number of european and american cities. *Water, Air and Soil Pollution: Focus*, 2:459–469, 2002.

[43] S. Di Sabatino. A simple model for spatially-averaged wind profiles within and above an urban canopy. *Boundary Layer Meteorology*, 127, 2008.

[44] J. Marshall Shepherd. A review of current investigations of urban-induced rainfall and recommendations for the future. *Earth Interact.*, 9:1–27, 2005.

[45] Teresa Simoes, Paulo Costa, and Ana Estangueiro. A first methodology for wind energy resource assessment in urbanized areas in Portugal. 2009.

[46] Di Sabatino S. Aquilina N. Dudek A.V. Britter R Solazzo, E. Coupling mesoscale modelling with a simple urban model. *Boundary-Layer Meteorology*, 137:441–457, 2010.

[47] Roberto Sozzi and Maurizio Favaron. Method for estimation of surface roughness and similarity function of wind speed vertical profile. *American Meteorological Society*, 1998.

[48] Andrew Stepek and Ine L. Wijnant. Interpolating wind speed normals from the sparse dutch network to a high resolution grid using local roughness from land use maps. *KNMI*, 2011.

[49] Ronald Stull. *Meteorology for Scientist and Engineers*. Brooks Cole, 2 edition, 1999.

[50] I. Troen. WAsP forums. *http://www.wasptechnical.dk/forum/viewtopic.php?id=305*, 2011.

[51] I. Troen. WAsP forums. *http://www.wasptechnical.dk/forum/viewtopic.php?id=258*, 2011.

[52] J. W. Verkaik. Evaluation of two gustiness models for exposure correction calculations. *Journal of Applied Meteorology*, 39:1613–1626, 1999.

[53] J. W. Verkaik. *On Wind and Roughness over Land*. Wageningen Universiteit, 2006.

[54] Christoph A. Vogel and William R. Pendergrass. Spectral characteristics of turbulence from rooftop meteorological stations in washington, dc. *NOAA Atmospheric Turbulence and Diffusion Division, Oak Ridge, TN, USA*, 1999.

[55] I. S. Walker, D. J. Wilson, and T. W. Forest. Wind shadow model for air infiltration sheltering by upwind obstacles. *HVAC&R Research*, 2, 1996.

[56] Graeme Watson, Neil Douglas, and Stuart Hall. Comparison of wind flow models in complex terrain. *EWEC conference paper*, 2004.

[57] J. Wieringa. Updating the davenport roughness classification. *Journal of Wind Engineering and Industrial Aerodynamics*, 41-44:357–368, 1992.

[58] J. Wieringa. Does representative wind information exist? *Journal of Wind Engineering and Industrial Aerodynamics*, 65:1–12, 1996.

[59] D. J. Wilson. Flow patterns over flat-roofed buildings and application to exhaust stack design. *ASHRAE Transactions*, 85:284–295, 1979.

[60] WINEUR. Report on resource assessment: Wineur deliverable 5.1. 2007.

[61] Man Sing Wong, Janet E. Nichol, Pui Hang To, and Jingzhi Wang. A simple method for designation of urban ventilation corridors and its application to urban heat island analysis. *Building and Environment*, 45:1880–1889, 2010.

[62] Fikirte Yemer. *Urban Wind Map for Delft, Rotterdam and Zoetermeer*. Masters Thesis Delft University of Technology, 2010.

Appendix A

User Guide for DEM derived z_0 in WAsP

Given that the rooftop is located above the surrounding roofs and no clear shelters are present, on may apply the following sequence to obtain a wind climate based on DEM analysis.

step 1: Calculating surface parameters

Surface parameters are calculated using the MATLAB program *getparam64.m*. It requires a ground-level filtered DEM, loaded in the workspace and coordinates of the roof with 5m precision. It is advised to use a radius of 160 cells (800 m) and average the solution over a 10x10 cell grid (50x50m) centered on the roof.

step 2: Generating the roughness map file

The estimated urban surface roughness lengths found in the previous step should now be integrated in the wheel-like roughness structure so that WAsP can use them in the simulation. This could be done manually, but is very time consuming so a small Python script was written that automatically generates the roughness structure.
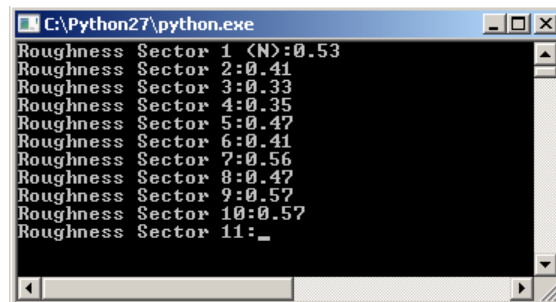
Figure A.1: Command line interface generating the WAsP map file

If the program is ran successfully, a WAsP map file *urbanroughness.map* is generated.

Step 3: Setting up the WAsP workspace

To perform a WAsP simulation, we first need to set up the WAsP workspace. The WAsP workspace combines the roughness map, the reference wind climate and the turbine site or turbine specifications and form the base for the simulation.

Once WAsP has been started, click on *Create New Workspace*. Then, in the workspace hierarchy, right click on the WAsP project and click *Insert New > Wind Atlas*. A wind atlas appears together with a meteorological station in the workspace hierarchy. The meteorological station is where the reference wind climate should be stored. To load the Zestienhoven wind climate, right

click on the met. station, choose *Insert New From File > Observed Wind Climate* and navigate to the Zestienhoven wind climate file.

Now we should load the urban roughness map that was created in the previous step. Right click on the WAsP project, choose *Insert New From File > Vector Map* and navigate to the urbanroughness.map file. Now we just need to add the wind turbine to the workspace. To do that, right click on the WAsP project and choose *Insert New > Turbine Site*. In the dialog, fill in the x and y-coordinates as 50 000; this positions the turbine site in the middle of the wheel. Select the height as the effective building height (z_d corrected).
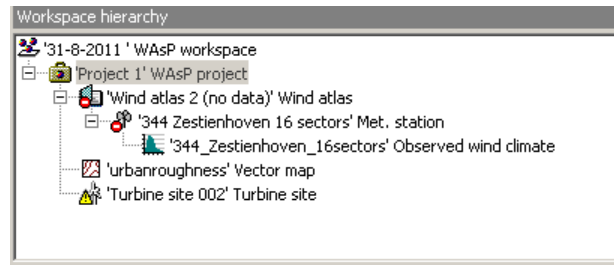
Figure A.2: WAsP's workspace hierarchy

The workspace should now look like figure A.2. WAsP indicates by the red warning signs that the met. station does not have a specified position on the map. Since the met. station holds potential wind speed data, the best position in our map would be infinitively far away from the wheel, surrounded by an infinite area of standard roughness (0.03m). This can be accomplished by double clicking the met. station icon and unchecking the check box *Require and use map location*. WAsP will now directly use the potential wind speed data to generate the wind atlas without considering any site effects or map influences. Since the data are potential wind speeds, we can assume these effects have been taken care of by the KNMI.

Step 4: Performing the simulations

The red signs have disappeared and we can now calculate a wind atlas by selecting the wind atlas and pressing F9. Then, we select the turbine site and click F9 to make the prediction. Double clicking the turbine site gives information about the mean wind speeds per sector. The dialog box also holds a *Site Effects* -tab, giving the effective reference roughness per sector. These values should be very close to the values used in generating the map. Small deviations aways occur due to some numerical errors.

Appendix B

Accuracy of WAsP

In a cross prediction, the WAsP model is used to extrapolate the observed wind climate at one station to a prediction for of another station, and visa versa. It enables estimation of the typical error accompanied with this WAsP extrapolation. For the Netherlands, such a cross prediction was previously done by Fikirte Yemer, between KNMI station Geulhaven and Zestienhoven, using the WAsP map with artificial orography [62]. These results indicated an 8% omni-directional prediction error. Although there may be many causes for this error, it seems obvious from the peculiarity of the wind rose at Geulhaven that shelter effects or local direction changes contributed to this.

To assess the accuracy of the current map, we chose to couple KNMI station Zestienhoven with KNMI station Hoek van Holland. Hoek van Holland is further away than Geulhaven but it is believed to have records which have not been affected by direction changes or shelter. For both, datasets are obtained for the period 1981-2011, normalized to potential wind speed (standard roughness and 10 m height).

Hoek van Holland is located in a coastal area characterized by dunes and low vegetation. Measurement position is 15 m above ground level and the local elevation is 12.1 m above sea level. Station Hoek van Holland is 25.5 km away from the Veilingweg in Rotterdam and 23.8 km away from measurement station Zestienhoven, which, in turn, is located in an area characterized by grassland and urban areas to the Southeast – the suburbs of Rotterdam. The measurement position here is 10 m a.g.l and the local elevation -4.6 m a.s.l. A map indicating the locations is given in figure B.1.

There are a few reasons why station Hoek van Holland, distant as it is, was still chosen as to assess the accuracy of WAsP over the current area. First, the station is nicely within the extend of the ground level elevation and roughness map produced earlier; saving time on further map extensions. Second, the wind frequency rose of Hoek van Holland seemed very similar to the one at Zestienhoven, indicating a less likely situation of wind shelter or local turning of the wind. This has been a main reason not to choose station Geulhaven, as it had a peculiar wind frequency rose, and is currently also not listed as an active station on the KNMI wind climate website.

The relatively large distance between Hoek van Holland and Zestienhoven/Veilingweg does constrain a proper accuracy assessment of WAsP to some extend, mainly because the criterion of a similar mesoscale wind climate may not be fulfilled. In this light, it would be better to compare Zestienhoven to a station further inland, which is expected to be subject to the same diurnal cycle. Hence, chances are that conclusions about the accuracy as they are drawn from the current

	Hoek van Holland	Zestienhoven
Local Elevation [m a.s.l]	12.1	-4.6
Anemometer Height [m a.g.l.]	15	10
Surface Characteristics	Dunes, Coastal Area	Grassland, Airport
Time series	1981-2011 hourly	1981-2011 hourly
Instrument	Cup Anemometer	Cup Anemometer

Table B.1: Measurement properties of the two long-term stations

Figure B.1: Map overview of the measurement stations Hoek van Holland (red) and Zestienhoven (green) in relation to the Veilingweg Rotterdam (blue). Courtesy of maps.google.com

Sector	$\overline{U}$ Observed	$\overline{U}$ Predicted	Error [m/s]	Error [%]
1 (N)	3.84	4.80	0.96	25
2	4.02	4.99	0.97	24.1
3	4.17	5.95	1.78	42.7
4	4.38	5.03	0.65	14.8
5	3.88	4.35	0.47	12.1
6	4.20	4.24	0.04	1
7 (S)	4.98	4.87	-0.11	-2.2
8	6.66	5.28	-1.38	-20.7
9	6.90	6.19	-0.71	-10.3
10	5.63	5.88	0.25	4.4
11	5.45	5.39	-0.06	-1.1
12	5.02	4.80	-0.22	-4.4
All	5.22	5.26	0.04	0.8

Table B.2: Observed and predicted (potential) mean wind speeds per sector in m/s for station Zestienhoven

test-setup are conservative as compared to conclusions which could have been drawn when a more inland station than Hoek van Holland would have been selected.

B.1 Cross Prediction for Zestienhoven

For Hoek van Holland as reference, and Zestienhoven as target, table B.3 gives the observed mean wind speeds, the predicted mean wind speeds and the percentage error, subdivided by sector. The bottom row gives the frequency weighted mean wind speeds. Figure B.2 depicts the observed and predicted wind roses for Zestienhoven.

B.2 Cross Prediction for Hoek van Holland

For Zestienhoven as predictor, and Hoek van Holland as target. The results of this simulation are given in table B.3.
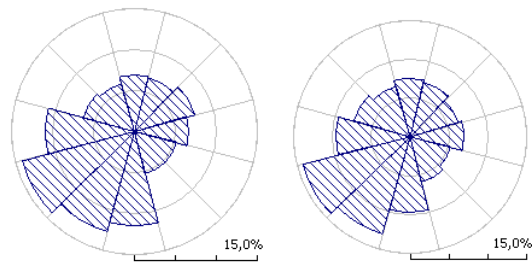
Figure B.2: Observed (left) and predicted wind frequency rose for station Zestienhoven

Sector	$\overline{U}$ Observed	$\overline{U}$ Predicted	Error [m/s]	Error [%]
1 (N)	6.56	5.73	-0.83	-12.7
2	6.51	5.16	-1.35	-20.7
3	5.82	4.05	-1.77	-30.4
4	5.02	4.26	-0.76	-15.1
5	4.71	4.21	-0.5	-10.6
6	5.34	5.41	0.07	1.3
7 (S)	6.15	6.47	0.32	5.2
8	7.23	8.72	1.49	20.6
9	8.11	8.90	0.79	9.7
10	7.59	7.79	0.2	2.6
11	7.25	7.24	-0.01	-0.1
12	6.83	7.10	0.27	4
All	6.68	6.69	0.01	0.1

Table B.3: Observed and predicted (potential) mean wind speeds in m/s for station Hoek van Holland.
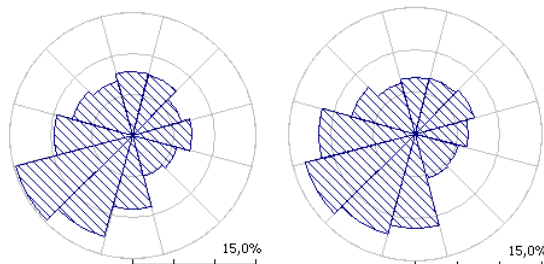
Figure B.3: Observed (left) and predicted wind frequency rose for station Hoek van Holland

B.3 Conclusion

The omni-directional (frequency-weighted sector averaged) wind speeds are surprisingly well extrapolated by WAsP, as in both tests the error is limited to below 1%. This result may be even better than expected, given the possible different mesoscale wind climate of both sites (coastal/inland). The mean wind speed accuracy between station Zestienhoven and Hoek van Holland is higher than the accuracy between Zestienhoven and Geulhaven, which leads us to conclude that having a similar wind rose is more important than the spatial distance between the predictor and target site.

Substantial errors are found in the sectoral wind speeds, mainly in sector 1 to 5. In these sectors, it seems as if the assumption of similar meso-scale wind climate is more vigorously violated than in other sectors. We also find the largest wind rose differences in these sectors. The wind speeds of Zestienhoven are overestimated by 12 to 42 percent in sector 1 to 5 when using Hoek van Holland as predictor. Interestingly, when using Hoek van Holland to predict the Veilingweg, a similarly large overestimation is found in exactly the same sectors 1 to 5. This further supports the hypothesis that these errors are due to a varying mesoscale wind climate which is not accounted for in WAsP.

Due to the small percentage of time of winds from the problematic sectors, the effect on the overall wind resource remains limited, at least for this occasion. In case of another wind frequency rose would be valid, such effects may have been more accentuated in the overall mean wind speed and energy density.

Concluding it can be stated that the large distance and presumable sea effects plays part in rightfully estimating typical errors encountered in a WAsP extrapolation. It would be wrong to totally neglect sectors 1 to 5 in this accuracy analysis, as they are still part of the cross prediction. Therefore, a middle route is chosen. It is decided to consider the mean absolute sectoral error of these samples to be a slightly biased estimator of the true mean sector error in any other WAsP prediction. Averaged over all sectors we find a mean absolute error in this sample of 0.67 m/s. Without sector 1-5 this is reduced to 0.42 m/s. Based on this it can be stated that a typical sectoral prediction error in WAsP is approximately 0.5 m/s. Errors higher than 0.5 m/s are from now on considered as above-average and may indicate violation of some of the assumptions in WAsP.

Appendix C

Resource Maps

This appendix presents several maps. The first is an overview of the measurement locations. Then follows the omni-directional zero-plane displacement height map. After that, four WAsP resource outputs are presented for the region. At last, we present a simple flowchart indicating which steps are required to

C.1 Omni-directional zero-plane displacement height

Figure C.1 shows a contour plot of the zero-plane displacement height in 1 m precision as it was calculated by the omni-directional analysis of the digital elevation model ($\sigma = 500$m). The plot may be used to estimate the effective building height for the logarithmic profile. X and Y-coordinates are given in *Rijksdriehoekscoordinat*en.[1]
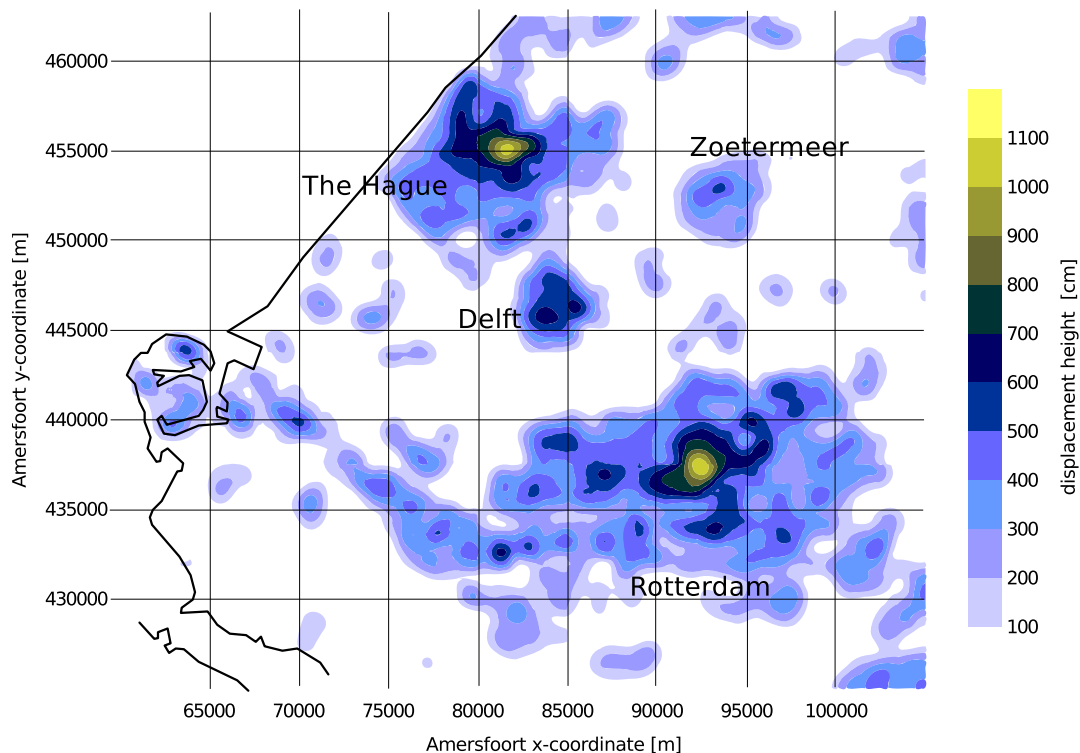
Figure C.1: Contour plot of the omni-directional zero-plane displacement height of the region.

---

[1]These coordinates may be found by tools on the internet, see for instance:
http://estevenh.home.xs4all.nl/1/frame/Index.html

C.2 Global overview of process required to produce the WAsP maps
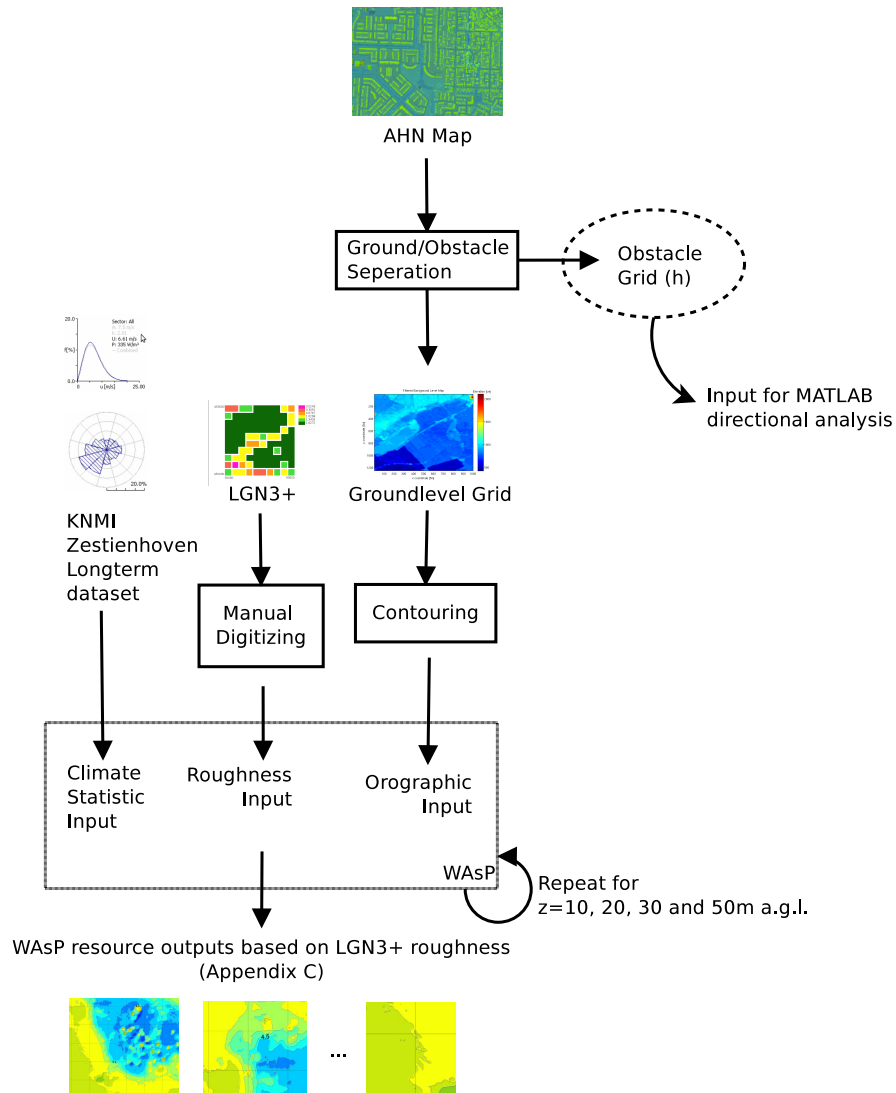
Figure C.2: Flow diagram indicating the integration of height, climate and roughness data to produce the set of WAsP maps. The most time-consuming step is preparing the LGN3+ roughness for use in WAsP. This involves manually digitizing a few hundred roughness contour lines which are subject to all kinds of geometric inconsistencies. Once this is done, the actual production of a single WAsP map takes about 4 hours on a regular PC.

C.3 Mean wind speeds based on LGN3+ roughness

WAsP simulations are executed at four different heights: 10; 20; 30 and 50 m above ground level, using LGN3+ land-use roughness, ground level orography and the Zestienhoven wind climate. The following four figures give the resulting mean wind speeds, and can be used for a quick, initial estimate of the wind resource for typical building heights.

The figures reflect the increasing wind velocity as well as the increasing roughness diffusivity at increasing heights. Numbers are given in m/s and indicate the minimum mean wind speed as predicted by WAsP in the region enclosed by the contour, while gradual color transitions indicate small local variation to the prediction.
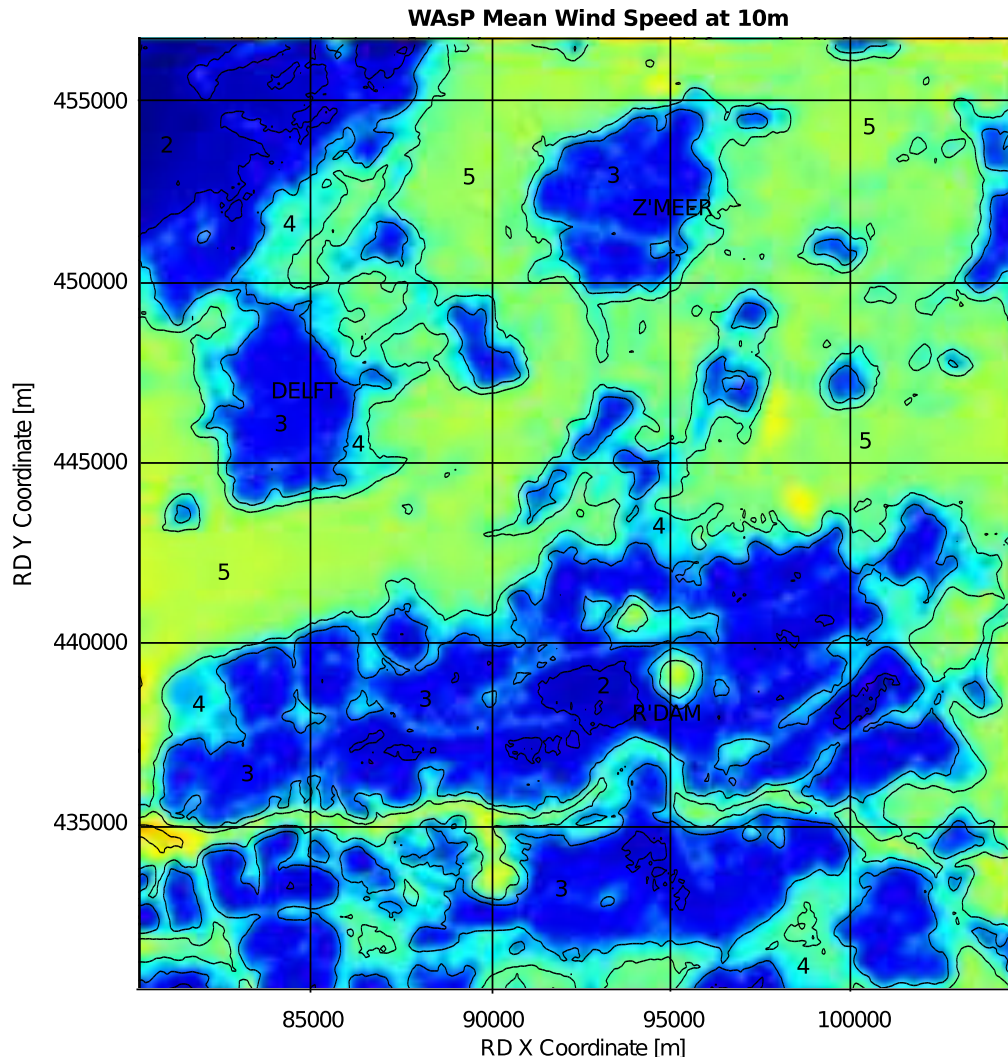
Figure C.3: Contour plot of the mean wind speed at 10 m agl.
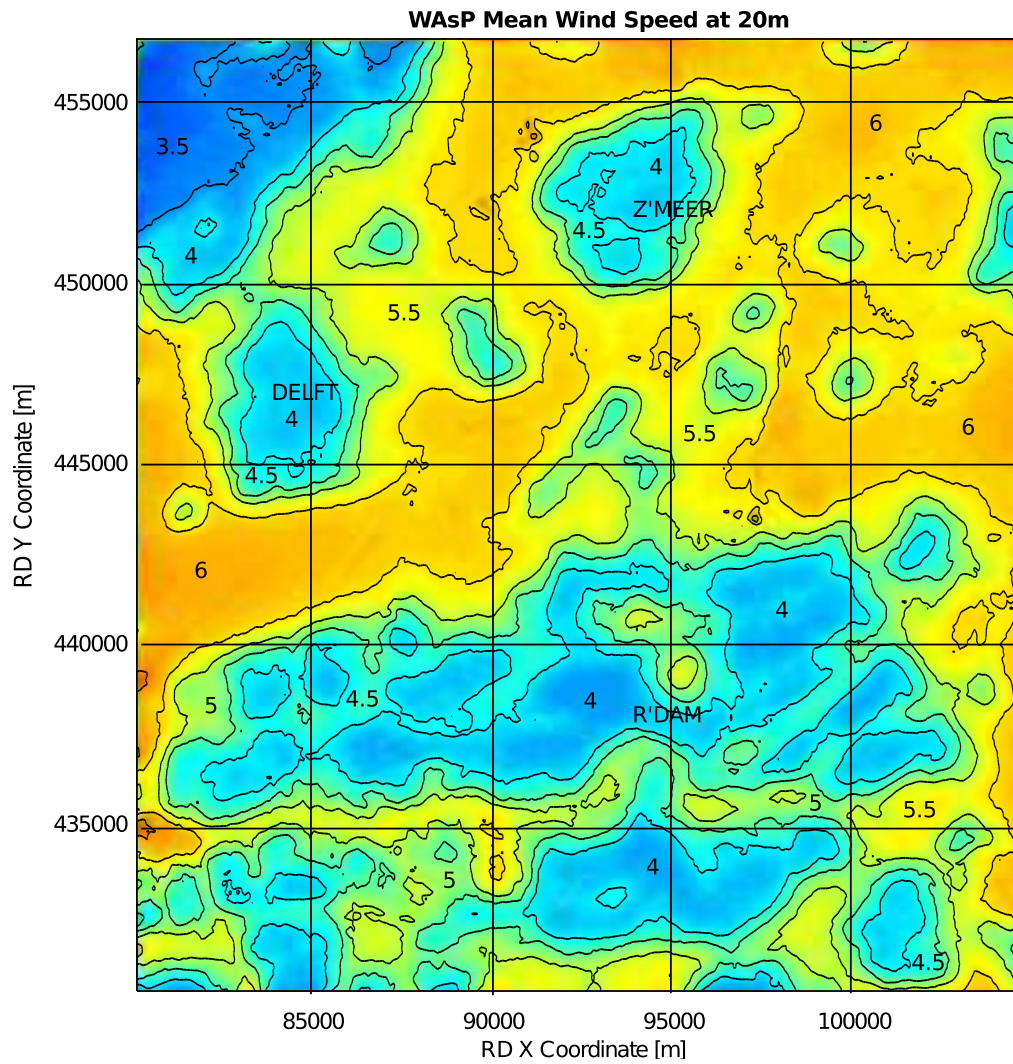
Figure C.4: Contour plot of the mean wind speed at 20 m agl. This figure shows most clearly very small orographic speedups which are modeled by WAsP around coordinate (91000,454000). This is the location of a small waste hill in Zoetermeer.
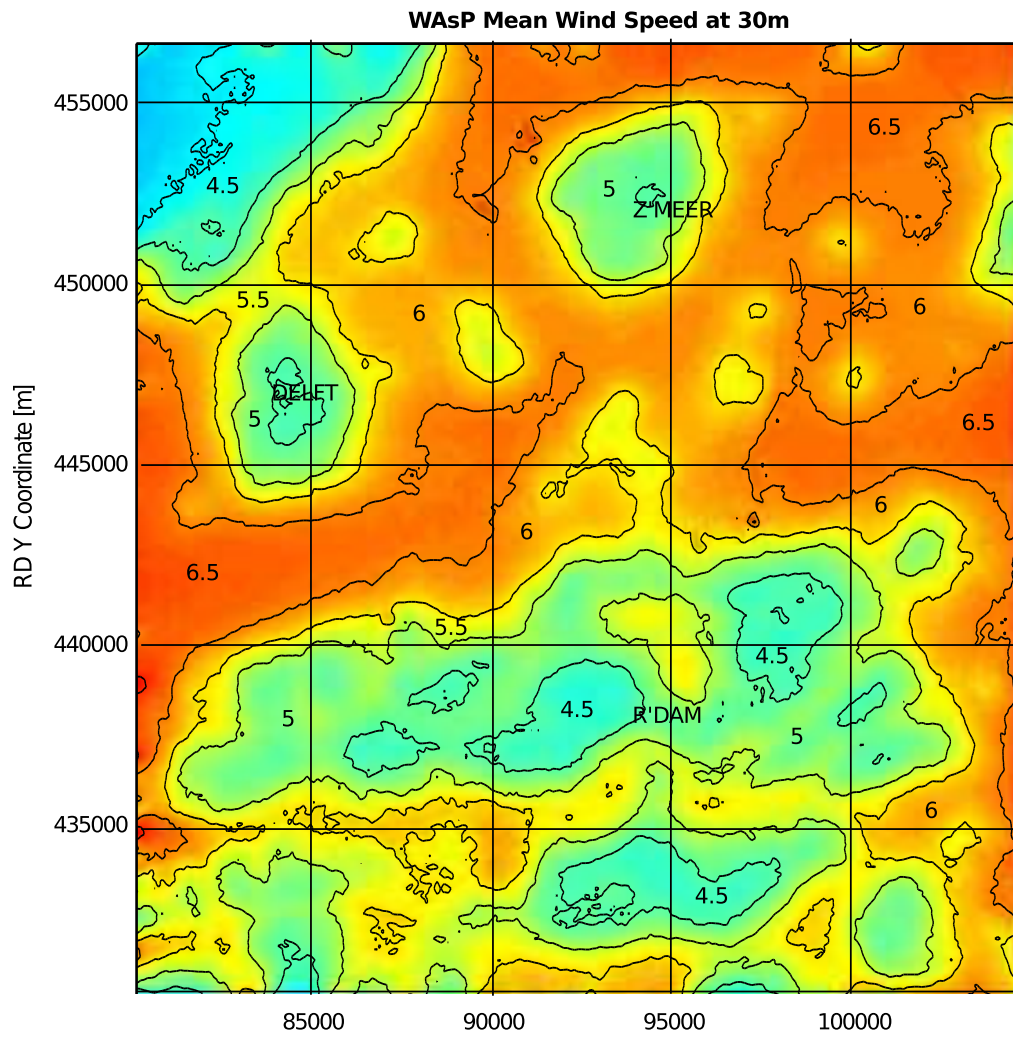
Figure C.5: Contour plot of the mean wind speed at 30 m agl.

WAsP Mean Wind Speed at 50m
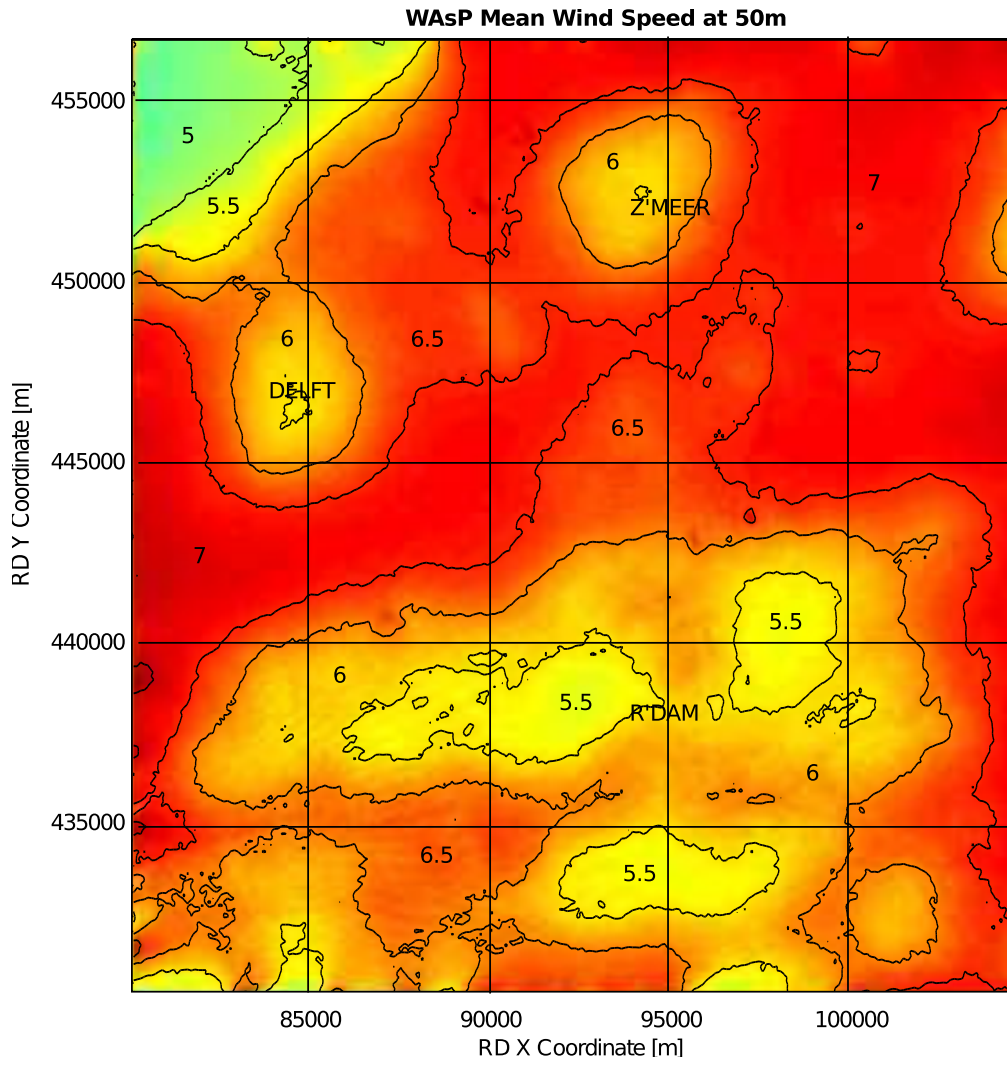
Figure C.6: Contour plot of the mean wind speed at 50 m agl.

Appendix D

Measurement Details

This appendix lists some additional measurement details from both campaigns, as well as results of a small sensitivity study on the measured roughness estimates.

D.1 Overview of the measurement locations

Map of the region indicating the two measurement locations
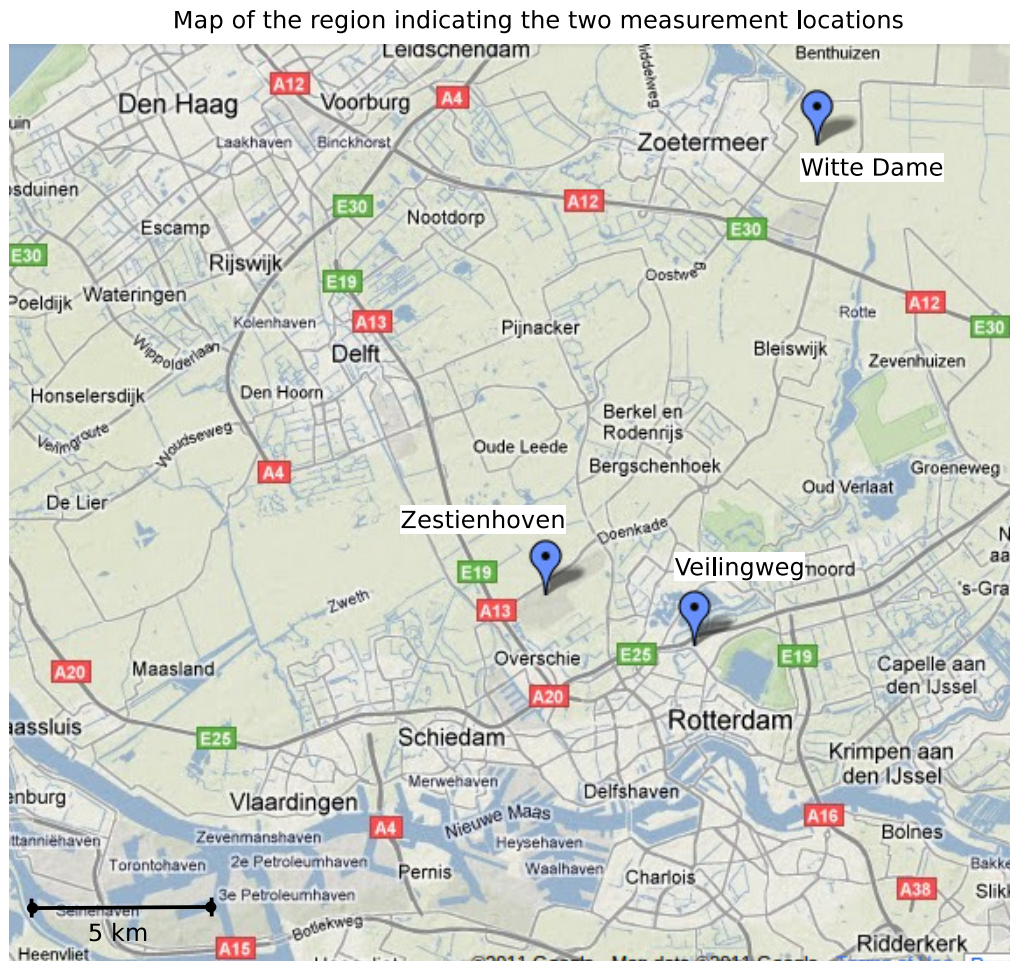
Figure D.1: Map of the Rotterdam - Delft - Zoetermeer region with the two measurement locations

D.2 Overview of data collected

The tables below gives some statistics of both measurement campaigns performed for this thesis. All data reported here are after the spike correction.

Sec   Measurement sector

N Number of 10-min data points collected within assigned sector

St   Number of stable data points

Sp   Percentage of spikes in the stable data

U Mean of the 10-min means

maxU   Maximum 10-minute mean within that sector

T.I.   Median of the turbulence intensity recorded

It should be noted that the sector division on the Witte Dame was susceptible to directional changes towards sector 10, in the analysis we therefore used the direction from KNMI Zestienhoven which was collected simultaneously. This led to small (<10%) differences on the mean and max wind speeds. Also, no distinction was made on different stability classes.

Table D.1: Measurement details of the ultrasonic campaign at the Veilingweg

Veilingweg (Aug 1 - Aug 29) - 7m above roof

Sec	N	St	Sp	U [m/s]	$\max U$ [m/s]	T.I. [-]
1	61	57	0	2.79	5.32	0.21
2	107	95	0	3.07	5.86	0.23
3	94	74	0	3.28	8.13	0.19
4	147	114	<0.1	3.72	8.01	0.18
5	192	106	0.9	3.67	6.89	0.18
6	123	63	<0.1	3.26	5.96	0.19
7	74	46	0.3	3.01	5.40	0.20
8	84	35	<0.1	3.16	5.14	0.22
9	133	80	<0.1	3.46	6.22	0.21
10	269	237	<0.1	4.12	7.72	0.24
11	828	552	<0.1	4.95	9.33	0.22
12	673	462	0.2	6.15	11.34	0.23
13	467	247	0.1	5.69	11.19	0.22
14	305	149	<0.1	4.36	10.12	0.21
15	284	194	<0.1	5.03	10.70	0.20
16	70	63	0	3.16	5.92	0.20

Table D.2: Measurement details of the ultrasonic campaign at the Witte Dame, low setup

Witte Dame (Aug 30 - Oct 2) - 6m above roof

Sec	N	St	Sp	U [m/s]	$\max U$ [m/s]	T.I. [-]
1	226	62	0	3.05	4.76	0.08
2	70	0	0	2.79	5.54	0.16
3	96	6	0	3.13	4.56	0.19
4	176	12	0	3.20	4.94	0.12
5	348	28	0	3.78	8.82	0.11
6	220	46	0	4.36	9.50	0.14
7	126	36	<0.1	4.04	7.67	0.16
8	162	96	<0.1	4.11	7.54	0.20
9	476	210	<0.1	3.78	10.31	0.24
10	735	501	0.1	5.53	12.37	0.34
11	658	434	0.22	5.59	13.71	0.32
12	734	472	<0.1	6.34	12.05	0.27
13	464	202	<0.1	6.15	11.39	0.29
14	78	54	0	2.70	7.5	0.39
15	30	18	0	3.00	7.19	0.38
16	4	0	0	3.49	6.06	0.17

Table D.3: Measurement details of the ultrasonic campaign at the Witte Dame, high setup. ΔT.I. gives the measured change in T.I. as compared to the low setup.

Witte Dame (Oct 2 - Oct 12) - 7.3m above roof

Sec	N	St	Sp	U [m/s]	$\max U$ [m/s]	T.I. [-]	ΔT.I. [%]
1	8	-	0	4.12	5.03	0.16	100.0
2	26	-	0	2.70	3.85	0.10	-37.5
3	84	-	0	3.55	5.28	0.09	-52.6
4	112	-	0	3.53	5.48	0.15	25.0
5	90	-	0	3.88	6.58	0.14	27.3
6	192	-	0	4.56	6.62	0.13	-7.1
7	102	-	0	4.73	6.64	0.10	-37.5
8	61	-	0	3.21	4.48	0.16	-20.0
9	42	-	0	4.61	7.17	0.30	25.0
10	53	-	0	4.42	8.84	0.25	-26.5
11	142	-	<0.1	9.22	12.98	0.24	-25.0
12	193	-	0.4	9.78	14.01	0.24	-11.1
13	44	-	0.4	7.92	11.80	0.23	-20.7
14	123	-	<0.1	6.97	12.24	0.31	-20.5
15	163	-	<0.1	6.70	12.80	0.24	-36.8
16	19	-	<0.1	5.35	8.35	0.20	17.6

D.3   Measured sectoral roughness

Table D.4: Sectoral roughness lengths found at the Veilingweg through turbulence measurements using only neutrally stable classes. The two most right columns give the lower and upper boundary of a 95% confidence interval on the median

sector	N	plateau	z_0 [m]	l.b. [m]	u.b. [m]
1	57	poor	0.38	0.19	0.48
2	95	good	0.59	0.45	0.67
3	74	good	0.27	0.21	0.39
4	113	good	0.18	0.13	0.24
5	101	good	0.18	0.14	0.26
6	59	poor	0.34	0.18	0.56
7	41	no	0.17	0.03	0.40
8	32	poor	0.67	0.39	1.11
9	77	good	0.53	0.34	0.93
10	235	good	0.77	0.69	0.87
11	552	good	0.59	0.54	0.62
12	481	good	0.61	0.56	0.66
13	248	good	0.52	0.46	0.58
14	147	good	0.30	0.23	0.38
15	193	good	0.28	0.22	0.33
16	63	poor	0.37	0.19	0.50

Table D.5: Sectoral roughness lengths found through turbulence measurements at the Witte Dame (low setup). The two most right columns give the lower and upper boundary of a 95% confidence interval on the median.

sector	N	plateau	z_0 [m]	l.b. [m]	u.b. [m]
1	226	poor	<0.01	<0.01	<0.01
2	70	poor	0.15	0.01	0.42
3	96	poor	0.10	0.01	0.34
4	176	poor	0.01	<0.01	0.02
5	348	poor	0.01	<0.01	0.02
6	220	good	0.04	0.01	0.10
7	126	good	0.11	0.03	0.20
8	162	good	0.30	0.19	0.44
9	476	good	0.84	0.57	1.13
10	735	good	2.66	2.54	2.75
11	658	good	2.19	2.03	2.32
12	734	good	1.33	1.24	1.44
13	464	poor	1.54	1.37	1.80
14	78	good	3.79	2.88	4.74
15	30	good	3.42	2.85	4.00
16	4	no	-	-	-

D.4 Sensitivity z_0 estimate for TI reduction

The longitudinal turbulence intensity may under some conditions be reduced due to localized speed ups of the mean wind speed. This rapid distortion effect was observed in complex terrain above hilltops [13, 19], although not for all hills. A small sensitivity study was performed at the effect on such speed ups to the roughness estimates in our measurements.

By application of equation 5.3, the results of figure D.2 are obtained. It indicates that even with a small TI reduction, estimated roughness may be affected substantially, especially for lightly turbulent conditions.

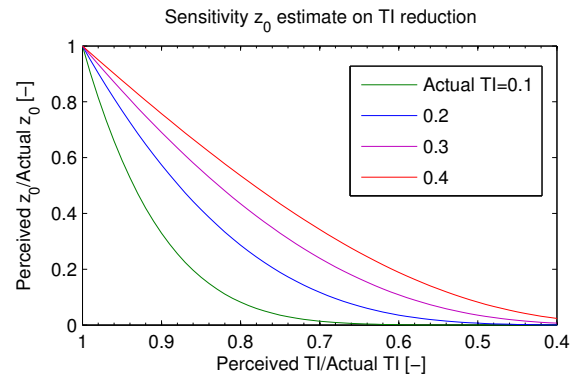Figure D.2: Effect of turbulence intensity reduction on roughness estimates from the ultrasonic campaign

D.5 Photos

Some photos that were taken of the measurement setup on the Witte Dame and on the Veilingweg.

Figure D.3: Mast installation in July 2011 on the Veilingweg (7m).

Figure D.4: Mast installation in August 2011 on the Witte Dame. Here shown is the 6 m setup, which was later extended to 7.3 m.

Appendix E

Witte Dame long-term prediction

Using the model applied in this thesis, the long-term wind climate at the Witte Dame is predicted. WAsP is used with the following inputs:

$H - z_d$ 44 m

z_0 as produced by DEM

ref   Zestienhoven 1981-2011

Table E.1 gives the wind climate. Also included is a wind climate if a user corrected speed-up is applied to sectors 15 to 8, which was found during the measurements. It these colums, a 30% potential speed up is proposed, as a conservative intepretation of the actual speed-up found.

Table E.1: Long-term wind climate of the Witte Dame

Sec	Freq [%]	U [m/s]	P [W/m2]	U_{corr}[m/s]	P_{corr}[W/m2]
1	5.96	4.17	88	5.42	192
2	4.27	4.67	116	6.06	255
3	5.64	4.56	98	5.93	215
4	5.26	4.37	80	5.68	176
5	5.75	4.31	77	5.61	169
6	3.44	3.96	62	5.14	136
7	2.95	4.08	69	5.3	151
8	6.74	4.63	103	6.02	226
9	10.06	5.20	143	5.20	143
10	8.58	7.02	327	7.02	327
11	9.21	6.76	319	6.76	319
12	9.86	6.29	277	6.29	277
13	8.97	5.72	221	5.72	221
14	4.32	5.49	193	5.49	193
15	3.75	5.20	158	6.76	346
16	5.22	4.84	131	6.29	288
All		5.32	176	5.98	233

Appendix F

LGN3+ Roughness Classes

Table F.1: Roughness classes as defined by the LNG3+ database [5].

ID	Description	z_0[m]
0	No data	0.03
1	Grass	0.03
2	Maize	0.17
3	Potatoes	0.07
4	Beets	0.07
5	Cereals	0.16
6	Other crops	0.04
7	Land abroad	0.15
8	Greenhouses	0.1
9	Orchards	0.39
10	Bulb cultivation	0.07
11	Deciduous forest	0.75
12	Coniferous forest	0.75
16	Fresh water	0.001
17	Salt water	0.001
18	Urban area	1.6
19	Rural area with buildings	0.5
20	Deciduous forest in urban area	1.1
21	Coniferous forest in urban area	1.1
22	Forest with dense urban area	2
23	Grass in urban area	0.03
24	Bare soil in urban area	0.001
25	Main roads and railways	0.1
27	Runways	0.0003
28	Parking lots	0.1
30	Salt marshes	0.0002
31	Beaches and dunes	0.0003
32	Dunes with sparse vegetation	0.02
33	Dunes with vegetation	0.06
34	Heathlands in coastal areas	0.04
35	Shifting sands	0.0003
36	Heathlands	0.03
37	Heathlands with some grass	0.04
38	Heathlands with grass	0.06
39	Raised bogs	0.06
40	Forest in raised bogs	0.75
41	Vegetation in wetlands	0.03
42	Reed in wetlands	0.1
43	Forest in wetlands	0.75
44	Pasture in peat areas	0.07
45	Other herbaceous vegetation	0.03
46	Bare soil in natural areas	0.001

This project is financed with support of the European Fund for Regional Development.